UNIVERSITÀ DEGLI STUDI DI TRIESTE

XXIV CICLO DEL DOTTORATO DI RICERCA IN NANOTECNOLOGIE

BIO-SAMPLE ENVIRONMENT MANIPULATION USING ADVANCED MICROSCOPY TECHNIQUES

Settore scientifico-disciplinare: FIS/01 FISICA SPERIMENTALE

Dottoranda:
Elisa D'ESTE

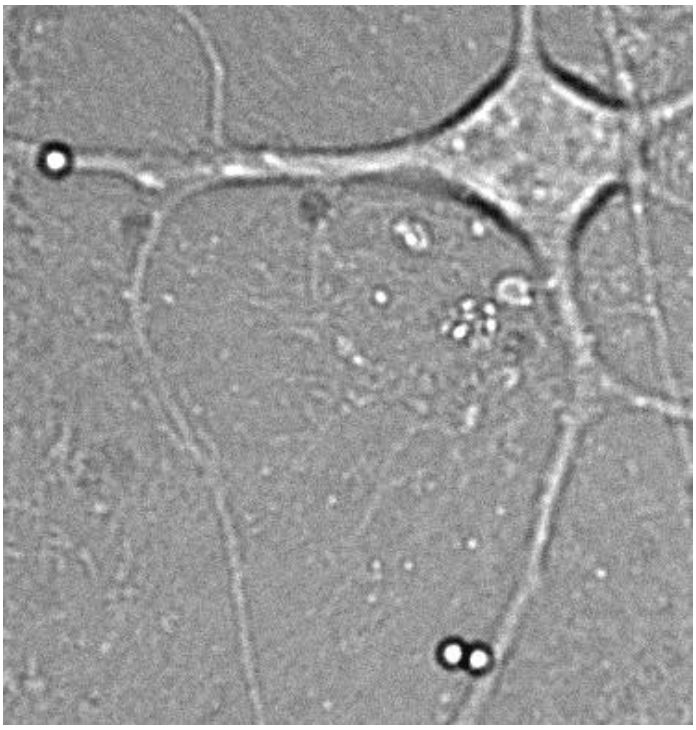

Coordinatore Dottorato di Ricerca:
Prof. Maurizio FERMEGLIA

Supervisore:
Prof. Alberto MORGANTE
Università degli Studi di Trieste

Tutore:
Dott. Dan COJOC
CNR - IOM Laboratorio TASC

Correlatore:
Prof. Enrico TONGIORGI
Università degli Studi di Trieste

ANNO ACCADEMICO 2010/2011

UNIVERSITÀ DEGLI STUDI DI TRIESTE

XXIV CICLO DEL DOTTORATO DI RICERCA IN NANOTECNOLOGIE

BIO-SAMPLE ENVIRONMENT MANIPULATION USING ADVANCED MICROSCOPY TECHNIQUES

Settore scientifico-disciplinare: FIS/01 FISICA SPERIMENTALE

Dottoranda:
Elisa D'ESTE

Coordinatore Dottorato di Ricerca:
Prof. Maurizio FERMEGLIA

Supervisore:
Prof. Alberto MORGANTE
Università degli Studi di Trieste

Tutore:
Dott. Dan COJOC
CNR - IOM Laboratorio TASC

Correlatore:
Prof. Enrico TONGIORGI
Università degli Studi di Trieste

ANNO ACCADEMICO 2010/2011

“And sometimes is seen a strange spot in the sky
A human being that was given to fly”

Eddie Vedder

“Le' inutil insegna' al mus, si piart timp. In plui si infastidis la bestie.”
(Teaching to the donkey: useless. And you bother it)

Common saying from Friuli

TABLE OF CONTENTS

ACRONYMS

AFM – Atomic Force Microscopy

ATP – Adenosine-5'-TriPhosphate

BDNF – Brain Derived Neurotrophic Factor

BLP – Biotinylated-Lipid Particles

BSA – Bovine Serum Albumin

Ca^{2+} – Calcium

cAMP – Cyclic Adenosine Monophosphate

CCD – Charge Coupled Device

C domain – Central domain

cGMP – Cyclic Guanosine Monophosphate

COOH – Carboxylic group

CW – Continuous Wave

D – Distance

DCC – Deleted in Colorectal Cancer

DIC – Differential Interference Contrast

DIV – Days *In Vitro*

DNA – Deoxyribonucleic acid

DRG – Dorsal Root Ganglion

E. coli – *Escherichia coli*

ECM – Extra Cellular Matrix

EDAC – 1-Ethyl-3-[3-dimethylaminopropyl]carbodiimide hydrochloride

EGF – Epidermal Growth Factor

f_L – Focal Lenght

GABA – Gamma-Aminobutyric Acid

GC – Growth Cone

GSD – Ground State Depletion microscopy

IL-8 – Interleukin-8

IP_3 – Inositol trisphosphate

IR – InfraRed

LTD – Long-Term Depression

LTP – Long-Term Potentiation

MAPK – Mitogen-Activated Protein Kinase

MNPs – superparaMagnetic NanoParticles

NA – Numerical Aperture

NGF – Nerve Growth Factor

N_{mol} – Number of molecules encapsulated within a liposome

P domain – Peripherial domain

PALM/STORM – PhotoActivation Localization Microscopy, STochastic Optical Reconstruction Microscopy

PI3K – Phosphatidylinositol 3-Kinase

PLC-γ – Phospholipase Cγ

PSF – Point Spread Function

Qdots or QD – Quantum Dots

RESOLFT – REversible Saturable OpticaL Fluorescence Transitions

RNA – Ribonucleic acid

RT – Room Temperature

Sema3A – Semaphorin 3A

SPEM/SSIM – Saturated Pattern Excitation Microscopy or Saturated Structured Illumination Microscopy

SQT – Single Quantum dot Tracking

STED – STimulate Emission Depletion

T zone – Transition zone

Trk – Tropomyosin-Related tyrosine Kinases receptors

TRPC – Transient receptor potential channels

VB – Vesicle Breaking

WD – Working Distance

ABSTRACT

Under physiological conditions in the brain, molecules are released with high spatial and temporal resolution. A lot of efforts have been done in the last years in order to develop techniques that mimic this situation. Among them, we mention the use of micropipettes for the ejection of fluids, the use of AFM (Atomic Force Microscopy), microfluidic devices and optical manipulation. The latter approach exploits light to manipulate the samples, e.g. to create transient pores in the cell membrane or to move small objects carrying a stimulus.

This Thesis concerns with the development of new techniques for the local delivery of molecules based on optical manipulation technologies, and in particular on optical tweezers. Sub-micrometer particles in a compact trap, such as the single-beam gradient or optical tweezers, can be localized within a small fraction of a wavelength of light or moved over long distances of many centimeters without any mechanical contact. A three-dimensional trap is simply created by focusing a laser beam through a microscope objective with high numerical aperture. We studied three types of vectors for local delivery of molecules, which can be optically manipulated: microbeads, micron-sized liposomes and Quantum dots (Qdots).

Silica microbeads can be covalently functionalized on their surface with the protein of interest and placed in contact with the desired part of a cell. In order to validate the technique, we functionalized beads with a secretory molecule, the neurotrophin Brain-derived neurotrophic factor (BDNF). BDNF is a key regulator of neuronal development and plasticity. We showed that single BDNF-coated microbeads can be extracted with optical tweezers from small reservoirs and positioned with submicrometric precision to specific sites on the dendrites of cultured hippocampal neurons. Localized contact of microbeads functionalized with BDNF induced focal increase of Calcium signaling in the stimulated dendrite, specific activation of the TrkB receptor pathway and influenced the development of growth cones. Remarkably, a single BDNF-coated bead positioned on a dendrite was found to be enough for TrkB phosphorylation, an efficient and long-lasting activation of Calcium signaling in the soma, and c-Fos signaling in the nucleus, comparable to bath stimulation conditions. Moreover, since BDNF is covalently cross-linked to the bead surface we could demonstrate that activation of some of the TrkB receptor pathway does not necessarily require BDNF endocytosis.

In the case of liposomes, the molecules of interest were encapsulated within their lumen. Single liposomes were trapped and transported by means of optical tweezers to the site of stimulation on cultured neurons. Finally, the release of liposome content was induced by application of UV-pulses that broke the liposome membrane. In order to test the effect of the UV-induced release, liposomes with a diameter ranging from 1 to 10 μm (fL to pL volumes), were filled with KCl and tested on neuronal cells. Neuronal cultures, loaded with Ca^{2+} dye, were monitored by imaging intracellular Ca^{2+}. An efficient release from the liposomes was demonstrated by detectable Calcium signals, indicating induced depolarization of the neuronal cells by KCl. Afterwards, this technique was used to address a biological issue, that is the effect of two proteins (Semaphorin 3A and Netrin-1) on growth cones. The growth cone is an intracellular apparatus located at the tip of the neurite of developing neurons. Its motility governs axonal path-finding and the construction of neuronal networks. Growth cones are highly dynamic structures that respond to external stimuli turning towards or away from the chemical gradient. We were able to demonstrate an attractive effect of Netrin-1 on the growth cones of primary hippocampal neurons. On the contrary, Semaphorin 3A showed a repellant behavior.

To correlate the high resolution of vector manipulation with high resolution of imaging we used STimulated Emission Depletion (STED) to investigate the intimate organization of two main cytoskeleton components: actin and tubulin filaments. STED microscopy allowed imaging of actin bundles in the filopodia and organized network in lamellipodia with un-precedent resolution, beyond the diffraction barrier.

Lastly, we used liposomes to encapsulate Quantum dots. Qdots are bright and photostable nanocrystals. Due to their small size, similar to that of proteins, Qdots may be endocyted along the receptor-mediated endocytosis pathway, when they are functionalized with the appropriate ligand. As case study we considered the BDNF-TrkB endocytotic pathway. We optimized the protocol for the direct binding of BDNF to Qdots and we demonstrated the possibility of encapsulating and releasing them from liposomes.

Concluding, two different approaches for local stimulation of neurons, based on optical manipulation of microvectors, were presented and validated in this thesis. Indirect optical manipulation of nanovectors (Qdots) encapsulated in liposomes has been demonstrated as well. The techniques were then successfully applied to address some biological issues, that in turn required the optimization of other imaging tools (super resolution microscopy and Qdots).

The results of the research have been published in three papers and make the subject of other two papers in preparation:

- D'Este, E., Baj, G., Beuzer, P., Ferrari, E., Pinato, G., Tongiorgi, E., and Cojoc, D. (2011). Use of optical tweezers technology for long-term, focal stimulation of specific subcellular neuronal compartments. Integr Biol (Camb) *3*, 568-577;
- Pinato, G., Lien, L. T., D'Este, E., Torre, V., and Cojoc, D. (2011a). Neuronal chemotaxis by optically manipulated liposomes. Journal of the European Optical Society Rapid Publications *6*, 11042;
- Pinato, G., Raffaelli, T., D'Este, E., Tavano, F., and Cojoc, D. (2011b). Optical delivery of liposome encapsulated chemical stimuli to neuronal cells. J Biomed Opt *16*, 095001.

1.INTRODUCTION

LOCAL ENVIRONMENT MANIPULATION AND IMAGING OF CULTURED CELLS

1.1 OPTICAL TWEEZERS

1.1.1 HISTORICAL INTRODUCTION

In the 17th century Johannes Kepler noticed that the tails of the comets were always directed opposite to the sun (Kepler, 1619). This observation suggested that the sun was exerting a sort of "radiant pressure" that shaped the tail of the comet. Two centuries later James Clerk Maxwell proved theoretically that light can exert force on matter (Maxell, 1873) but only in 1968 Letokhov proposed the use of light beams to trap atoms (Letokhov, 1968). One year later Arthur Ashkin proved experimentally that micron-sized particles could be accelerated and trapped in stable optical potential wells using only the force of radiation pressure from a continuous laser (Ashkin, 1970). Ashkin used two counter-propagating Gaussian beams to confine the particles: only particles with a high refractive index were attracted into regions of high light intensity, while low index particles were always pushed out of the light beam. Up-to-date optical tweezers were born in 1986, when three dimensional trapping of dielectric particles was achieved with a single-beam gradient force optical trap (Ashkin et al., 1986).

Shortly after, laser tweezers started to be used for the manipulation of biological samples (Ashkin and Dziedzic, 1987). Since then a lot of uses have evolved and the interest in optical tweezers has grown exponentially (for reviews see Ashkin, 2006; Dholakia et al., 2007; Grier, 2003; Moffitt et al., 2008; Neuman and Block, 2004; Snook et al., 2009; Stevenson et al., 2010a).

1.1.2 BASIC PRINCIPLES

A single beam gradient optical trap is formed by tightly focusing a continuous-wave laser beam through an objective lens with a high numerical aperture (NA). The basic principle behind optical tweezers is related to radiation pressure forces that arise from the momentum of light itself. An easy explanation can be given for micron-sized dielectric particles. If an object bends the light, changing its momentum, conservation of momentum requires that the object must undergo an equal and opposite momentum change. This gives rise to a force acting on the object.

According to the size of the trapped particles, two different regimes describe the forces acting within optical tweezers:

- the Mie regime, when the diameter of the particle is large compared to the wavelength ($d>\lambda$);
- the Rayleigh regime, when the diameter of the particle is much smaller compared to the wavelength ($d<<\lambda$).

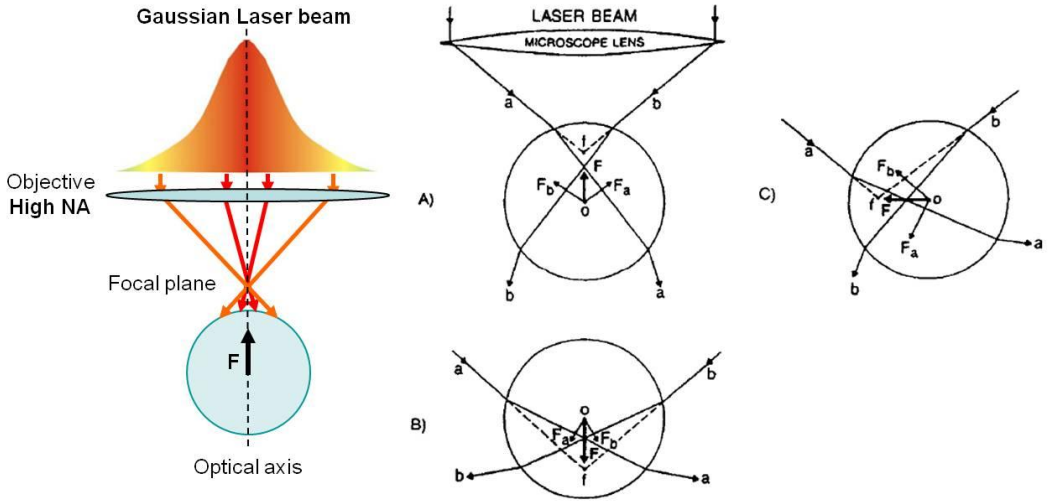

Figure 1.1: Simplified illustration of the principle of optical trapping. (**Left**) The ray-optics diagram. Rays coming from different parts of the Gaussian laser beam have different intensities. When they are focused through a high numerical aperture objective, they hit a particle that is in the neighbourhood of the focus with different angles. These rays undergo different refraction (see right part of the figure), generating a net force on the particle, that pulls it in the focus of the objective. (**Right**) Qualitative view of the trapping in of dielectric spheres. The refraction of a typical pair of rays (*a* and *b*) of the trapping beam gives forces F_a and F_b whose vector sum F is always restoring for axial and transverse displacements of the sphere from the trap focus *f*. Modified from Ashkin, 1992.

For Mie regime, ray optics analysis of the deviated light path gives the change in momentum flow and hence the reaction force acting on the object (**Figure 1.1**). A dielectric particle in a focused laser beam experiences a force called the gradient force that tends to bring the particle towards the focus. This force arises from the momentum imparted to the bead as it scatters the laser light. As depicted in

Figure 1.1, two components are essential for a three dimensional trapping to occur: a high numerical aperture objective and a Gaussian laser beam. The combination of these two elements has some advantages:

- rays coming from the inner parts of the Gaussian laser beam are more intense then rays coming from the outer parts. As a result, the force they exert on the particle is higher, and they tend to push the particle away from the focus (**Figure 1.1A**) along the optical axis. These forces are counterbalanced by the outer and less intense rays, that are more divergent and pull the object toward the focus (**Figure 1.1B**);
- the beam is symmetric and thus forces on the right and on the left of the beam are equal. As a result, particles always tend to align to the optical axis of the system (**Figure 1.1C**);
- once the particle is in the focus of the objective, the net sum of all the forces is null and the particle is confined in along the three axis x, y and z (Ashkin, 1992; Shaevitz, 2006).

The forces of a single-beam gradient radiation pressure optical trap on micron-sized dielectric spheres were first described quantitatively by Ashkin (Ashkin, 1992). These forces can be discussed in terms of scattering and gradient forces on a sphere. As they are derived considering the refraction of the light rays though the sphere, they are functions of the power of the incident light ray, the angles of incidence and refraction, and the Fresnel reflection and transmission coefficients. The total force can be described as

$$F = \frac{Q\, n_m P}{c}$$

Where Q is the dimensionless efficiency, n_m the index of refraction of the suspending medium, P is the incident laser power at the specimen plane, and c is the speed of light. Q depends on the numerical aperture of the objective (NA), on the laser (wavelength, polarization state and mode structure) and on the particle (relative index of refraction and geometry) (Ashkin, 1992; Ashkin et al., 1986). Considering standard parameters (Q=0,3 and a n_m=1,33) the force acting on the particle can thus be estimate to be in the pN range.

For the Rayleigh regime, a simple dipole model can be used (Harada and Asakura, 1996). In this case, the scattering force, which arises from the absorbed or reflected light, points towards the propagation of the laser beam. The gradient force is caused by the laser beam, which polarized the object. This force points in the direction of the intensity gradient. Also in the Rayleigh regime, the key parameters influencing the force of the trap are the light intensity, the refractive indexes of both particle and medium, the cross-section of the sphere and its radius.

For particles in between the Mie and Rayleigh regime, the previous calculations are not consistent with experimental data. Indeed, when the beam is highly localized, the electromagnetic field is essentially constant over the diffraction-limited spot (Tlusty et al., 1998) and the interactions arise from steep variations in amplitude of the electromagnetic fields. The dipole approximation can thus be used. The optical gradient force is given by dipole interaction energy as the coordinates of the particle change and the localized electromagnetic fields near the focal point can be approximated by a three-dimensional Gaussian beam. The interactions of the polarization form a potential well in which there is a restoring force that pulls the particle to the centre of the beam.

Finally, also particles with a low refractive index (e.g. air bubbles) or made from strongly scattering materials (e.g. metallic particles) can be trapped. In these cases the gradient force is reversed and more complex beam arrangements are required. For instance, the annular intensity distribution Laguerre-Gaussian was used to trap objects with lower refractive index than their surroundings (Cahagan and Swartzlander, 1998).

1.1.3 PHOTODAMAGE INDUCED BY OPTICAL TWEEZERS ON BIOLOGICAL SAMPLES

Optical tweezers are widely used for biological applications on living samples. Since the power of laser used can be quite high, the issue of photodamage should be considered. If one looks at the absorption coefficient of important organic molecules, such as hemoglobin and oxyhemoglobin, a large drop in the infrared (IR) region can be noticed (**Figure 1.2**). There is a window of relative transparency around 750 – 1200 nm, between the absorption of proteins in the visible and the increasing absorption of water towards the infrared which can be exploited. Several papers analyzed the effects of the wavelength within this window on the lethal dose and cloning efficiency of both prokaryotic and eukaryotic cells (Ashkin et al., 1990; Liang et al., 1996; Neuman et al., 1999).

Ashkin and colleagues demonstrated that using 1064 nm wavelength, trapped cells (*Escherichia coli* and yeast cells) could duplicate (Ashkin et al., 1987). Trapping of other cell types, such as red blood cells, plant cells, protozoa, diatoms, algae, was successfully tested at this wavelength.

For this reason many optical tweezers setups for biological application use IR lasers, such as Nd:YAG (Neodymium:ytterbium-aluminium-garnet, 1064 nm), Nd:YVO_4 (Neodymium:ytterbium-orthovanadate, 1064 nm) or Nd:YLF (Neodymium:ytterbium-lithium-fluoride, 1047 or 1053 nm). At these wavelengths the damage caused by the light is relatively low, even if an increase in the expression of heat shock proteins (chaperone molecules) was observed in trapped cells (Leitz et al., 2002).

Besides the wavelength, cell survival during optical manipulation depends on other factors: power and duration of manipulation, oxygen (in anaerobic conditions or in the presence of oxygen-scavenging molecules cells had a increased viability) and particular treatment performed prior to the manipulation (Neuman et al., 1999).

Finally different tolerances to optical tweezers were observed between both different bacterial species and intraspecies.

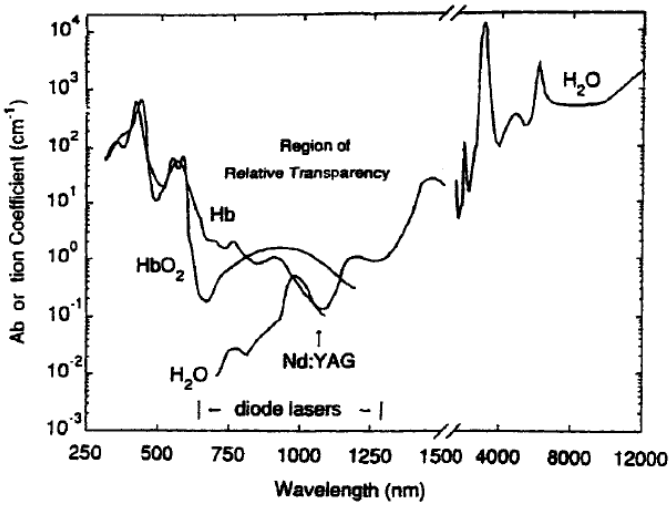

Figure 1.2: Plot of the optical absorption coefficients of hemoglobin (Hb), oxyhemoglobin (HbO_2) and water versus wavelength. Nd:YAG emission at 1064 nm is indicated. From Ashkin, 2006.

1.1.4 BIOLOGICAL APPLICATIONS OF OPTICAL TWEEZERS

The main applications of optical tweezers in the biological field are force measurements, studies on the dynamics of single molecules, and manipulation at the cellular level (Ashok and Dholakia, 2011; Grier, 2003; Moffitt et al., 2008; Stevenson et al., 2010a).

The first two applications arise from the possibility of converting the trap into a true force measurement apparatus. A trapped object in optical tweezers works rather like a calibrated microscopic spring: the tightly focused laser beam, indeed, creates a parabolic potential energy well for the trapped object. Thus, small displacements away from trap center correspond in a directly proportional way to the force. Hence, a simple accurate evaluation of the position of the object allows absolute force measurements (Ashkin, 1992; Ashkin et al., 1990; Block et al., 1990).

In single molecule studies, rather than trap a molecule directly, the molecule of interest is chemically attached to a micro- or nanosphere. Forces are measured on the terminal using optical tweezers and are in the range of pN, meaning that optical tweezers are unable to sever covalent bonds but are sufficient to analyze protein-protein interactions. With this technique, the activity of many different enzymes was unraveled (RNA- and DNA-polymerase, helicases, exonuclease, DNA restriction enzymes), the transport of DNA through a nanopore was measured, as well as the translation of RNA into protein, the dynamics of rotary and linear molecular motors (e.g. actin-myosin, kinesin motion on microtubules), and the folding of proteins (Bustamante et al., 2003; Fazal and Block, 2011; Perkins, 2009; Stevenson et al., 2010a).

Optical traps are not restricted to the world of single molecules. Indeed, they can be used to trap and organize cells, allowing us the understanding of numerous facets of cell biology. This application field takes strong advantage on the development of multiple trapping systems, that permit generation of arrays of planar or three dimensional traps in space. 2D and 3D pattern may have a strong effect on tissue

engineering, since it is well established that the microenvironment of a cell influences its differentiation and activity. The control of cell-cell contacts is thus a highly important topic and it can help to elucidate the mechanisms of phenotype maintenance. So far, arrays of cells have been demonstrated for the creation of artificial neural networks (Townes-Anderson et al., 1998) or to deliver single cells to microfabricated sensors or wells (Luo et al., 2007; Pine and Chow, 2009). Patterns of live cells (both bacteria and mammal cells) were created in a photopolymerizable hydrogel. Cells could be subsequently fixed into defined positions inducing the polymerization of the gel (Akselrod et al., 2006). Optical tweezers were also used to guide the development of the axon of growing neurons (Carnegie et al., 2009; Ehrlicher et al., 2002) and other mammalian cells (Ehrlicher et al., 2007).

Another major application of optical tweezers at the single-cell level is the sorting of cell types, particularly in microfluidics environment. By means of optical manipulation, biologically tagged cells can be actively drag from a flow stream. Cells can also be sorted on a potential energy landscape by relying on differing physical attributes (e.g. size) of one cell type compared to another (Dholakia et al., 2007; Stevenson et al., 2010a). Optical chromatography achieves microscale optical manipulation through the balance of optical and hydrodynamic forces acting on micron sized particles, which are in microfluidic flow travelling counter to the propagation of a mildly focused laser beam. The optical pressure force on a particle is specific to each particle's size, shape and refractive index and hence allows the separation according to physical characteristics of the particle itself (Hart et al., 2006).

In the last decade optical trapping was combined with other optical methods, such as spectroscopy. In particular Raman spectroscopy was combined with optical tweezers for a variety of studies of lymphocytes and erythrocytes (Bankapur et al., 2010; Dasgupta et al., 2011; Ramser et al., 2004; Rao et al., 2009; Snook et al., 2009). The advantages of this approach are several: the cell can be separated from any local surface and can be exposed to different buffer media. Moreover the cell can be rotated and oriented and Raman signal can be recorded from different subcellular regions.

Cell tweezers can also be combined with other light fields that are designed to perform very precise cutting or controlled transient perforation with submicrometric resolution. "Optical scissors" and nanosurgery were employed to study intracellular organelles (mitotic spindle, chromosomes, mitochondria) (Kohli and Elezzabi, 2009), to fuse cells (Steubing et al., 1991) or for transfection, transiently permeabilizing the cell membrane (Barrett et al., 2006).

The use of optical tweezers for local delivery of molecules and for cell stimulation will be discussed specifically in **section 1.2.7**.

1.2 MICROENVIRONMENT MANIPULATION OF BIOLOGICAL SAMPLES

In physiological conditions, molecules are released at low concentrations and in a spatially restricted fashion. Moreover polarized cells usually interact with a polarized environment and it may be very useful having the possibility to study reactions promoted by stimuli in different and definite parts of the cells. Different techniques have been developed to reach a good efficiency of localized delivery but they all have some drawbacks. Thus, obtaining a cheap, reliable and repeatable technique could have a great impact in modern research, where bath stimulation is still the method of choice.

The now-a-day available local stimulation techniques will be reviewed in the following paragraphs, namely: microfluidics, ejection, uncaging, AFM, phototransfection and optical tweezers.

1.2.1 MICROFLUIDICS

Microfluidic systems represent a new kind of cell culture vessel that expands our capacity to control the local cellular environment. They enable patterning of molecules and cells, as well as both passive and active cell handling and environmental control. This is possible because the flow conditions at low Reynolds numbers (where inertial forces are minimal) provide unprecedented spatial and temporal control over fluids entering and leaving an experimental system (Meyvantsson and Beebe, 2008).

Microfluidic systems allow a fine control of the biochemical and physical environment in which cells are growing. First of all they permit spatially defined treatments, often impossible to achieve with conventional means. By simply controlling the stream, the concentration of soluble factors can be modified. For instance, laminar flows were used to expose only a small part of a cell to a epidermal growth factor and to observe the intracellular propagation of cell signaling (Sawano et al., 2002). Laminar streams were also used to stimulate different regions of rat brain slices and then analyze the effect of the treatments on the electrical activity (Blake et al., 2007).

In microfluidic devices gradients of molecules can be generated as well. This opportunity is fundamental when studying soluble factors involved in chemotaxis. Several approaches have been used to achieve this goal. In a simple cross-shaped device, growing neurites were exposed to guidance cue gradients orthogonal to the direction of growth (Kothapalli et al., 2010). Jeon et al. generated gradients of interleukin-8 (IL-8) by successive splitting and mixing of flows and observed different migration sensitivity of neutrophils (Li Jeon et al., 2002). To address the same topic, Irimia et al. used a gradient-switching device. They studied the response of neutrophils to time-dependent step-up, step-down, and reversal of IL-8 gradients (Irimia et al., 2006). Laminar flow-based gradients have been used to separate wild-type and chemotactic mutant strains of *E. coli* bacteria. In this assay cells were collected in different channels downstream depending on their position within the laminar flow (Mao et al., 2003). Recently, a single-cell assay platform that allows quantitative analysis of single cell chemotaxis by dynamic morphogenetic gradients was also proposed and applied to the study of molecular regulatory mechanism of chemotaxis in yeast (Lee et al., 2012). Multi-channel microfluidic perfusion platform for culturing living animals (zebrafish embryos) is also possible. In this device the development of up to 8 embryos stressed with gradients of different drugs can be monitored (Choudhury et al., 2012).

Within microfluidic devices extra cellular matrix (ECM) can be mimicked. This aspect is primary, since cell attachments to the ECM are not merely mechanical anchors, but receptors that sense the biochemistry and mechanics of the environment. The response of cells to gradients of ECM proteins can be analyzed. For instance, the orientation of the axons of rat hippocampal neurons grown on a gradient of laminin was analyzed. This gradient was produced using a flow-based gradient (Dertinger et al., 2002). Three-dimensional photopatterned hydrogels in which cell-adhesive peptides were incorporated, were used to produce 3D hepatic tissues (Liu Tsang et al., 2007). By means of microchannels and chambers the migration of cancer stem cells through the interstitial spaces of the brain can also be mimicked (Huang et al., 2011).

In microfluidic systems the control of gas concentration, a crucial parameter for cells, is possible. These systems offer a rapid response even if the supply strongly depends on the device geometry, material, and perfusion conditions. This issue was tackled creating a perfusion bioreactor system that forms steady-state oxygen gradients (Allen and Bhatia, 2003) or producing multicompartment devices (Park and Shuler, 2003).

Finally, microfluidic devices allow the precise control of physical parameters (e.g. forces, flow, temperature, geometry) of the cell microenvironment. In particular, the shear stress acting on bone tissue

can be mimicked (Leclerc et al., 2006), as well as the leukocyte interaction with a biological substrate under flow conditions (Schaff et al., 2007).

In special types of microfluidic systems the compartmentalization is possible. Compartmentalization can be employed to specifically manipulate or analyze different parts of a single cell. For instance, two-compartment microfluidic system were used to culture polarized neurons with cell bodies and axons in separate compartments and to study region-specific gene expression after injury (Taylor et al., 2005). Using a similar device, in which cell bodies and from axons were in two distinct compartments, the death of axons following chemical insult that mimics neuropathology was analyzed (Ravula et al., 2007).

Another advantage of these devices is the possibility of coupling them with analytical methods, such as microscopy, PCR, capillary electrophoresis or biosensors.

All in all, microfluidic devices, even though they are very powerful and precise, require a different tailor for every specific issue and facilities for their fabrication.

1.2.2 EJECTION

Delivery of small volumes (nanoliters to picoliters) of solutions can be achieved releasing soluble molecules from glass pipettes by pressure pulses.

In 1992 the use of repetitive pulsatile ejection method was developed to produce microscopic chemical gradients near the growth cone of embryonic neurons in culture. Micropipettes have a inner diameter of the tip of 1-2 µm. They are filled with test solution and connected to an electrically gated pressure application system that controls the delivery. The released volume can be down to 0,3pL (Lohof et al., 1992). Usually, pipettes are positioned tens-hundreds of micron away from the target cell and hence the gradient that is generated is broad and not localized on a particular cell structure.

In hydraulically coupled microejection systems, a solution-filled glass micropipette is connected to a motor-driven, liquid-filled syringe. The volume ejected from the micropipette is the same as the volume displaced by movement of the syringe plunger. In this way the ejection rate and duration can be precisely controlled (Pakhomov et al., 2006). Puffer pipettes have a small, sharp tip, which makes them suitable for applying a small quantity of a compound to a well-defined location. This system has two shortcomings: solution leaking from the tip of the pipette can contaminate the signal, and it is difficult to apply more than one test solution exactly to the same local area of the specimen. Due to its relatively easy handle, the ejection systems are still the most popular in neurosciences (Henle et al., 2011; Thompson et al., 2011).

Another application system is the “U-tube” system, that has a pressure head of the test solution applied to one end, and a vacuum head applied to the other end. There is a hole at the base of the U. At rest, the vacuum and pressure heads are nearly balanced to prevent flow out of the hole. When a switch blocks the vacuum, the solution in the U-tube flows out of the hole. This out flow can rapidly apply a compound to a cell positioned next to the hole. A major limitation for neurons stimulation is that the U-tube hole has a relatively large diameter (Pidoplichko and Dani, 2005) and hence single synapse stimulation is not possible.

1.2.3 MICROBEADS (BULK APPLICATION)

Pioneer experiments of focal stimulation of cells using functionalized microbeads were performed by Fan, who coupled an enriched collapsin-containing preparation made from chick brains to 1µm large beads (Fan and Raper, 1995). Later on, Nerve growth factor (NGF) was covalently bound to

polystyrene beads (Gallo et al., 1997). The diameter of the beads was 10 µm in this case. Functionalized beads were then added to the cell culture in bath and the effect of a localized source of neurotrophins on growth cone guidance was studied.

Afterwards, 10 µm large Brain-Derived Neurotrophic Factor-coated beads were used by Zhang in *Xenopus* nerve-muscle cultures to show that a single bead in contact with the pre-synaptic axon resulted in potentiation of transmitter secretion and in a persistent local elevation of Calcium (Zhang and Poo, 2002). In these experiments, beads were manipulated using a micropipette.

The use of microbeads coated with neurotrophins became then popular. Beads were not only used to locally stimulate dendrites (Yoshii and Constantine-Paton, 2007) but also to analyse the effect of the protein of interest at the membrane level (MacInnis and Campenot, 2002). The retrograde transport of the neurotrophin, when this is covalently bound to a bead, is indeed prohibited.

Larger beads (75-300 µm) heparin-coated beads soaked with the molecule of interest have been proposed for single cell chemotaxis assays. A gradient of diffusing molecules is generated around the bead and cell movement can be analyzed (Theveneau and Mayor, 2011). The large dimension of the beads allows their manipulation with tweezers or eyebrow knife.

1.2.4 UNCAGING

The idea behind the caging technique is that a molecule of interest can be rendered biologically inert (or caged) by chemical modification with a photoremovable protecting group. Illumination with the appropriate light, results in a concentration jump of the biologically active molecule that can bind to its cellular receptor, switching on (or off) the targeted process (Ellis-Davies, 2007). Uncaging, in particular when coupled with two-photon microscopy, can be temporally and spatially defined, intracellular or extracellular, and controlled by chancing the amplitude or the frequency of the stimulus (Berridge et al., 1998; Ellis-Davies, 2011). Stimulation with this technique can activate neurons at a single dendritic spine level in a way that closely resembles synaptic activity.

Many different compounds are commercially available. They can be divided into four main categories: Calcium chelators, neurotransmitters (Glutamate, GABA, carbamoylcholine), phosphates (IP_3, cAMP, ATP) and fluorophores (fluorescein) (Ellis-Davies, 2007). A drawback is that most of the caged compounds turned out to produce undesired effects, being able to block both glycine and GABA receptors (Canepari et al., 2001).

Moreover the caging of peptides and macromolecules is not so straightforward. There are no general schemes that can be adopted for their design and the activity of the compound should be tested for every specific situation. As a result, the applications of protein caging are still limited. Among the strategies that have been adopted for the caging of proteins there are:

- Single amino acid mutagenesis (Mendel, 1991);
- Protein ligation to assemble a caged semi-synthetic protein (Muralidharan and Muir, 2006);
- Site-specific crucial modification with a small caging molecule (Walker et al., 1998);
- Addition of a peptide at the N- or C-terminus via a photocleavable cross-linker (Bosques and Imperiali, 2003);
- Genetically encoded fusion protein that can be reversibly activated (Wu et al., 2009);
- Antibody caging (Kossel et al., 2001).

In this latter case, in particular, an antibody against BDNF (see **paragraph 2.1.2**) was caged. The authors, were able to demonstrate an effect of the protein in the range of hundreds of microns from the uncaging point. Thus, the spatial resolution achieved was really low.

Concluding, the use of caged compounds is powerful but it has strong limitations due to the limited availability of tailored molecules and to the low flexibility. Moreover the instrumentation required is highly expensive.

1.2.5 AFM

Atomic force microscope (AFM) can be used for the local delivery of molecules in different ways. The first and simplest approach is to use the AFM tip for delivering and patterning molecules extremely locally on a surface by means of the so-called Dip-pen lithography (Piner et al., 1999).

More elaborated techniques allow the intracellular delivery of molecules into cells. For instance a transfection procedure was proposed, in which the AFM tip was decorated with the DNA of interest. The approach relies on the possibility to reversibly penetrate through the cell membrane with an AFM tip and without causing permanent damages to the cell or provoking leakage of intracellular fluid, which could irreversibly alter the cell integrity (Cuerrier et al., 2007).

A less invasive method uses "nanoneedles" placed on the top of the AFM tip. Chen proposed the use of carbon nanotubes as needles. Nanotubes were functionalized with cargo via a disulfide-based linker. Penetration of cell membranes with this "nanoneedle" was controlled by the AFM. The following reductive cleavage of the disulfide bonds within the cells interior resulted in the release of cargo inside the cells, after which the nanoneedle was retracted by AFM control (Chen et al., 2007). The needle can also be a etched on the top of the AFM tip, and the molecule of interest adsorbed on the surface (Han et al., 2008).

Finally, in a recent paper "fluidFM" (fluid force microscopy) was proposed (Meister et al., 2009). FluidFM has a nanofluidic channel in the cantilever, that allows soluble molecules to be dispensed through a submicrometer aperture in the AFM tip. An advantage of this technique, is that the delivery can be both intracellular and at the cell surface.

1.2.6 PHOTOTRANSFECTION

By using ultrashort (femtosecond), high-intensity and tightly focused laser beam, the plasma membrane of cells can be locally perforated, allowing foreign molecules to enter the cell (Tirlapur and Konig, 2002). Many different laser wavelength, repetition rate and power have been tested, having as a readout the synthesis of fluorescent proteins, whose DNA was phototransfected (Stevenson et al., 2010b). A brilliant application of phototransfection in the local delivery field was proposed by Barrett (2006). She used this focal transfection procedure to introduce the mRNA of a transcription factor (Elk-1) into specific regions (dendrites or cell bodies) of live, intact primary rat neurons. The authors demonstrated that introduction and translation of Elk-1 mRNA in dendrites produced cell death, whereas introduction and translation of the very same mRNA in cell bodies did not produce cell death (Barrett et al., 2006).

Beside DNA and RNA, also nanoparticles can be introduced inside cells. This nanoparticles can both carry proteins and be exploited as sensors that permit spectroscopic analyses in real time of different regions of a living cell (McDougall et al., 2009).

1.2.7 OPTICAL TWEEZERS FOR MICROENVIRONMENT MANIPULATION

By means of optical tweezers, micrometric objects placed in the focus of the objective can be transported in a cell culture dish over hundreds of microns and positioned at the desired site with high spatial resolution.

At the beginning, optical tweezers were used to put a single bead in contact with a specific part of cell. Usually the aim of these experiments was the investigation of the mechanical properties of the cell (Dai and Sheetz, 1995; Raucher, 2008; Valero et al., 2008) or the measurement of forces exerted by the cell (Cojoc et al., 2007; Galbraith and Sheetz, 1999). Positioning of more beads on the same cell is possible as well. To tackle this issue, however, the use of microreservoir to stock beads is suggested. The desired number of beads can then be extracted with optical tweezers from the reservoir and positioned on the target cell (Monneret et al., 2007).

Delivering defined packages of stimuli to single cells with both high spatial and temporal resolutions exploiting optical tweezers was first proposed by Sun: optical trapping was used to manipulate individual vesicles that encapsulate the bioactive molecules of interest. Once a selected vesicle is placed adjacent to the target cell, a single UV-laser pulse, which is aligned with the trapping laser, is used to photolyze the optically trapped vesicle and to release the encapsulated molecules (Sun and Chiu, 2003). In their brief communication, the authors released carbachol from single 0.6 μm large vesicle and showed the response it induced on Calcium levels in epithelial cells overexpressing muscarinic acetylcholine receptor.

Optical tweezers allow also the setting up of molecular concentration patterns that are chemically, spatially and temporally flexible by using optically manipulated microsources, which steadily release molecules. The technique enables the control of molecular concentrations over length scales down to about 1 μm and timescales from fractions of a second to an hour. The authors demonstrated this technique by manipulating the motility of single human neutrophils. They induced directed cell polarization and migration with microsources loaded with a chemoattractant stimulus. Furthermore, they triggered highly localized retraction of lamellipodia and redirection of polarization and migration with microsources releasing cytochalasin D, an inhibitor of actin polymerization (Kress et al., 2009).

1.3 DIFFRACTION LIMITED IMAGING

Until not very long ago, it was widely accepted that lens-based (far-field) optical microscopes cannot visualize details much finer than about half the wavelength of light because of diffraction (**Figure 1.3**). This limit was revealed by Ernst Abbe in 1873 (Abbe, 1873), who stated:

$$r = \lambda/2n \sin\alpha = \lambda/2NA$$

where "r" is the resolution (minimum distance between two point objects which can be resolved by the microscope), "λ" is the wavelength of the illuminating light, "n" is refractive index of the medium between the specimen and the objective, "sinα" is the semi-angle aperture of the objective lens, and "NA" is the numerical aperture. Along the optic axis, the maximum achievable resolution is even poorer, being it related to the square of sinα.

Spatial resolution could be improved by employing shorter wavelengths (for live cells imaging the minimum is around 400 nm, which is in the spectrum of near-UV light) and objectives with a higher numerical aperture. As a result, the maximum resolution in the focal plane would be 200 nm in x, y and 500 nm along the z axis (**Figure 1.3**).

In the Fifties, when fluorescence staining techniques were developed, light microscopy became a powerful biological tool. Nowadays specific molecules (proteins, DNA, RNA, etc.) can be marked and imaged using fluorophores. The dimension of cellular organelles is in the range of hundreds of nanometers – few microns. It can be easily understood why conventional optical microscopy does not provide a satisfying resolution. Moreover, when looking at proteins, their size is in the range of tens of nanometers, far smaller than our imaging capabilities.

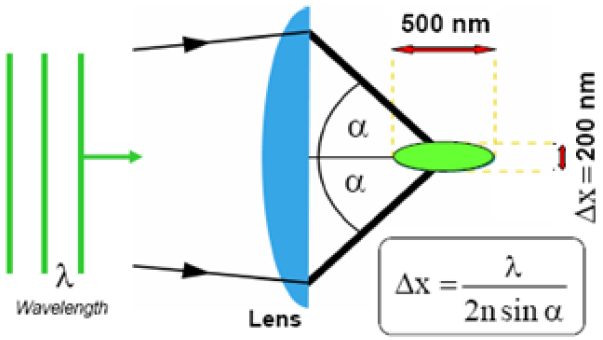

Figure 1.3: Abbe diffraction limit. The resolution of an optical system is related to the wavelength used for the illumination (λ), the refraction index of the medium (n) and the semi-angle aperture of the objective lens (α). The maximum achievable lateral resolution (200 nm) is given by the formula in the box. In the z-dimension is scales up with the square of sinα and thus it is poorer (500 nm). Modified from Stefan Hell's presentation available at the link www.biop.dk/biophotonics09/After/Hell/Handout_StefanHell.pdf.

Electron microscopy overcomes these limitations by changing the illumination source wavelength. Although the achievable resolution is really high (it can be less than 1 nm), electron microscopy requires a complicated sample preparation. Indeed, specimens should be fixed, dehydrated and cut in thin sections. It is thus impossible to use this type of microscopy for living cells.

For all these reasons, big efforts have been done in optical microscopy since 60's to break the resolution limit imposed by diffraction.

A first improvement was achieved with confocal microscopy. With respect to normal wide-field fluorescence microscopy, in which the entire specimen is illuminated, confocal microscope uses a focused laser beam to illuminate a small part of the sample being observed (**Figure 1.4 left**) and two optically-conjugated pinholes. The first one restricts the illumination spot, and the second one is placed in front of the detector, in a way so that only the light that comes from the focal plane can pass through it (**Figure 1.4 right**). As only one point in the sample is illuminated at a time, image acquisition requires scanning of the specimen, both in 2D and 3D.

An alternative to confocal microscopy is two-photon microscopy (Denk et al., 1990), which provides distinct advantages for three-dimensional imaging, especially within thick tissues such as brain slices, embryos, and even entire animals.

Two-photon microscopy employs two-photon excitation process, according to which two photons of comparably lower energy than needed for one photon excitation can excite a fluorophore in one quantum event (Goeppert-Mayer, 1931). Each photon carries approximately half the energy necessary to excite the molecule. The probability of the near-simultaneous absorption of two photons is extremely low and hence a high flux of exciting photons is typically required.

Even if confocal and two-photon microscopy significantly improved the quality of fluorescence imaging, they are still limited by Abbe's resolution equation.

In the last decades super-resolution techniques that break this limit have been developed. These techniques will be described in **section 2.4**.

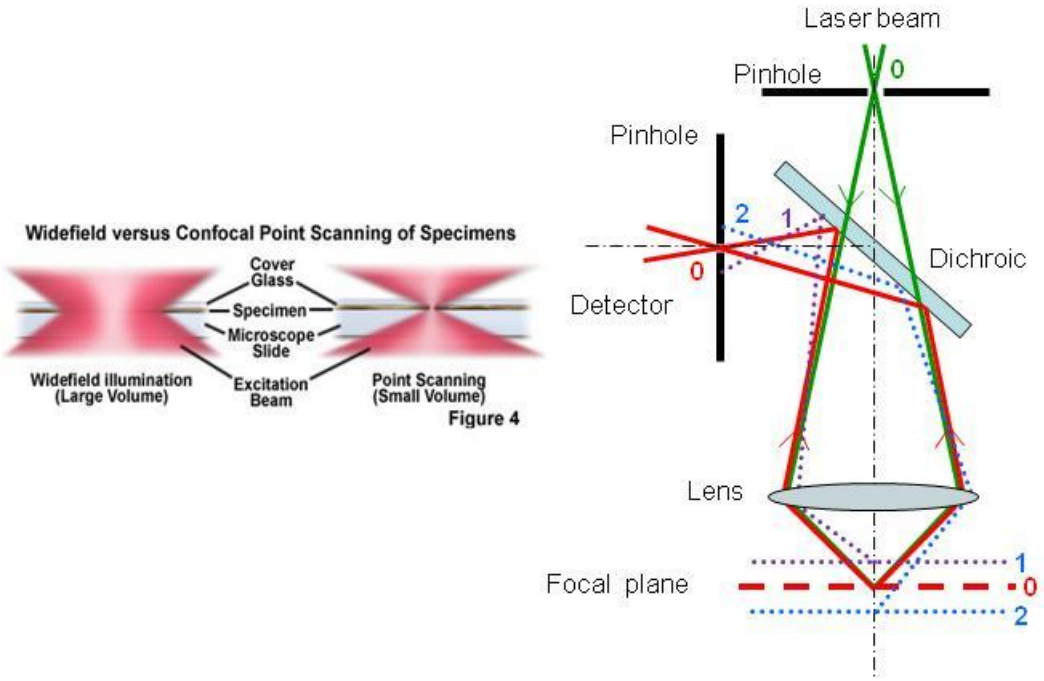

Figure 1.4: General scheme of a confocal microscope. (**Left**) In widefield microscopy the whole specimen is illuminated, while in scanning microscopy only a spot of the sample is exited. From www.microscopyu.com. (**Right**) Scheme of a confocal microscope. The exiting laser beam (0-green) passes through a first pinhole and is focused by the lens. Only emission coming from the focal plane (0-red) can pass through the pinhole in front of the detection camera. Rays coming from upper (1-violet) or lower (2-blue) planes are blocked by the pinhole.

GOAL OF THE THESIS

The goal of this Thesis is the development of new techniques to locally change the microenvironment of biological samples. These techniques should improve the limitations of the currently available systems and thus should have a high spatial resolution, a high flexibility and handiness, and finally should be affordable.

The techniques will be validated by tackling different biological issues related to neurobiology.

More in details, two different kind of vectors carrying the molecules of interest will be developed: microbeads, that allow the focal and prolonged stimulation of cells, and micron-sized liposomes, through which a gradient of molecules can be generated. A high spatial precision of stimulation will be achieved using optical tweezers, an instrument that allows the manipulation and movement of such vectors.

Since optical tweezers allow the manipulation of a sample and its imaging at the same time, a lot of efforts have been placed also in the development of new live imaging tools (functionalized Quantum dots) or in the use of innovative imaging techniques, such as far –field optical nanoscopy.

The next part of the Thesis will be organized as follows: the development and the use of beads and then liposomes will be presented within the appropriate biological frame. Finally, the preparation of tool to better the imaging will be presented.

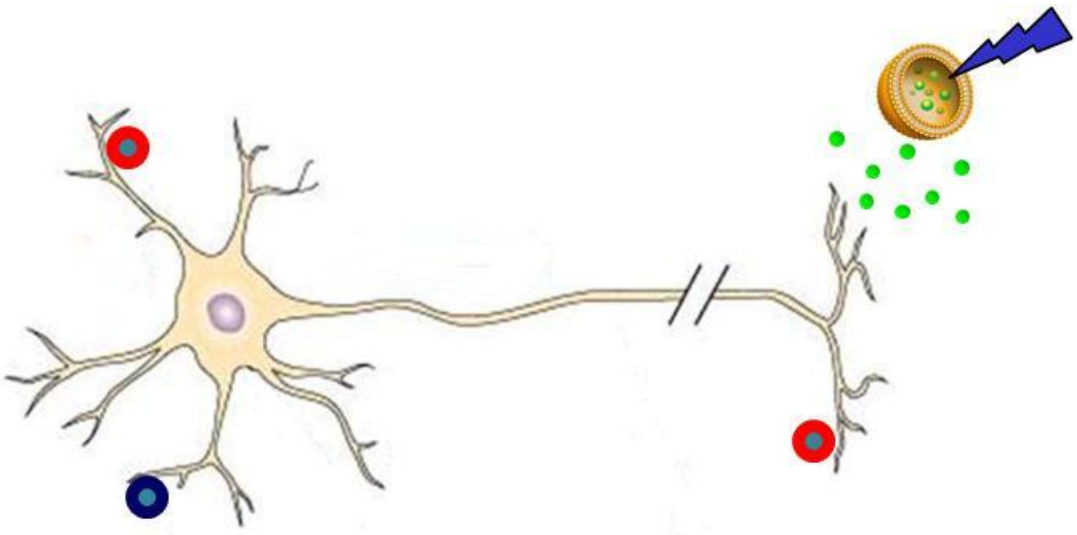

Figure 1.5: Goal of the Thesis. Local stimulation of specific neuronal compartments with different vectors. Both beads with different coatings and micron-sized liposomes are depicted. In the case of liposomes, the release is achieved by breaking the vesicle with a UV pulse.

2.RESULTS

HIGH RESOLUTION OPTICAL MANIPULATION OF MICRO AND NANO-VECTORS FOR MICRO-ENVIRONMENT CONTROL

2.1 FUNCTIONALIZED MICROBEADS

Dielectric microbeads are widely used in optical tweezers since they are easy to fabricate and trap. The main characteristics that make these particles suitable for trapping are: the refractive index and the symmetric shape. Moreover, beads of almost any dimension and surface functionalization are commercially available. This means that a molecule of interest can be covalently attached to their surface. Then, beads can be manipulated at will and put in contact with a cell. The questions are: is this molecule attached to the surface of the bead still biological active, being it cross-linked and manipulated with an IR laser? Is it able to bind and activate its cognate receptor present on a cell membrane even if the ligand cannot be internalized? To answer these questions we used Brain-Derived Neurotrophic Factor (BDNF) as model system.

2.1.1 FUNCTIONS AND IMPORTANCE OF FOCAL DELIVERY OF BDNF

Brain-Derived neurotrophic factor is a member of the neurotrophins' family of proteins (Barde et al., 1982). Neurotrophins are small secreted proteins that play key roles in the development of nervous system, since they control survival, differentiation, synaptogenesis, and activity-dependent forms of synaptic plasticity (Chao, 2003; Chao et al., 2006; Reichardt, 2006). They also mediate additional higher-order activities, such as learning, memory and behavior.

The importance of BDNF is demonstrated by the fact that knockout mice display severe abnormalities in the nervous system (Ernfors et al., 1995; Linnarsson et al., 2000) and usually die soon after birth. Heterozygote mutants have an impaired learning caused by a reduction of LTP (Korte et al., 1995). Alterations in BDNF levels have been implicated in neurodegenerative disorders, such as Alzheimer's disease and Huntington's disease, as well as psychiatric disorders, including depression and substance abuse (Chao et al., 2006).

Neurotrophins are produced as propeptides, with a prodomain followed by the mature neurotrophins. Thus, each gene product must be processed by proteolysis to form the mature protein (Mowla et al., 2001). Mature neurotrophin proteins are non-covalently associated homodimers.

The neurotrophins interact with two entirely distinct classes of receptors **Figure 2.1**:

- p75 neurotrophin receptor (p75), which is a low-affinity receptor for mature neurotrophins but has a stronger affinity for all the proneurotrophins (Frade and Barde, 1998; Rodriguez-Tebar et al., 1990). Mainly it promotes apoptosis and growth inhibition (Underwood and Coulson, 2008);

- tropomyosin-related tyrosine kinases receptors (Trk). Three different Trk receptors exist (TrkA, TrkB, TrkC) and each of them has a different affinity for the mature neurotrophins. Trk receptors mediate several processes, such as survival, neurite outgrowth and long term potentiation (Chao, 2003; Huang and Reichardt, 2003);

The affinity of Trk receptors for neurotrophins can be regulated by receptor dimerization, structural changes or association with the p75 receptor (Arevalo et al., 2000; Esposito et al., 2001; Schecterson and Bothwell, 2010), that can act as a co-receptor for Trk receptors.

Upon ligand binding, Trks dimerize and become catalytically active, resulting in trans-autophosphorylation. Activated receptors initiate several signal transduction cascades, including mitogen-activated protein kinase (MAPK) pathways (which promotes neuronal differentiation), the phosphatidylinositol 3-kinase (PI3K) pathway (which promotes survival and growth of neurons and other cells), and the phospholipase Cγ (PLC-γ) pathway (which promotes synaptic plasticity) (Kaplan and Miller, 2000; Patapoutian and Reichardt, 2001). These signaling pathways culminate in the activation of transcription factors that alter gene expression (**Figure 2.1**).

The signals generated by the two neurotrophins receptors can either augment or oppose each other, regulating almost all aspects of neuronal development and function, including precursor proliferation and commitment, cell survival, axon and dendrite growth, membrane trafficking, synapse formation and function, as well as glial differentiation and interaction with neurons.

The responsiveness and specificity of responses are determined by the ability of Trk and p75 to present different binding sites and affinities to particular neurotrophins. The ratio of receptors is important in dictating the numbers of surviving cells, and interactions between them provide another level of regulation (Chao, 2003).

The effects of neurotrophins can be also modulated by the subcellular location of the neurotrophin-receptor complex. Signaling locally was shown to regulate growth cone motility, while signaling in the cell soma controlled cell survival and gene expression (Reichardt, 2006). In this latter case, neurotrophins can be internalized by the target cell into vesicles, the so-called "signaling endosomes" (Grimes et al., 1996), which are transported to the cell body. Activated Trks initiate signaling throughout the transport process, both in the axons and at the cell body and hence signaling endosomes should be capable of engaging multiple second messenger cascades. Difference in the gradient of these molecules along the axons may thus activate different pathways, which in turn lead to different outcomes (Heerssen and Segal, 2002).

A further level of complexity is given by the kinetics of activation of the receptors. A receptor may be acutely activated by an immediate increase in ligand concentration as a result of its regulated secretion or it may experience a gradual increase in the concentration, when the ligand is secreted from a distant source. The control of the kinetics of signal transduction may be an important mechanism to ensure the functional specificity of extracellular factors. Since BDNF is secreted through both constitutive and regulated secretory pathways (Canossa et al., 1997; Lessmann et al., 2003), Ji and colleagues used it as a model to study the effects of different delivery kinetics. In cultured rat hippocampal neurons, acute and gradual increases in BDNF elicited transient and sustained activation of TrkB receptor and its downstream signaling, respectively, leading to differential expression of two downstream target genes (Homer1 and Arc). Transient TrkB activation promoted neurite elongation and spine head enlargement, whereas sustained TrkB activation facilitated neurite branch and spine neck elongation. In hippocampal slices, fast and slow increases in BDNF enhanced basal synaptic transmission and LTP, respectively. Thus, the kinetics of TrkB activation is critical for cell signaling and functions (Ji et al., 2010).

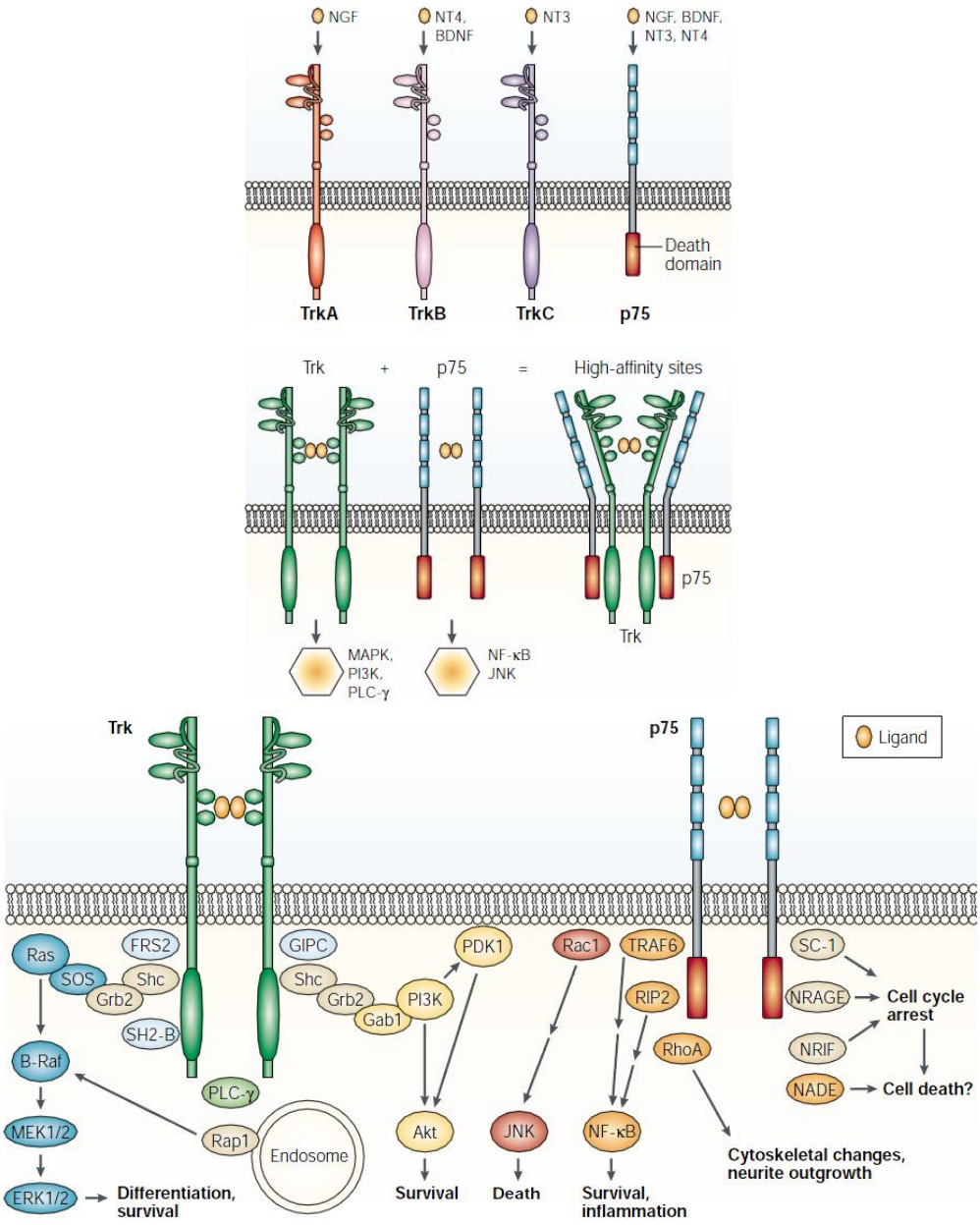

Figure 2.1: Neurotrophins' receptors and signaling pathways. **Upper panel**: Neurotrophin binding results in dimerization of each receptor. Neurotrophin binds selectively to specific Trk receptors, whereas all neurotrophins bind to p75. Each receptor activates several signal transduction pathways. Interactions between Trk and p75 receptors can lead to changes in the binding affinity for neurotrophins. **Lower panel**: intracellular signaling pathways and their responses. Trk receptors mediate differentiation and survival through extracellular signal-regulated kinase (ERK), phosphatidylinositol 3-kinase (PI3K) and phospholipase Cγ (PLCγ). p75 signals to active NF-κB and Jun N-terminal kinase (JNK) and affects apoptosis, survival, neurite elongation and growth arrest. From Chao, 2003.

Finally, neurotrophins have different effects on specific cellular compartments. In visual cortex, not only each layer responds in a different way to a specific neurotrophin, but also within the same layer, neurons respond with a distinct constellation of dendritic changes (McAllister et al., 1995). For instance, the effect of BDNF on layer 6 of visual cortex changes between basal and apical dendrites. More in detail, BDNF increases dendritic growth in layers 4 and 5, and decreases it in layer 6. In this latter layer, however, the negative effect is observed only on basal dendrites. On apical dendrites BDNF has weak

positive effect. This distinction can be explained with structural and functional differences between apical and basal dendrites, that lead to diverse responses to the same extracellular signal.

Overall, the development of techniques that allow the delivery of neurotrophins and BDNF in particular in a spatially and temporally defined way may help the understanding of the complex cellular responses. In many occasions, indeed, bath application of molecules led to different experimental outcomes and does not unveil the signaling pathway that are effectively activated in physiological conditions in a specific subcellular compartment, with its peculiar characteristics.

2.1.2 LOCALIZED DELIVERY OF BDNF

Several attempts to achieve local control of neurotrophins concentration have been proposed. The use of caged antibody against BDNF, through which a decrease in potentiation for several synapses has been obtained in the range of hundreds of microns from the uncaging point (Kossel et al., 2001), was previously mentioned in **section 1.2.4**.

Another method that uses of neurotrophin donor-recipient pairs of neurons (Horch and Katz, 2002) was proposed. Authors produced "donor neurons" in ferret cortex brain slices that co-expressed BDNF and red fluorescent protein (RFP). Using two-photon microscopy, they analyzed their effects on "recipient neurons" that expressed green fluorescent protein (GFP) alone and demonstrated that BDNF release from dendrites and cell bodies acts directly on nearby recipient neurons to increase dendritic branching in a distance-dependent manner.

The approach that exploits micropipettes and Picospritzer delivery was also considered for BDNF. Li and colleagues (Li et al., 2005) produced a microscopic gradient of BDNF by pulsatile application of BDNF-containing solution with a micropipette near growth cones of cerebellar granule cells. This system permitted to demonstrate that the chemoattractive turning effect of BDNF on growth cones requires Calcium elevation and TRPC (transient receptor potential canonical) channel. Micropipettes delivery was used also to demonstrate that in developing hippocampal neurons focal application of BDNF evoked fast and local dendritic Calcium transients. These transients required activation of TrkB receptors as well as activation of voltage-gated sodium and Calcium channels (Lang et al., 2007).

As we already mentioned, also coated beads (Naka et al., 2004; Yoshii and Constantine-Paton, 2007; Zhang and Poo, 2002) were used to deliver BDNF and potentiate the nearby synapses (Yoshii and Constantine-Paton, 2007; Zhang and Poo, 2002). Beads, however, were simply dropped in the culture dish or manipulated with pipettes.

2.1.3 MATERIALS AND METHODS

2.1.3.1 CELL CULTURES

Primary hippocampal neurons were prepared from P0-P1 rats as described before (Tongiorgi et al., 1997) with slight modifications. Cells were plated on Poly-Ornithine and 2% Matrigel (BD Biosciences) coated homemade glass bottom Petri dishes at a density of 10^5cells/mL per dish. Neurons were cultured for at least 5 days in a 5% CO_2-humidified incubator, in Minimum Essential Medium with Earle's salts and Glutamax I (MEM, Life Technologies, Invitrogen) with 10% FBS (Gibco), 35 mM D-glucose (Lancaster), 14 mM Hepes (Sigma), 1 mM vitamin B12 (Sigma), 0.36 mM d-Biotin (Sigma), 30 μg/mL insulin (Sigma), 100 μg/mL bovine transferrin (Sigma), and antibiotics (Euroclone). The medium was changed every 2 days from the second day in culture onwards.

2.1.3.2 BEADS FUNCTIONALIZATION

1,5 μm large silica beads coated with COOH groups (Kisker-biotech, cat. PSi-1.5COOH) were functionalized using PolyLink Protein Coupling Kit (Bangs Laboratories Inc., cat. PL01N) following the manufacturer's protocol. Briefly, about 1,4 x 10^5 beads were incubated with 500 ng of BSA or BDNF in presence of 20 μg/μL EDAC for 1 hour at room temperature and stored in Storage Buffer at 4°C.

2.1.3.3 ELISA

ELISA test was performed using BDNF $E_{max}^{®}$ ImmunoAssay Systems (Promega, cat. G7611) and following the manufacturer's protocol. Supernatants diluted 1/10 obtained after beads functionalization and three washes were analyzed. Release of BDNF was tested also after treatment of beads in different conditions, i.e. normal storage at 4°C, 1 hour at 37°C or 5 min at 100°C. This latter condition was also used to test whether the immunoassay was able to detect the protein after it was boiled.

2.1.3.4 IMMUNOHISTOCHEMISTRY

Coated microspheres were washed in PBS and incubated for 1 hr at room temperature with anti-BDNF or anti-BSA (both 1:50, Sigma). Beads were then centrifuged, washed and incubated for 30 min at room temperature with anti-rabbit Alexa 488 (Invitrogen) and finally analyzed using confocal microscopy (Nikon C1-Si).

For pTrkB and c-Fos analysis, neurons were incubated either with functionalized beads, BDNF 50ng/mL or K252a 200nM for 15min. Neurons were then washed in PBS, fixed in PFA 4% for 15 min, permeabilized with Triton X-100 0,1% for other 15 min and then incubated with primary antibodies (anti-c-Fos antibody 1:50, Lab Vision; and anti-BDNF 1:50, Sigma; anti-BSA 1:50, Sigma; anti-pTrkB 1:250, kind gift of M.V. Chao) in PBS in presence of 2% NGS for 2 hr at room temperature. After washing them in PBS, they were incubated for 1 hr at room temperature with anti-rabbit Alexa (488 or 568) or anti-mouse Alexa (568 or 647) (Invitrogen), 5 min with Hoechst and mounted in Mowiol. In the pTrkB experiments actin was marked using phalloidin FITC (Sigma cat. P8252) 15min. For data analysis of the c-Fos experiments, the neurons touched by the beads and the neurons un-touched (untreated) were classified in c-Fos positive and c-Fos negative, according to the nuclear staining. The percentage of c-Fos positive untreated neurons was normalized to 1.

2.1.3.5 OPTICAL MANIPULATION

A custom optical tweezers setup was built on a mini breadboard MS12B (Thorlabs, USA) and coupled to the lateral port of an inverted microscope Nikon TE-300 (**Figure 2.2**) in the Molecular and Cellular Neuroanatomy Laboratory at the University of Trieste. The setup could be easily implemented to all inverted microscopes with more output ports and quickly removed or mounted if necessary. The laser trapping beam (1064 nm) from an Ytterbium fiber laser YLM-5 (IPG Photonics, USA) was focused by a convergent lens (L1, f_L= 200 mm) into the lateral port (LP) plane of the microscope. The trapping beam was then collimated by the microscope tube lens (TL) and focused by the microscope objective (60X, 1.4 NA, Nikon) onto the sample. The sample imaging before and during trapping was accomplished on an external camera (WAT1000, Watec LTD, Japan) using a relay lens (L2, f_L= 60 mm). The vectors were loaded in square capillaries with 50 μm inner size (VitroCom, US, cat. 8505), which were used as reservoirs. They were pre-treated with 1% BSA to reduce beads binding to the walls.

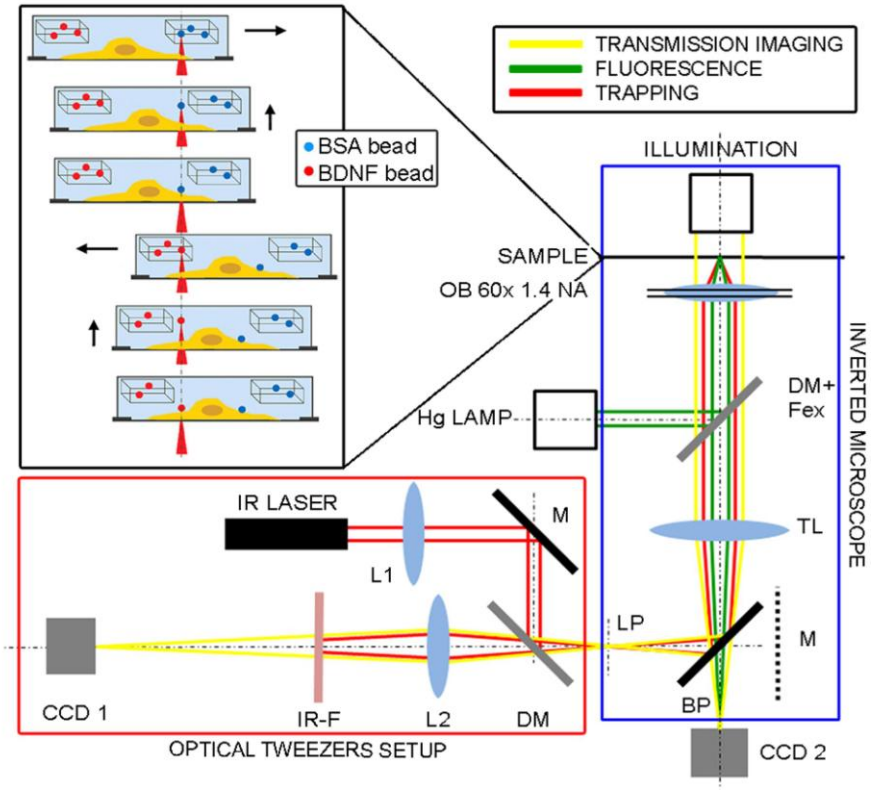

Figure 2.2: Optical manipulation and Calcium imaging experimental setup. A custom optical tweezers setup (red box) is coupled to the lateral port (LP) of the inverted microscope Nikon Eclipse TE300 (blue box). The colors indicate the different optical paths: trapping beam in red, transmission in yellow, fluorescence in green. During trapping the sample is imaged on CCD-1 camera, using the relay optics (L2). Calcium imaging is recorded on CCD-2 camera, turning out the microscope mirror (M). L1, L2 - Lenses; M - Mirror; DM - Dichroic Mirror; TL - Tube Lens; OB - Objective (60x PlanApo NA 1.4); CCD - Charge Coupled Device; IR-F - Infrared filter; Fex - Excitation Filter. **Inset**: Layout of beads manipulation. Two reservoirs, one with BSA beads (blue) and the other with BDNF beads (red) are laid on the bottom of the cells chamber. A BSA-bead is trapped inside the reservoir and then pulled out and positioned at the desired site of the cell by moving the stage of the microscope. The same sequence is repeated to trap and position the BDNF-bead from the second reservoir. From D'Este et al., 2011.

To bring a single functionalized bead to the desired sites on a neuron, we used the custom optical tweezers setup described previously (**Figure 2.2**). The laser beam of 1064 nm wavelength was focused by a lens and reflected by a mirror and a dichroic mirror into the lateral port of the microscope. The tube lens of the microscope collimated the beam which was then focused on the sample by the objective 60x (NA 1.4, oil immersion). During trapping, the sample was imaged using a first camera (CCD-1). After beads positioning on the cells, achieved by optical manipulation, the mirror inside the microscope was switched vertically to allow fluorescence and transmission imaging through the direct port below the microscope, on a second more sensitive CCD camera (CCD-2).

Since the optical trap remained fixed, its relative position to the sample-cell could be changed by moving the stage of the microscope (**Figure 2.2 inset**). BSA- and BDNF-coated beads were prepared and stored separately in small reservoirs (square capillaries, 50μm inner size). The capillaries were laid on the bottom of the cell culture dish. Single beads were optically trapped inside the reservoirs, pulled out and then positioned with sub-micrometric resolution to desired sites on the neurons selected for stimulation (**Figure 2.2 inset**).

2.1.3.6 GROWTH CONE MOBILITY

The experiments on growth cones were performed on 1 DIV (day *in vitro*) hippocampal neurons using a 100x 1.4 NA oil immersion objective (Nikon) equipped with DIC (differential interference contrast) imaging. Images were collected for 5 minutes every 20 seconds before the stimulation and 40 min at the same frame rate after stimulation.

2.1.3.7 CALCIUM IMAGING

Fluorescence and transmission images were recorded by a second cooled video camera (CCD-2) (Sensicam, PCO Imaging, Germany) located at the bottom port of the microscope. Fluorescent dye used was Fluo-3, AM Ester (Biotium, Inc, USA). Neurons were incubated for 40 min with 7mM Fluo-3 prior to use. Images were acquired every 2min with the Sensicam camera. Analysis was performed using NIH Software ImageJ (http://rsbweb.nih.gov/ij/index.html). Every stack was normalized by its background and then all values were normalized to the first stack after bead placement. For the analysis of dendrites, measurements were taken on segments of 20 μm length, centered on the bead position.

2.1.4 RESULTS

We tested the possibility of using functionalized, optically manipulated microbeads for the local stimulation of cultured hippocampal neurons. First of all, the coating and the biological activity of our vectors was tested following bulk application. Subsequently, we demonstrated the possibility of extracting a single bead from a reservoir, position it on the desired cellular compartment and induce a response. In particular, the effects of manipulated microbeads on growth cone navigation and on Calcium levels were studied.

2.1.4.1 BIOLOGICAL ACTIVITY OF FUNCTIONALIZED BEADS

Microspheres are most frequently used in biology and beads of different materials with different sizes and functionalizations are commercially available. For our experiments we chose silica beads coated with carboxylic groups, because they can be cross-linked with a variety of proteins and have a refractive index (1.45 against 1.33 of water) that makes them suitable for optical trapping. The dimension selected was 1.5 μm in diameter, which is similar to the width of dendrites and can be easily visualized in transmission microscopy. We cross-linked either BDNF or BSA as a control to the spheres. The carboxylic groups present on the beads surface formed an amide bond with the amine of the proteins in presence of the coupling reagent EDAC (1-Ethyl-3-(3-dimethylaminopropyl) carbodiimide). The reaction was performed in a large excess of protein in solution and thus we can assume that the coating has a high density of proteins. In this way the effect observed is not dependent of the number of ligands but of the number of receptors present on the cell surface. Coating of the bead surface was tested by immunofluorescence with anti-BDNF or anti-BSA antibodies (**Figure 2.3a**). Neither primary nor secondary antibodies attached on untreated beads, confirming that the signal observed on the functionalized beads was specific. Since the amide bond between BDNF and silica is very strong, the only possible source of BDNF leakage is due to molecules adsorbed but not covalently linked to the bead surface. To rule out this possibility of leakage from the beads, we also performed an ELISA assay. Free BDNF was found at the end of the functionalization process and in the first wash but was absent in the following washes. BDNF-functionalized vectors were also stored at 4°C for a week or kept 1 hour at 37°C to mimic the conditions that will be used in the experiments. The protein was undetectable in the supernatants of these samples, showing the absence of protein leak from the beads (**Figure 2.3a**). Since BDNF occurs as a dimer, we finally tried to separate the monomers by boiling beads for 5 min. In these conditions the dimers in which only one molecule is covalently bound to the bead should separate and

thus be detected. We again did not detect any signal. We can thus state that BDNF never detaches from the surface of microspheres during the *in vitro* experiments.

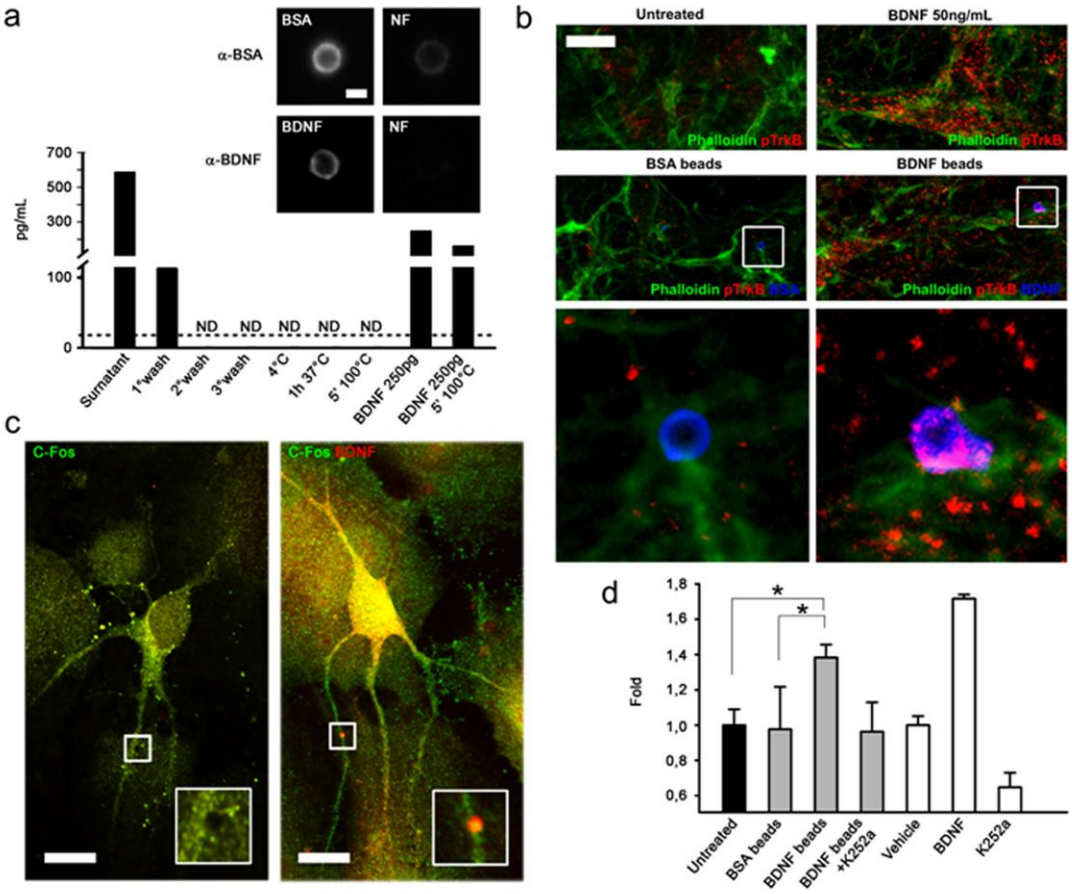

Figure 2.3: BDNF-coated beads trigger TrkB signaling pathway. (**a**) ELISA assay on the supernatants (1/10 dilution) of beads collected right after the functionalization, the washes or the indicated conditions. Dashed line indicates the threshold of sensitivity on the test (ND – not detectable). Immunofluorescence images of BSA- and BDNF- beads (left) and of non-functionalized beads (NF) (right) incubated with the corresponding primary antibodies are shown at the up-right corner. Scale bar 1 μm. (**b**) Confocal microscopy images showing that no activation of the TrkB (pTrkB) is detectable for the control (untreated neurons) or BSA-coated beads (images on the left, scale bar 15 μm) while TrkB is phosphorylated (red dots) for the neurons incubated with BDNF 50ng/mL or BDNF-beads (images on the right). Magnified images at the bottom show the difference between the pTrkB induced by BSA and BDNF coated beads. The actin is marked by phalloidin (green) while the BSA and BDNF in blue. (**c**) Neurons touched by BSA (left) and BDNF (right) beads have negative and respectively positive nuclear staining for c-Fos. Enlarged images of the region surrounding the beads are shown in insets. Rat hippocampal neurons P0-1, 6 days in vitro, prepared as described in methods have been used. Scale bars 10μm. (**d**) c-Fos positive neurons for different treatments were counted. Untreated cells mean of the counts per experiment, n_{mean}=705. BSA-beads (control) n_{mean}=91, BDNF-beads n_{mean}=94, BDNF-beads+K252a n_{mean}=68. The last three bars refer to bath experiments: vehicle n_{mean}=414, BDNF 50 ng/mL n_{mean}= 463, K252a 200nM n_{mean}=779. P-value: *<0.05. Analysis performed with one-way ANOVA. From D'Este et al., 2011.

Since the amide bond between BDNF and silica is very strong, the only possible source of BDNF leakage is due to molecules adsorbed but not covalently linked to the bead surface. To rule out this possibility of molecules release from the beads, we performed an ELISA assay. Free BDNF was found at

the end of the functionalization process and in the first wash but was absent in the following washes. BDNF-functionalized vectors were also stored at 4°C for a week or kept 1 hour at 37°C to mimic the conditions that will be used in the experiments. The protein was undetectable in the supernatants of these samples, showing the absence of protein leak (**Figure 2.3a)**. Since BDNF acts most of the times as a dimer, we finally tried to separate the monomers by boiling beads for 5 min. In these conditions the dimers in which only one molecule is covalently bound to the bead should separate and thus be detected. We again did not detect any signal. We can thus state that BDNF never detaches from the surface of microspheres during the *in vitro* experiments.

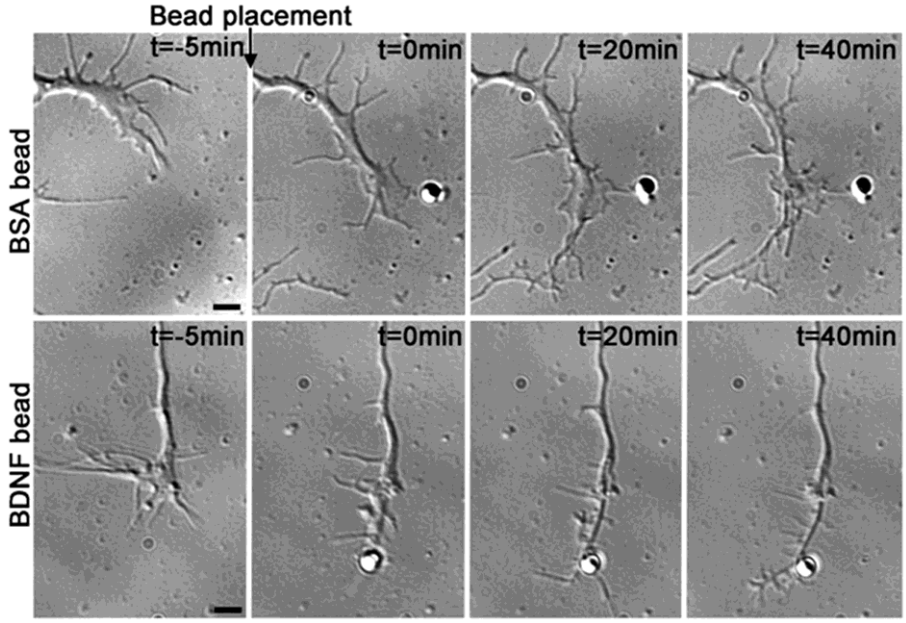

Figure 2.4: Growth cone motility. DIC images showing different effect induced by BSA- and BDNF-coated beads respectively. (**Upper panel**) A BSA coated bead positioned by optical manipulation on the filopodia does not affect the motility of the growth cone. (**Lower panel**) The BDNF coated bead stimulates the neurite development. The first image for each case shows the neuron 5 min before the bead placement. Scale bar 2 μm. From D'Este et al., 2011.

In 1986, Rosenberg *et al.* reported loss of biological activity of neurotrophins if their surface lysines residues were modified (Rosenberg et al., 1986). More recent works, however, used COOH-beads functionalized with BDNF or Nerve Growth Factor (NGF) and reported a biological effect (Gallo et al., 1997; Yoshii and Constantine-Paton, 2007; Zhang and Poo, 2002). Hence, we used the same reaction to couple BDNF on the COOH-beads and we tested whether after immobilization, BDNF maintained its biological function, i.e. it was able to activate TrkB receptor. TrkB activation was first demonstrated by incubating neurons with beads and visualizing TrkB phosphorylation by immunofluorescence (**Figure 2.3b)**. pTrkB dots were barely visualized in control cultures (untreated or incubated with BSA-beads) while a strong activation of the receptor was observed for the stimulated cells with BDNF (bath applied or bound to the microspheres). A particularly striking finding, was the observation of spatially restricted activation of pTrkB on the dendrites right under the beads (**Figure 2.3b**) which supports the effectiveness of this methodology in inducing a local stimulation of BDNF signaling. Since in our system we assume no neurotrophins internalization and TrkB phosphorylation alone is not sufficient to demonstrate the activation of the intracellular signaling pathway (Du et al., 2003), we analyzed the levels of c-Fos within the nucleus by immunofluorescence (Finkbeiner et al., 1997)(**Figure 2.3c**). Neurotrophins, are known to induce the immediate-early gene c-Fos by pathways that do not require new protein synthesis (Sheng et al., 1990). The amount of cells not in contact with beads (untreated) was normalized to 1. Neurons

contacted by BSA-beads showed nuclear levels of c-Fos similar to untreated neurons (0,98±0,23 s.e.), while BDNF-beads induced a marked increase in nuclear c-Fos with respect to untreated neurons (1,38±0,07; p-value 0,008) and with respect to BSA-beads (p-value 0,019) similarly to the effect induced by bath-applied BDNF (1,72±0,02)(**Figure 2.3d**). Incubation of neurons with the Trk inhibitor K252a abolished the effect observed (0,96±0,17), indicating a specific TrkB involvement. These results demonstrated the possibility to use BDNF-coated beads as microvectors for local stimulation of neurons, since even a single bead was able to activate BDNF receptor and induce a cellular response.

Finally we analyzed the effect of our vectors on the growth cone development since BDNF is a key mediator of axonal guidance (for a review Shen and Cowan, 2010). Bead manipulation was achieved as previously explained (**paragraph 2.1.3.5**). While BSA-beads did not influence the growth of these structures (**Figure 2.4**), BDNF-beads were able to affect the development of the growth cones guiding the migration of lamellipodia and filopodia (**Figure 2.4**).

2.1.4.2 Effect of bath applied BDNF

TrkB is known to activate PLCγ1 which produces IP3, leading to Ca^{2+} release from internal stores (Reichardt, 2006). Hence, to obtain the experimental evidence that stimulation of the BDNF/TrkB pathway after bead manipulation with optical tweezers had occurred, we measured Calcium levels in neuronal soma and dendrites. To make sure that stimulation with BDNF could produce measurable Calcium signals in our experimental system, we carried out a first experiment with bath application of BDNF 50 ng/mL. Basal fluorescence of neurons loaded with Fluo-3 dye was monitored for 10 minutes, acquiring images every 2 minutes. BDNF was then bath-applied and fluorescence was recorded for 40 minutes. A rapid raise of the Calcium signal both in soma and dendrites was observed after the stimulation (**Figure 2.5a**). A plot of the normalized fluorescence values showed this progressive increase in Calcium signal which reached a plateau at about 15 minutes after BDNF stimulation in both soma and dendrites (**Figure 2.5b**).

2.1.4.3 Dendrites stimulation with sub-micrometric resolution

For focal stimulation experiments, we first placed a BSA-bead on a dendrite and recorded basal Fluo-3 fluorescence for 10 minutes, acquiring images every 2 minutes. A BDNF-coated bead was then positioned on another dendrite of the same neuron, at the same distance from the soma, and fluorescence images were acquired every 2 min for a period of 40 min, as done for bath application. An example of the stimulation of Ca^{2+} signaling induced in a pyramidal neuron is illustrated in **Figure 2.6**. To assure that the contact between the beads and dendrites had occurred, transmission images in phase contrast were acquired immediately after positioning the beads (**Figure 2.6**, t= -10' and t=0'). Only a low Ca^{2+} signal fluctuation was observed after BSA-bead positioning (t= -9'; t= -5'; t= -1'). On the contrary, the fluorescence signal clearly increased in the cell body after positioning the BDNF-bead. Moreover, a difference in the signal obtained from the two stimulated dendrites was recognized, indicating a selective activation of the BDNF-stimulated neurite (**Figure 2.6, inset**).

To rule out the possibility that the effect observed with BDNF-beads could be due to the mechanical stimulation of the dendrites, we ran a set of control experiments in which a pair of BSA-beads was positioned on two different dendrites of the same neuron. An example of time lapse analysis of Calcium fluorescence is illustrated in **Figure 2.7**, showing an almost constant Calcium level, and hence non-activation of the TrkB receptor for a pair of BSA-beads. After positioning the first BSA-bead (BSA-1), the curves of the control and experimental groups of cells were overlapping (**Figure 2.8a**). When the second bead was coated with BSA (BSA-2) there was no increase in Calcium levels in the soma, but

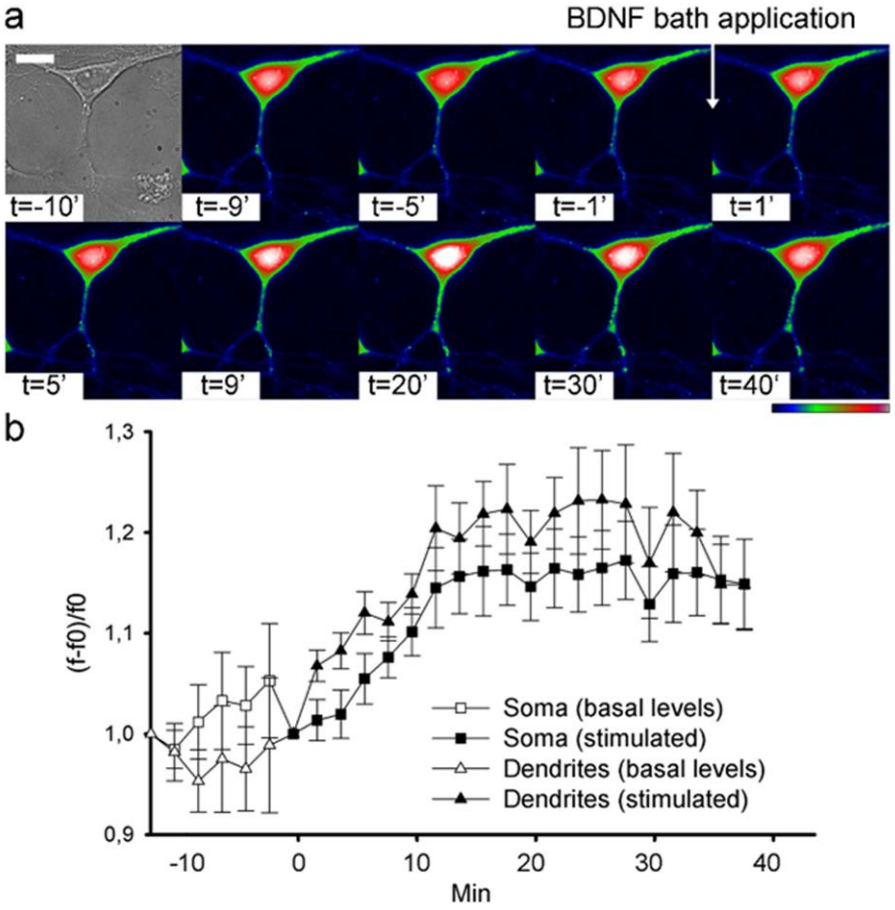

Figure 2.5: The effect of BDNF bath administration. BDNF 50ng/mL induced an increase of Calcium levels. (**a**) Transmission image of a neuron and its fluorescence levels in false colors. BDNF application is indicated by the arrow. (**b**) Normalized Calcium levels in soma (n=10) and dendrites (n=16). Scale bar 10 µm. From D'Este et al., 2011.

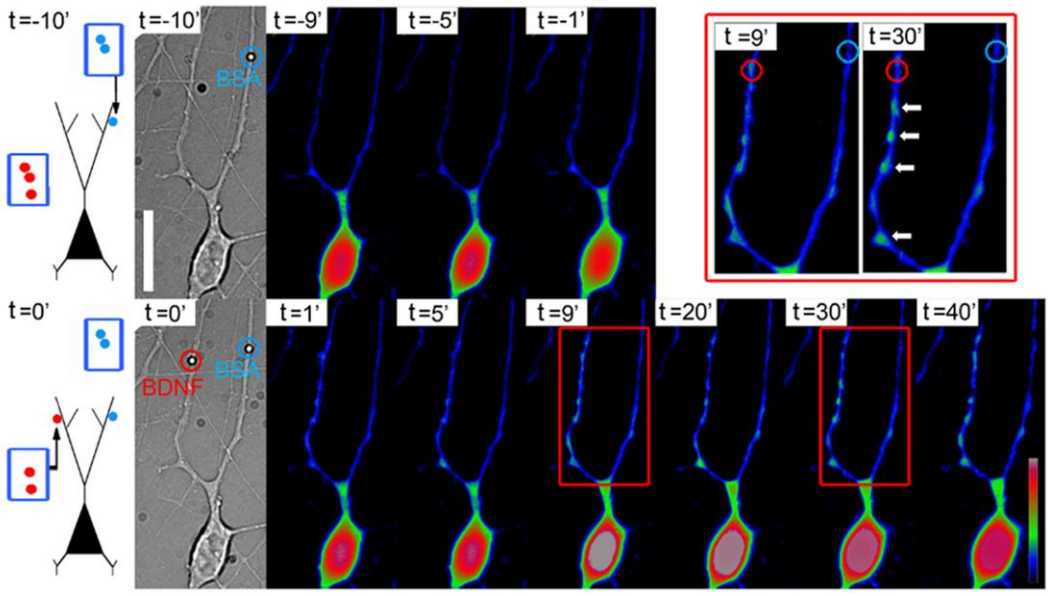

Figure 2.6: Focal stimulation of primary rat hippocampal neurons by optically manipulated functionalized beads. Activation of BDNF-dependent Calcium signaling pathway. A BSA-bead was placed at 35,5 µm from soma (first transmission image), as schematically depicted on the left (t=-10'). Raw Calcium levels detected by Fluo-3 fluorescence are visualized in false colors at the indicated

times (selection from the image sequence acquired every 2 min). A BDNF-bead was then placed at the same distance from the cell body (t=0'). The fluorescence images show a clear increase in Calcium levels within the cell body. In the inset, enlargement of dendrites 9 and 30 min after stimulation clearly showing a difference between the two stimulated dendrites. Arrows indicate high Calcium concentration. Scale bar 15µm. From D'Este et al., 2011.

when the second bead was coated with BDNF, the curves began to split showing a sudden increase in somatic Calcium levels (**Figure 2.8a**). A binning of values between -10 to 0, 1 to 10, 15-25 and 30 to 40minutes outlines this difference, having a significant p-value (<0,001) for the last two sets of times (**Figure 2.8b**). The effect on Calcium levels obtained with local application of BDNF, was similar to that observed after bath application of 50ng/mL BDNF (**Figure 2.8b**). These results suggest that there was a strong activation of neurons induced by BDNF-functionalized beads, further confirming that BDNF immobilized on the bead surface was active and able to stimulate an intracellular signaling cascade.

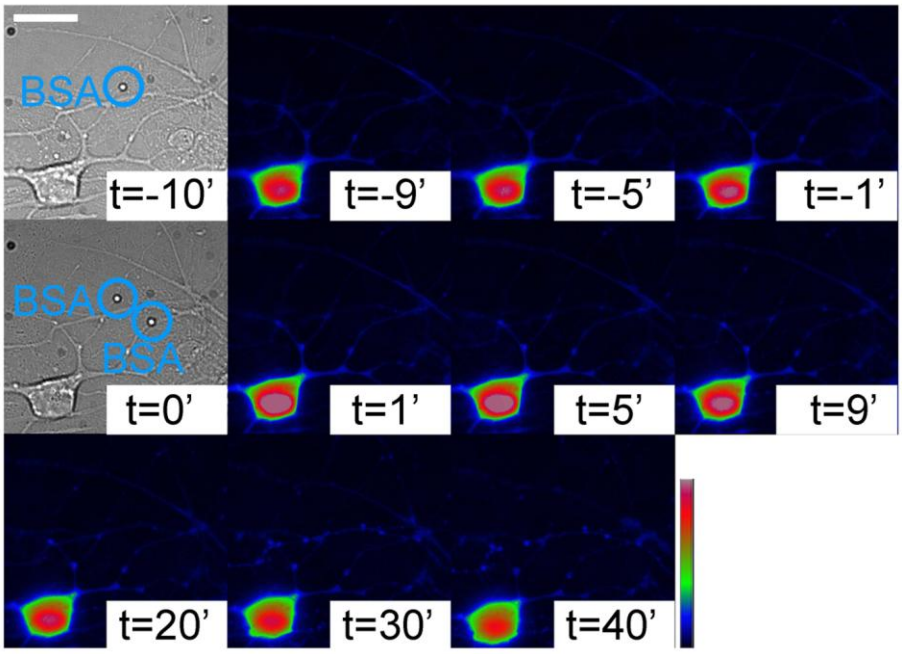

Figure 2.7: Focal stimulation with two BSA-coated beads. Similar to Figure 2.6 except that two BSA beads were placed instead of a BSA- followed by BDNF-bead. Calcium levels, represented in false colors, remain almost constant showing non-activation of the TrkB receptor. Scale bar 15µm. From D'Este et al., 2011.

To determine if this method allows for local stimulation of TrkB-signaling in the cell periphery, we carried out a semi-quantitative analysis of Calcium levels in dendrites. BSA-beads did not alter Calcium concentration and the curves of the two dendrites in control experiments were superimposed at all times, demonstrating that there was no activation due to the mechanical stimulation of neurons or effects produced by BSA itself (**Figure 2.8c, d**). On the contrary, dendrites stimulated with BDNF-beads showed increased Calcium levels and, at 15 and 25 min after placement of the second bead, a statistically significant difference with respect to dendrites in contact with the BSA-bead, (**Figure 2.8e, f**; p=0.002). These results indicate selective TrkB activation only in dendrites in contact with BDNF-beads. In dendrites, Calcium signals showed a different kinetic behavior with respect to soma, starting about 10 minutes after the stimulation with the neurotrophin-coated bead, but like in the soma, were prolonged in time. Interestingly, in the last 10 minutes of the experiment a rise in Calcium concentration, probably caused by ion diffusion, was observed also in the first dendrite stimulated with BSA. This was not

surprising since the whole cell (and thus also the control dendrite) was activated, as indicated by the large increase of Ca^{2+} in the soma.

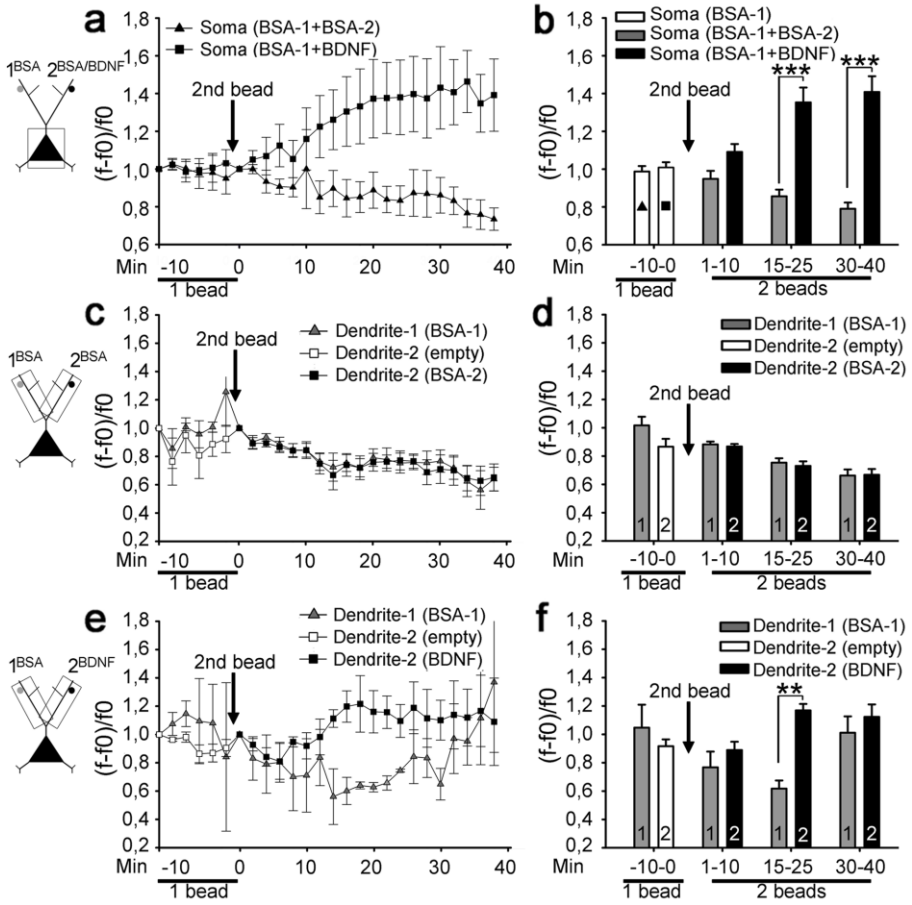

Figure 2.8: Neurons stimulation with BDNF- beads increase Ca^{2+} levels while BSA- beads do not. (**a,b**) Normalized values of Calcium levels measured in the cell body of the neurons stimulated with two subsequent BSA-beads (BSA-1+BSA-2) (n=5) or with a BSA- and then a BDNF-bead (BSA-1+BDNF) (n=4). Arrows indicate the moment of second bead placement. A clear divergence is observed immediately after placing the second bead. (**b**) Binning of values represented in (a) at the indicated time gaps underlies the differences observed. (**c, d**) Normalized values of Calcium levels measured along the two dendrites (10µm before and after each bead) both stimulated with BSA beads and (**d**) binning of data. The two curves are almost identical for all the times. (**e, f**) Same as (c, d) but for dendrites stimulated with BSA and then BDNF. Calcium levels increased in dendrite-2 about 10 min after stimulation and values are statistically different between 15 and 25 min. P-value: **<0.005; ***<0.001. Analysis performed with one-way ANOVA. From D'Este et al., 2011.

2.1.5 DISCUSSION

Since neurons are morphologically and functionally complex cells and the cellular response to a particular stimulus, critically depends on how and where it is delivered (Reichardt and Mobley, 2004), local stimulation has always been an objective in neuroscience. Already in the '70s Campenot noticed a specific local effect of the neurotrophin NGF on distal neurites causing their growth while local NGF was not required at the somas and proximal portions of the neurites (Campenot, 1977). Later, a different response of basal and apical dendrites to the same bath applied neurotrophin was demonstrated (McAllister et al., 1995). More recently, also the effect induced by different kinetics in neurotrophins administration was explored (Ji et al., 2010; MacInnis and Campenot, 2002) and differences in the

activation of signaling pathways were found. Techniques controlling both aspects are developing, however they have drawbacks. In fact, most delivery techniques generate gradients of molecules that can diffuse to the nearby region of the cell or have minimal flexibility, since they are efficient only for small compounds (photo-uncaging Ellis-Davies, 2007) or require protein engineering (photo-activable proteins Wu et al., 2009).

The use of functionalized beads for local delivery of neurotrophins, was proposed by Gallo (Gallo et al., 1997), who used 10 μm large vectors settled in cell culture dish or, in later works, microbeads were positioned by means of micropipettes (Yoshii and Constantine-Paton, 2007; Zhang and Poo, 2002). Considering an average number of 7 spines every 10 μm in a mature hippocampal neuron (Desmond and Levy, 1985) it can be immediately understood that this technique does not allow a precise focal stimulation. Smaller magnetic beads (250 nm large) were also used (Naka et al., 2004), however these particles are at the limit of optical resolution and their position cannot be controlled with precision. Here we proposed a new approach that, by coupling the use of micro-beads and optical tweezers, allows a high resolution stimulation of cells.

We show that this novel approach has several advantages. First, we demonstrated the possibility to individually manipulate different beads stored in small reservoirs by means of optical tweezers and that several reservoirs with beads coated differently can be used. Secondly, with our system, more than two kinds of beads can be manipulated, analyzing the response of the same cell to each of them. Indeed, we showed that it is possible to stimulate the same cell simultaneously with one activator (BDNF) and a control (BSA) bead placed on two different dendrites and obtain a specific response on one dendrite only. Third, the use of optical tweezers instead of micropipettes for the manipulation of the vectors has the advantage that the effective contact between the bead and the cell can be easily verified since the particle does not follow the optical trap anymore when it is in touch with the cellular membrane. Fourth, beads down to 0,3 μm diameter can be used and placed on the cell with sub-micrometric precision ensuring focal stimulation of a single spine/synapse. Moreover, because beads did not move during the 50 minutes of time-lapse recording, this study demonstrated that this technology is particularly well suited to monitor long-term responses induced by BDNF. Thus it is possible to study cellular phenomena linked to Long Term Potentiation or Depression, as for instance rearrangements of endoplasmic reticulum, trans-Golgi network and secretory vesicles, mRNA granules trafficking and translation within the spines following BDNF stimulation (Ostroff et al., 2002; Tongiorgi, 2008; Toresson and Grant, 2005). These modifications relay on microtubule-based traffic (Shan et al., 2003) and need a persistent stimulation to occur, like the one provided by the functionalized beads.

In our study, BDNF was coupled to silica beads through a reaction between the carboxylic groups of the bead and the amine groups of the protein. We demonstrated that BDNF was still biologically active because a single functionalized bead in touch with a neuron was able to induce TrkB phosphorylation and a robust c-Fos translocation within the nucleus. Similarly, a single BDNF-coated bead was able both to influence the mobility of growth cones and to induce a large Ca^{2+} response in the stimulated dendrites and the soma that, after 30 min, spread also into the unstimulated dendrites. This striking cell-wide activation of TrkB receptor signaling by a single BDNF-bead positioned on a dendrite, represents a particularly important finding of this study because it supports the use of this technology to study cell changes induced by activation of a small set of synapses/spines - if not a single one. Of note, the use of functionalized beads, unlike systems that deliver free molecules, does not allow ligands to be endocytosed and thus the signaling deriving from retrograde transport of the neurotrophins' signaling endosomes is not activated. Indeed, distinct biological responses to neurotrophins, and in particular to NGF (i.e. neuronal differentiation or survival), can be controlled by receptors signaling from different locations within the cell (Cui et al., 2007; Zhang et al., 2000). In our study, the possibility that the signal can reach the cell body unaccompanied by the molecule that initiated it, cannot be ruled out (Du et al., 2003).

A local Calcium transient caused by local stimulation with BDNF has been reported in literature (Lang et al., 2007), and it has been demonstrated to be independent from internal stores. This transient is fast and can be observed only in the first seconds after stimulation. Since in our setup we need to switch from the camera used for trapping to another camera used for fluorescence imaging, we could not investigate these events. Indeed we have a time lag of 30 second between the actual bead deposition and the first frame of live Calcium imaging. Amaral and Pozzo-Miller (Amaral et al., 2007; Amaral and Pozzo-Miller, 2007) however showed that this signal is able to reach the soma and it induces the activation of the Calcium-dependent cationic current I_{BDNF} mediated by TRPC3 channels. This current causes a further increase of Ca^{2+} also in dendrites in a internal stores dependent manner.

We can speculate a mechanism similar to that described by Amaral and Miller for the effect we observe, since also the timing is comparable. To explore this hypothesis, our setup needs a further modification, to allow simultaneous optical manipulation of the microbeads and fluorescence imaging of neurons. The reported experiments seem to prove no mechanical stimulation of neurons caused by the beads. However we cannot exclude that a fast, immediate signal was induced by beads (both BSA and BDNF coated).

In conclusion, here we propose the use of optical tweezers as an approach to stimulate defined neuronal compartments by manipulating functionalized beads. This technique can be useful to study any growth factor, hormone or peptide signaling at sub-cellular levels and has several advantages:

- it overcomes problems related to other local delivery methods, such as unwanted diffusion of soluble compounds;
- it has a high flexibility since beads of any dimension can be functionalized with any desired protein or molecule;
- its high resolution allows studies of neural processes at single dendrite level, having the desired controls within the same neuron and thus reducing the variability of the system;
- it is a simple-to-implement setup, which can be easily applied in bio-laboratories not specialized in optical tweezers;
- the technique might be of interest not only for neurobiology, but also for molecular oncology, immunology and any other field in which single cell response to a specific and localized stimulus is studied.

2.2 LIPOSOMES

Many relevant biological events are sensitive to gradients of molecules, which influence the cellular response and morphology. In particular, during chemotaxis, cells move in the same or in the opposite direction of a given gradient. With beads, the stimulus is fixed and cannot diffuse, and the study of these events is not possible. Hence, we thought about using micron-sized liposomes filled with molecules. Their breaking should allow the generation of spatial and temporal gradients. As in the case of beads, however, this hypothesis should be tested. In particular the main questions about this kind of vector are: are we able to encapsulate the desired molecules inside liposomes? Can we trap and manipulate them? Can an UV pulse induce the photolysis of a trapped liposome? Do the molecules encapsulated inside it diffuse outside during the photolysis? Are they damaged by the UV pulse or do they preserve their biological activity? Do they reach surrounding cells and stimulated them? Does the UV pulse have an effect on the cell? To answer all these questions, we started by encapsulating and releasing a simple chemical compound (KCl) and then we turned to more complex systems, encapsulating proteins. In this case, the readout was the navigation of growth cones, extremely dynamic structures with a high sensitivity to small changes in the environment.

2.2.1 GROWTH CONES

During development of the nervous system, each neuron extends an axon through a complex and changing environment to reach its final destination. At the tip of each axon there is the growth cone. Its motility and highly dynamic behavior governs axonal path-finding and the construction of neuronal networks.

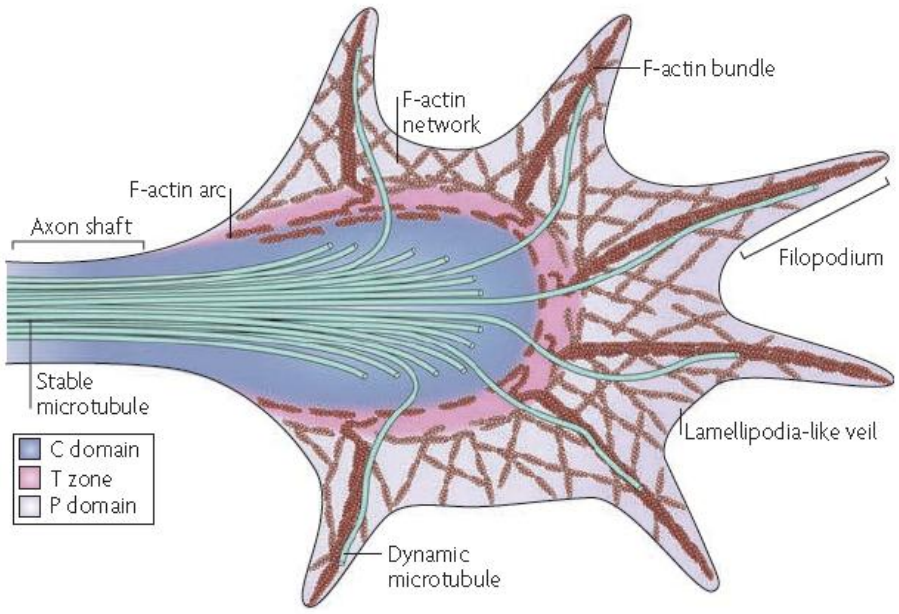

Figure 2.9: Structure of a growth cone with its cytoskeletal features. C domain is the central domain, T zone is the transition zone while P domain is the peripheral domain. From Lowery and Van Vactor, 2009.

Growth cones have a finger-like shape. Fingers are the filopodia, dynamic structures that have the function of antennas, since they explore the environment. Filopodia are connected through sheets of membrane, called lamellipodia. The shape of growth cones is determined by its cytoskeletal structure. The central domain (C domain) corresponds to the end of the axon shaft. It contains mainly stable

bundled microtubules, organelles and vesicles. Within this region also central actin bundles can be found. The peripheral domain (P domain) is it outer part of the growth cone. It has two main actin structures: actin bundles, that are inserted within filopodia, and mesh-like branched actin networks, that sustain lamellipodia. "Pioneer" microtubules may be linked to actin bundles inside filopodia. C domain and P domain are connected by the transition zone (T zone). In this region actin arcs are present. They are actomyosin contractile structures that are perpendicular to actin bundles of P domain and form a hemi-circumferential ring (Lowery and Van Vactor, 2009).

Navigation of the growth cone is affected by several cues and in particular by adhesive cues (that can be attached to the extracellular matrix or cell surface) or diffusible chemotropic factor. These factors activate specific signaling pathways that act locally to modulate the cytoskeletal dynamics and promote attraction, repulsion, growth cone collapse, or influence the rate of axon extension. Signals can thus foster the adhesion and migration of the cell in that direction or repel it, prohibiting this adhesion. Examples of attractive adhesive cues are laminin and fibronectin, while slit, ephrins and chondroitin sulphate proteoglycans are repellent. Diffusible molecules can be divided into three main families: Netrins, Semaphorins and trophic factors. Generally, trophic factors (such as BDNF) are attractive, Semaphorins are repellant, while Netrins can be both attractive and repellant (Tojima et al., 2011). However, it should be considered that response to attraction or repulsion is not due to intrinsic properties of the cue, rather than to specific receptors that are engaged in the growth cone and to the signaling pathway activated (for reviews see Bashaw and Klein, 2010; Conde and Caceres, 2009; Lin and Holt, 2007; Lowery and Van Vactor, 2009).

When a positive cue binds its receptor, an intracellular pathway is activated so that the actin cytoskeleton is stronger linked to the substrate. Actin polymerization continues in front of the adhesion site and lamellipodia and filopodia move forward, thus extending the leading edge (Mogilner, 2006). Engorgement occurs after actin clears from the corridor between the adhesion and the C domain. Actin arcs reorientate from the C domain towards the site of new growth and C domain is occupied by microtubules. Finally, the proximal part of the growth cone compacts at the growth cone neck to form a new segment of the neurite shaft.

Microtubules have two different roles in the outgrowth process: C domain microtubules guide the growth cone advance by fixing axonal direction, while individual pioneer microtubules in P domain act as sensors. These ladder microtubules generally follow actin bundles (Letourneau, 1983), which are thought to guide them within the P domain (Zhou and Cohan, 2004). This interaction has a major control in the regulation of the structure of growth cones. Indeed, positive guidance cues, increase the frequency of microtubule-actin uncoupling, leading to and increased exploration at the sites of cue binding by the microtubules. Repellant cues, on the contrary, foster this coupling, reduce microtubule exploration and promotes the formation on microtubule loops (Lowery and Van Vactor, 2009).

In vitro studies indicate that Calcium signals are most of the times required for growth cone guidance (Tojima et al., 2011). Higher Ca^{2+} levels are observed on the side of the growth cone facing the source of the cues, regardless of whether the cues are attractive or repulsive. Thus, localized Ca^{2+} elevations on one side of the growth cone can act as both attractive and repulsive signals (Gomez and Zheng, 2006; Zheng, 2000). The diverse spatiotemporal patterns of Ca^{2+} and cyclic nucleotide signals contribute to the response, together with the different subcellular localization of the effectors. In the case of repulsion, cGMP levels increase and Ca^{2+} influx only through plasma membrane channels occurs. This source of Ca^{2+} activates repulsive effectors and not attractive effectors. Conversely, attractive cues induce an increase of cAMP and the activation of attractive effectors by means of Ca^{2+} release from the endoplasmic reticulum and/or abundant Ca^{2+} influx across the plasma membrane (Tojima et al., 2011).

Growth cones may also undergo a fast desensitization, which is dependent on receptor endocytosis, and a slow resensitization, which is dependent on protein synthesis. If background levels of a particular guidance cue increase, growth cones make use of this adaptation mechanism to tune their responsiveness appropriately to higher levels of the guidance cue riding on top of the background levels (Bashaw and Klein, 2010; Piper et al., 2005).

It is thus evident that soluble cues should be released through the generation of gradients of molecules at really low levels and with an appropriate temporal pattern.

2.2.2 SEMAPHORIN 3A

Semaphorins are a family of proteins with more than 20 items. They have diverse functions in many physiological processes, such as cardiogenesis, angiogenesis, tumor metastasis and immune regulation (Kumanogoh and Kikutani, 2010). Semaphorin 3A (Sema3A) is a member of this family and is one of the best characterized axonal chemorepellents. It acts through the neuropili-1(NP1)/plexin-A(PlexA) receptor complexes. NP1 serves as a high-affinity ligand binding partner, while PlexA transduces the signal into the cell via its large intracellular domain. In the absence of ligand, NP-1stabilizes an inactive conformation of NP1-PlexA receptors. Binding of Sema3A to NP1 induces a conformational chance in this complex. The effects on cytoskeleton are given by the regulation of actin dynamics through the phosphorylation of the actin-binding protein cofilin. Phosphorylated cofilin is inactive and thus its ability to promote actin filament turnover is reduced, and ultimately, F-actin filaments dissolute. As a result, a redistribution of the F-actin cytoskeleton occurs and the growth cone membrane is endocyted (Fan et al., 1993; Fournier et al., 2000). These events lead to a dramatic collapse of the growth cone lamellipodium (Castellani et al., 2004; Jurney et al., 2002) (for reviews on the Sema3A pathway Bashaw and Klein, 2010; Huber et al., 2003).

In the hippocampus the repellent role of Sema3A was demonstrated by Chèdotal using mouse embryo extracts (Chedotal et al., 1998).

2.2.3 NETRIN-1

Netrins are a small family of highly conserved guidance cues (molecular weight 70–80 kDa). They can function as both neural chemoattractants and repellents depending on the cellular context in which the cue is encountered (Chisholm and Tessier-Lavigne, 1999). These opposing neuronal responses to netrins may depend in part upon activation of different receptor complexes, and they suggest that differential activation of intracellular signaling cascades defines netrin function.

One factor that determines the response of an axon to Netrin-1 is the composition of the receptor on the surface of growth cones, and in particular on the association between DCC (deleted in colorectal cancer) and Unc-5 family. The attractive effects of Netrin-1 are mediated by homodimers of DCC proteins. By contrast, Unc-5 proteins mediate repulsion, in the presence of DCC, in the absence of DCC and/or with recruitment of a distinct co-receptors (Round and Stein, 2007).

Furthermore the response depends on the internal state of the growth cone, and in particular on Ca^{2+} influx and on the ratio between cAMP e cGMP (Nishiyama et al., 2003). More in detail, The Netrin-1-induced turning response depends on Ca^{2+} influx through plasma membrane Ca^{2+} channels, as well as Ca^{2+}-induced Ca^{2+} release from cytoplasmic stores. Reduction of Ca^{2+} signals by blocking either of these two Ca^{2+} sources converted the Netrin-1-induced response from attraction to repulsion (Hong et al., 2000).

Signaling through both DCC and Unc-5 receptors affects growth cone cytoskeleton by modulating the activity of Rho GTPases (Li et al., 2002; Shekarabi and Kennedy, 2002). Rho GTPases

integrate the responses of upstream pathways and coordinate downstream effectors by modifying the function of cytoskeletal effectors. Activation or inactivation of cytoskeletal effectors leads to responses such as actomyosin contraction, filamentous (F)-actin disassembly or F-actin polymerization. The resulting growth cone turning response depends on the localization of the guidance signaling inside the growth cone (Lowery and Van Vactor, 2009).

2.2.4 LOCALIZED STIMULATION OF GROWTH CONES

The study of growth cone dynamics and turning obviously requires a gradient of molecules for the stimulation. Only being able to localize the source of stimulus, indeed, it is possible to see whether it affects the turning angle. The repetitive pulsatile ejection method (presented in **section 1.2.2**) is still the method of choice when performing growth cone turning assays (Han et al., 2011; Thompson et al., 2011) even if microfluidics platforms have been proposed (Kothapalli et al., 2010; Wang et al., 2008).

Chemical stimuli, encapsulated in optically manipulated liposomes and delivered by breaking the liposome with a pulsed UV laser were proposed as local delivery with precise temporal switch-on control (Sun and Chiu, 2003). A submicrometric diameter liposome (0.6 μm) was loaded with a Carbachol solution (0.1 M) and positioned at 0.5 μm from a CHO cell transfected with muscarinic acetylcholine receptor, stained with the fluorescent Calcium indicator Fluo-3. The content was then delivered by liposome photolysis with an UV laser pulse and the increase of the intracellular Calcium level monitored by fluorescence. This method has the advantage that any membrane impermeable molecules, including peptides and proteins, can be easily encapsulated into liposomes and delivered to cells. Moreover, the amount of released molecules can be varied easily by controlling either the size of the liposome or the concentration of the encapsulated compound (Walde and Ichikawa, 2001). Therefore, we wanted to extend this technique to investigate cultured neurons and in particular growth cones.

2.2.5 MATERIALS AND METHODS

2.2.5.1 OPTICAL SETUP

The optical setup was built in the Optical Manipulation lab at CNR-IOM. It was composed by three main modules (**Figure 2.10**):

- custom built IR optical tweezers;
- commercial UV micro-dissection system (MMI-CellCut Plus, MMI, Zurich, Switzerland);
- commercial inverted microscope Nikon Eclipse TE-2000-E.

The trapping laser beam was generated by a 1064 nm continuous wave single mode Yb fiber laser (YLM-5, IPG Photonics GmbH, Burbach, Germany). The laser head had a built-in collimator providing a TEM00 collimated beam. The direction of the trapping IR beam was aligned with the direction of the micro-dissection UV beam by two mirrors (M1 and M2 in **Figure 2.10**). A convergent lens, L, with the focal length, f_L = 150 mm was placed just before the entrance aperture of the micro-dissection system to adjust the convergence of the trapping IR beam to the convergence of the UV micro-dissection beam. Different objectives have been used: 100x water immersion NA=1, WD=1mm, Olympus; 60x water immersion, NA=1.2; WD=0.4, Nikon; 60x oil immersion NA=1.4, WD=0.13.

The alignment of the IR trapping beam was facilitated by a red guide laser beam (660 nm, 0.5 mW), emitted by the same source. Powers between 10 to 20mW were necessary at the sample location to stably trap the liposomes. Typically, the IR laser power at the output of the collimation head was regulated from 150 to 300 mW. The micro-dissection system was equipped with a solid-state pulsed UV

laser (355 nm, max 1 µJ / pulse, pulse duration < 0.5 ns, repetition rate < 5 kHz). The beam was collimated by internal optics and directed toward the microscope objective by two dichroic mirrors (D1, D2). The number of required pulses may vary with liposome morphology (single or multi-lamellar).

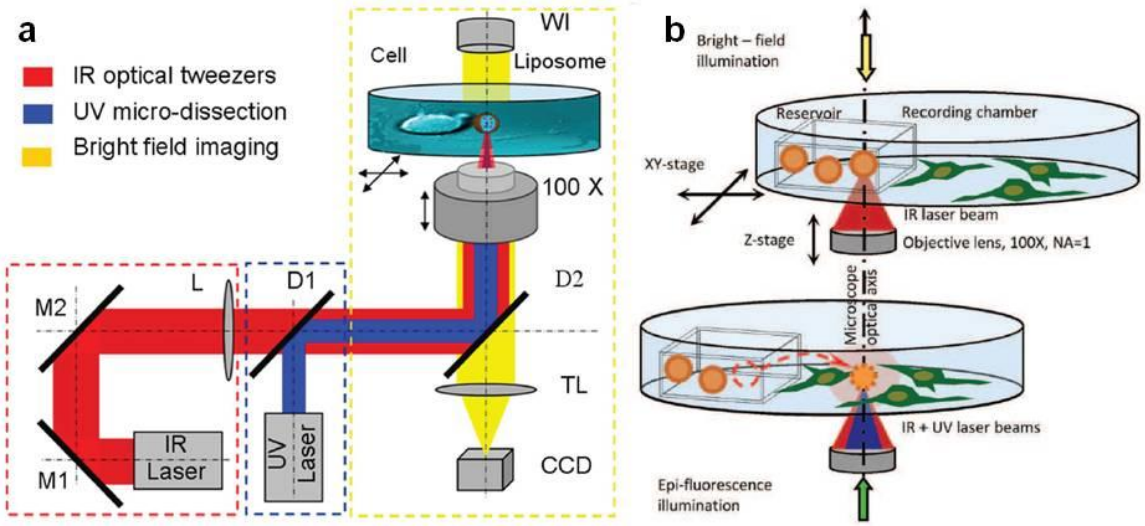

Figure 2.10: Optical manipulation approach. (**a**) Setup: the IR laser trapping beam direction is adjusted by two mirrors, M1 and M2, and its convergence by the convergent lens, L, to be aligned with the UV laser micro-dissection beam. Both laser beams are then directed into the entrance pupil of the microscope objective (100 X) by the dichroic mirrors D1 and D2. The sample is illuminated by a white light source (WI) and the image is formed through the tube lens (TL) on the CCD camera. (**b**) Optical manipulation and dissection of a single liposome. A selected liposome inside the capillary is first fixed in the optical trap (top) and then placed to the specific site near the cells by moving the stage and microscope objective (black arrows). A short train of UV pulses breaks the liposome to deliver the content to the surrounding environment (bottom) (adapted from Pinato et al., 2011a and Pinato et al., 2011b).

Short series of less than 50 pulses were usually enough to break the liposomes wall and deliver their content. The power and the focus of the UV laser beam were controlled by the MMI software, which controls also the XY motorized sample stage and the image recording on the CCD camera. The sample chamber on which the neuronal cell were cultured is a glass-bottom Petri-dish. Since the experiments last for tens of minutes, the Petri-dish was settled on a heating insert and kept at 37°C by a digital temperature controller (PeCon GmbH, Erback, Germany) to maintain physiological conditions.

2.2.5.2 LIPOSOME PREPARATION

For the preparation of liposomes, phospholipids were dissolved at the concentration of 10 mg/mL in a solvent composed of chloroform:methanol (2:1, v/v). The phospholipid composition was the following: Cholesterol: 9 µmol, L-α- Phosphatidylcholine: 63 µmol, Stearylamine: 18 µmol (Sigma-Aldrich, cat. L4395). Liposomes were obtained using the lipid film hydration method (Hub et al., 1982). Aliquots of the phospholipid solution were dried in vacuum overnight. The obtained lipid films were finally hydrated with the solution to be encapsulated. The ion concentration of the encapsulated solution was estimated to be the same as that of the rehydration solution in bulk. After a brief incubation, liposomes were formed. They were then gently centrifuged (5000 rpm x 3 min) and rinsed three times with an isotonic solution (100mM glucose in physiological buffered saline, PBS). Sucrose 100 mM was added to the hydration solution to improve liposome wash and to help the trapping of large liposomes as previously reported (Ichikawa and Yoshikawa, 2001). The size distribution of the liposomes was

6.30±4.04 μm. We could observe the presence of both multi- and mono/oligo-lamellar vesicles, based on qualitative optical criteria, i.e., shape and rim size. The stability was tested by filling the liposomes with fluorescein and maintained for days. Liposomes were finally charged in rectangular capillaries (Vitrotubes, #5005, VitroCom, New Jersey) and subsequently transferred to the recording chamber. This allows selection of a single liposome from the capillary and positioning it at the site of interest.

2.2.5.3 CELL CULTURE

Cell cultures were obtained as described in **paragraph 2.1.3.1**.

Before starting the experiment cultures were bathed in Ringer's solution (145 mM NaCl, 3 mM KCl, 1.5 mM CaCl2, 1 mM MgCl2, 5 mM Glucose, 10 mM HEPES, adjusted to pH 7.4 with NaOH).

2.2.5.4 CALCIUM IMAGING

Ca^{2+} imaging experiments were performed in epi-fluorescence using a blue excitation filter block (B-2A, Nikon). The fluorescence images were recorded with a CCD camera DVC-1412AM (DVC Company, Austin, TX, US). Frames (174x130 pixels in 8x8 binning mode) were collected at the rate of 22 Hz at 12-bits. Stock solution of the Calcium dye Oregon Green 488 BAPTA-1-AM (OGB-1-AM, Molecular Probes O-6807) was prepared in DMSO. Cell cultures were then incubated for 30 min with 1.5 μM of the Ca^{2+} dye. After incubation neuronal cultures were washed and transferred on the stage of the microscope. Measurements were performed at 37 °C. Data were analyzed with software ImageJ and Matlab (Mathworks, Natick, MA). Increases of Ca^{2+} are expressed in relative fluorescence changes (DF/F) as described in (Pinato et al., 2009).

2.2.6 RESULTS

There are several questions related to the use of micron-sized liposomes as vectors for the delivery of molecules, since two highly focused laser beams (UV and IR) should be used at the same time. Hence, they might damage encapsulated molecules or the cells. Moreover, the UV pulse causes only a transitional rearrangement in the liposome, during which molecules are supposed to escape from the lumen of the vesicle. Initially, we validated the technique by delivering a small chemical compound (KCl) and analyzing its effects on Calcium levels in neurons. Afterwards we encapsulated two chemotactic proteins (Netrin-1 and Semaphorin 3A) and studied their outcomes on growth cones.

2.2.6.1 PRELIMINARY STUDY WITH KCL AND CALCIUM

The technique was first tested by molecules encapsulation and subsequent release by breaking the liposome membrane with UV laser pulses. Liposomes with dimension ranging from 1 to 10 μm were produced. The efficiency of encapsulation and subsequent release induced by the UV pulse, was first qualitatively evaluated (**Figure 2.11**).

Liposomes were encapsulated with 1 mM fluorescein and collected in a reservoir consisting of a rectangular glass capillary. The reservoir was introduced in the recording chamber and a single liposome was optically trapped, positioned and visualized both in bright field and epi-fluorescence (**Figure 2.11a**). The fluorescence signal originated from the liposome allowed to check the correct encapsulation (**Figure 2.11a left**). After UV-pulse delivery, fluorescence disappeared from the liposome demonstrating complete depletion of fluorescein and a shape rearrangement of the vesicle induced by the microdissection occurred (**Figure 2.11a right**). The fluorescence signal from a large vesicle in close proximity was not influenced by the UV pulse (**Figure 2.11a**), demonstrating single vesicle photolysis.

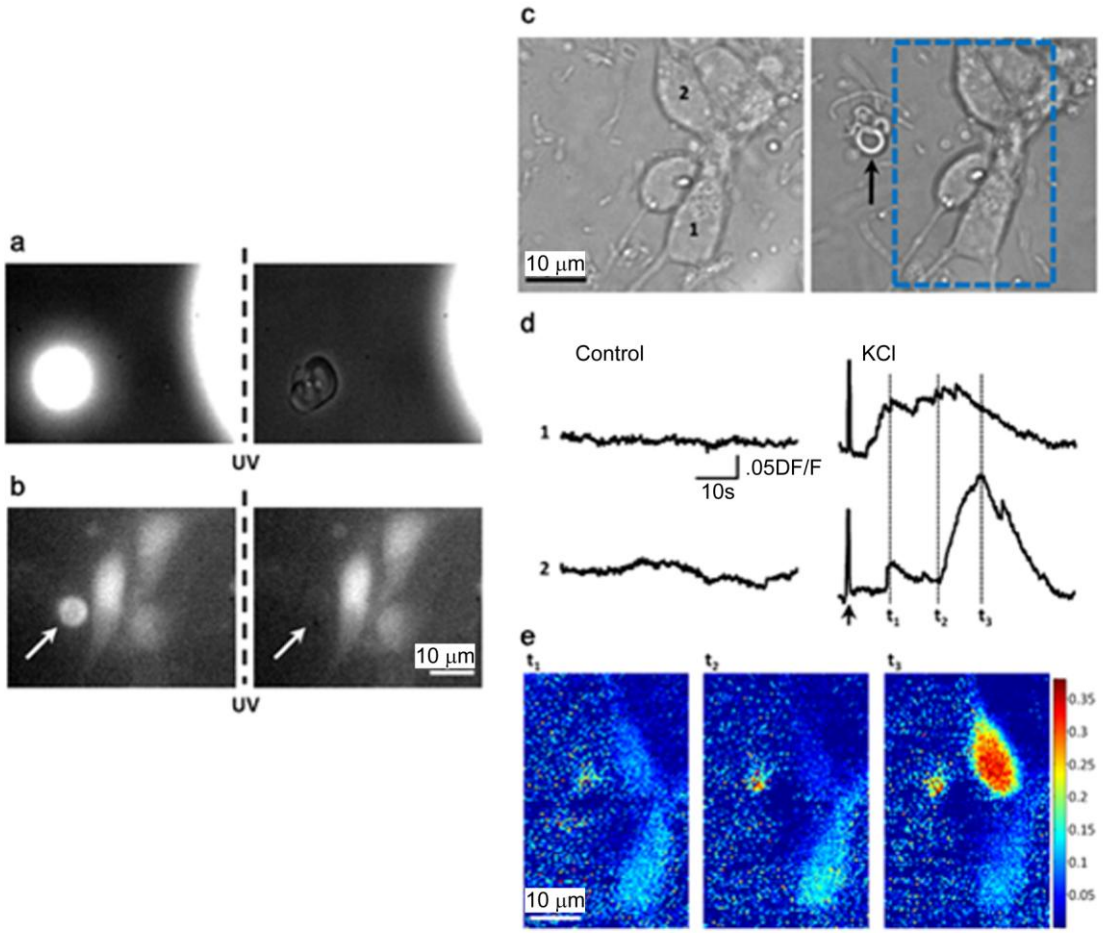

Figure 2.11: Encapsulation and release efficiency from single liposomes. (**a**) Simultaneous bright field and fluorescence images before (left) and after (right) UV-pulse release from a liposome containing 1 mM fluorescein. (**b**) A fluorescent liposome was optically trapped and brought in the vicinity of cultured neuronal cells treated with OGB-1-AM. Fluorescence was measured before and after the UV-induced release, allowing to test the efficiency of encapsulation and subsequent release. (**c, d, e**) Optical delivery of high KCl to neurons, and simultaneous measurements of Ca^{2+} elevation responses by fluorescence imaging. (**c**) Bright field images of cultured hippocampal neurons before (left) and after (right) the positioning of a single liposome (black arrow) encapsulated with KCl 100 mM. (**d**) Time dependence of DF/F, calculated from cell 1 and 2 as indicated in (c). Left traces report spontaneous fluctuations of Ca^{2+} fluorescence in absence of external stimuli (control), while right traces were recorded after UV-pulse induced KCl release (KCl). The presence of an artifact (arrow) indicates the time of release. (**e**) Three images reporting the values of DF/F expressed in pseudo-colors, over the area indicated in the box of panel (c) for the time points t1, t2 and t3 as indicated in (d) (adapted from Pinato et al., 2011b).

For mono/oligo-lamellar vesicles of 1-10 µm, i.e. the range used in our experiments, the efficiency of triggering release was 100%, while multi-lamellar vesicles often required separated and repeated UV trains.

Liposome content could be released in proximity of neurons without damage. As shown in **Figure 2.11b**, the fluorescent content of a single liposome positioned close to a group of neuronal cells stained with OGB-1-AM, was released. The fluorescence signal from the vesicle disappeared, revealing complete release of the liposome content, while the baseline fluorescence signal from the Ca^{2+} dye stained neurons was still present.

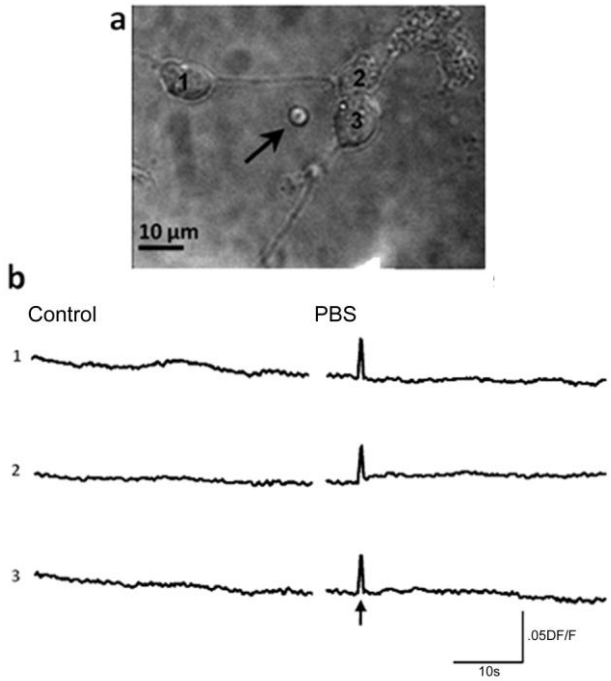

Figure 2.12: Photolysis of control liposomes containing PBS. (**a**) Bright field image of a neuronal culture treated with a control liposome containing PBS (indicated by the black arrow). (**b**) Time dependence of DF/F, calculated from cell 1 and 2 and 3 as indicated in (a). Left traces report spontaneous fluctuations of Ca^{2+} fluorescence in absence of external stimuli, while right traces were recorded after UV-laser photolysis of a control liposome (a, arrow). The artifacts indicate the time of release (arrow)(from Pinato et al., 2011b).

Subsequently, the effect of release from liposomes was tested on neuronal cells in culture (**Figure 2.11c**), by releasing encapsulated KCl. Neuronal responses were monitored with Ca^{2+} imaging technique, by loading the cells with OGB-1-AM. From the baseline fluorescence (not shown) it was possible to identify the contribution of single neurons and associate them to different regions of interest. The activity was monitored by calculating the value of DF/F over time. Cells were first monitored for few minutes before the stimulation in order to obtain a control of the spontaneous activity (**Figure 2.11d**, left traces, numbers 1 and 2 refers to the cells indicated in **Figure 2.11c**, left). After this period, a single liposome with a suitable volume was selected in the reservoir by visual inspection. The liposome could be trapped with the optical tweezers, and by moving the microscope stage it could be positioned at the location of interest as indicated by the arrow in **Figure 2.10c**. The liposome was then cut by UV dissection while monitoring fluorescence signals from the neuronal culture. In order to avoid any disturbance on the measurements of fluorescence emission from the Ca^{2+} dye, fluorescein was not included in these experiments. Following the dissection of the liposome, the time dependence of DF/F mediated over the different cells showed a large increase, followed by a return on the baseline level (**Figure 2.11d**, right) denoting a depolarization induced Ca^{2+} influx originated by the release of KCl. DF/F images (**Figure 2.11e**) were also calculated at different time points (t1, t2, t3, indicated in **Figure 2.11d**, right). These data show the distribution of activation within the area corresponding to the neuronal cells. Differences in cell responses (**Figure 2.11d, e**) can be ascribed to the heterogeneity of the intrinsic electrical properties of the neurons present in the cultures and to the presence of both inhibitory and excitatory synaptic connections that influence the electrical activity. Altogether these results confirm the possibility of focal delivering chemical stimuli to neuronal cells through release from liposomes. In order to exclude artifacts from the UV photolysis of the liposomes, control experiments were done by delivering PBS from liposomes. No response was observed after the PBS release, induced by UV pulse (**Figure 2.12**). This

control also excluded the possibility of any effect of the specific lipid composition of the liposomes on neurons, as membrane-distorting effects.

The possibility of using liposomes as vectors for local stimulation of hippocampal primary neuronal cultures, was thus assessed. A main advantage of the method is the possibility to accurately measure the volume of the liposome, that scales from femtoliters to picoliters for liposomes ranging from 1 to 10 μm, and consequently to estimate the amount of molecules released, given the concentration. The time precision of delivery is sub-milliseconds, although it must be taken into account the distance from the delivery point to provide a correction of both the actual concentration and precise occurrence of the stimulus.

Another advantage consists in the procedure of liposome production and encapsulation that is very simple and does not require expensive equipment and heating. Thus, proteins can be easily encapsulated within liposomes without affecting their structure and biological activity.

2.2.6.2 Effects of Netrin-1 and Semaphorin 3A on growth cones

We probed chemotaxis of single neurons, induced by signaling molecules which were optically delivered from liposomes in the neighborhood of growth cones. Two proteins were tested in our experiments: Netrin-1 and Semaphorin 3A (Sema3A).

To preclude potential leakage/diffusion of molecules out of the liposome, with the subsequent effect on the neuron morphology, we performed a second type of control experiments. The liposome filled with the protein of interest was positioned and held near the growth cone for more than 5 minutes before the liposome photolysis. Examining visually the neuron, we controlled that no significant changes of the neuron morphology occurred. Afterwards, we studied the guidance effect of the Netrin-1 molecules released from the liposomes. The liposome was positioned near a neurite, as shown in **Figure 2.13**, and its content released by laser photolysis. To see the effect induced by the Netrin-1 molecules, the neurite's growth cone was monitored for 5 minutes after the molecules release, recording images every 30 seconds. From **Figure 2.13** a neat activation of the growth cone movement and the neurite progression toward the liposome location can be observe, demonstrating the chemotaxis effect. The growth of the neurite was about 10 μm after 5 minutes.

In order to replicate the same experimental conditions we tried to select liposomes with the same diameter and position them at the same distance from the neurite. The behavior observed was similar and reproducible in all the different experiments (**Figure 2.14a**). The neurite movement was clearly accentuated after the release of Netrin-1 molecules and it was directed toward the liposome location. A plot of the edges of growth cones before and after the delivery of the stimulus highlights this effect. In particular, in **Figure 2.14b** in green the shape of the structure at the beginning of the time laps is drawn, and it is superimposed to the shape of the growth cone (in red) at the end of the period. Movements before the photolysis of the vesicle (-60s and -10s) are compared to movements after the breakage of the liposome (-10s and 240s). In the presented case, small rearrangements are observed before the stimulation, while after it occurred, a difference in the growth cone shape can clearly be noticed.

The effect of Netrin-1 is even more evident when we plot the distance (*D*) between the vesicle and the nearest tip of the growth cone over time (**Figure 2.14c**). Although only small oscillations are visible before the photolysis of the liposome, after the delivery of the stimulus a clear trend can be noticed: *D* decreases, indicating that filopodia of the growth cones are closer to the point of release. The effect of Netrin-1 on growth cones is really fast, since the navigation is affected starting from the very first seconds after the photolysis and it lasts for the following four minutes. Afterwards, in some cases (**Figure 2.14c** blue and green lines) it looks like the effect disappears and the growth cone start to develop

also in the opposite site with respect to the releasing point. This is not surprising, since it is highly possible that after such a long time no more diffusing molecules are present in the area of interest. While some of them could have been kicked out by diffusion processes, other ones could have been endocyted by the stimulated cell.

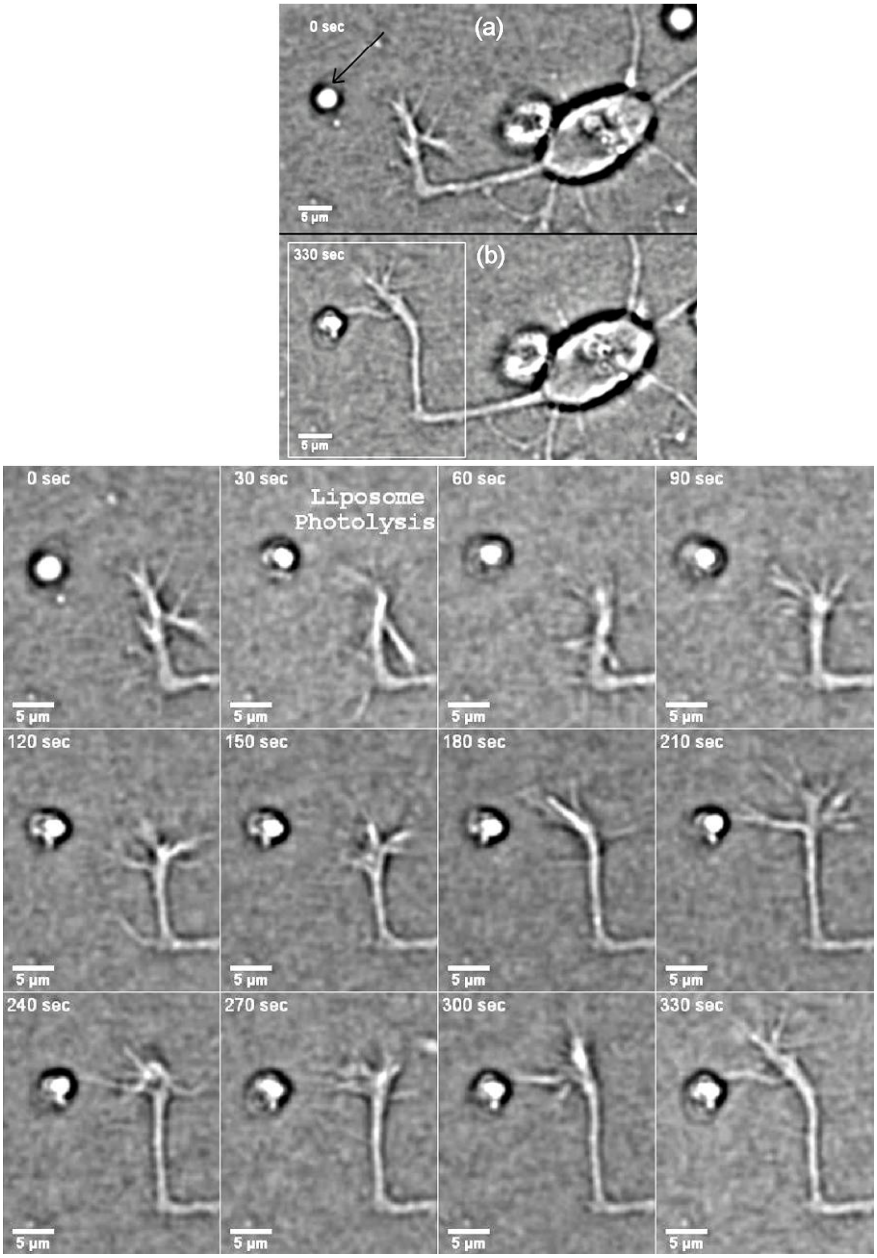

Figure 2.13: Neurite guidance by Netrin-1 released from a micrometric size liposome. Netrin-1 concentration was 5µg/mL. (**a**) A liposome (indicated by the black arrow) is positioned near the neurite of a neuron. The image was taken 30 seconds before liposome photolysis. (**b**) Neurite development 5 minutes after the release of the Netrin-1 molecules from the liposome. The progression of the region marked by the rectangle is shown below (from Pinato et al., 2011a).

Sets of experiments using Sema3A were performed in the same conditions as Netrin-1. In this way, a further control of the technique is provided, since Sema3A has opposite effects with respect to Netrin-1. As expected from literature, Sema3A was repellent and it induced both collapse (**Figure 2.16a**) and turning on the opposite side with respect to the releasing point (**Figure 2.15** and **Figure 2.16c**). In the case of collapse, the number of filopodia diminished and the lamellipodia retracted. In the second case an

expansion was observed, but in a direction different from that pointing towards the location of the vesicle (**Figure 2.15** and **Figure 2.16c**). Also in this case, the edges of the growth cones have been drawn, in order to compare the shape before and after the stimulation (**Figure 2.16b** and **d**). As in the case of Netrin-1, small differences are observed before stimulation, while after the delivery of Sema3A the cells are clearly departing from the liposome. The plot of the distance (*D*) from the vesicle to the nearest tip of the growth cone over time (**Figure 2.16e**) shows again only small oscillations before the photolysis of the liposome. After the release of Sema3A, *D* increases indicating a departure from the source of the gradient. As in the case of Netrin-1, the effect starts soon after the UV pulse and lasts for at least 4 minutes. Only in one case (**Figure 2.16e** red line) the cellular response is delayed of about 1 minute.

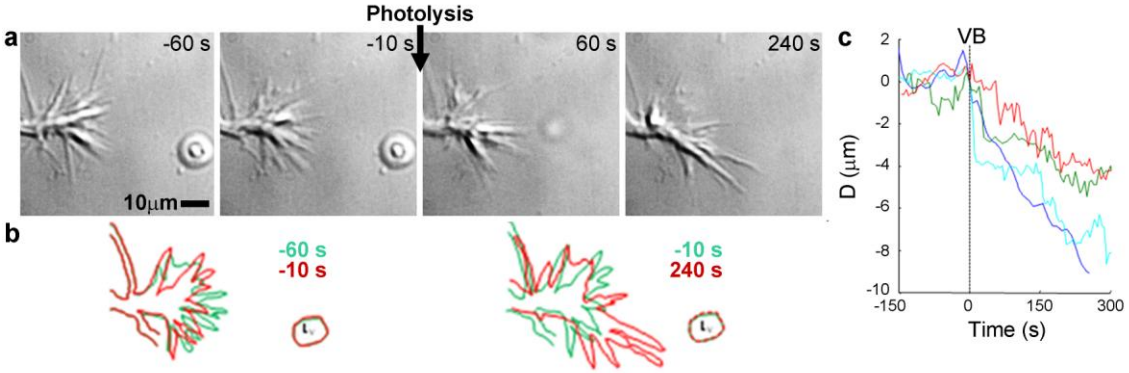

Figure 2.14: The release of Netrin-1 from vesicles induces attractive turning. (**a**) DIC images of a GC before Vesicle breaking (VB) (-60 s and -10 s) and after VB (60 s and 240 s). (**b**) Profiles before VB of the GC at -60 s (green) and at -10 s (red) (left). The GC before VB explored the environment, but after VB grew clearly towards the vesicle, as shown by its profile at -10 s (green) and 240 s (red) (right). In this experiment the laser pulse completely broke the lipid vesicle. The estimated number of molecules (N_{mol}) released was 1750. (**c**) Time evolution of the distance between liposome and the nearest tip of the GC for 5 different experiments. The vertical broken line indicated the time of VB. Following VB the GC started to grow with a delay varying from 20 to 60 s. From Pinato et al., paper in preparation.

The chemotactic effects of the two proteins are really fast. Thus, they can be mediated only by local signaling triggered by the two proteins, and caused by changes in the cytoskeletal structure. Indeed, the time scale of the events is not compatible with gene expression and they are fast also for the *de novo* protein synthesis to take place.

It should be considered that the number of molecules released in the experiments was between thousands and hundreds thousand. This number depends on the concentration of the rehydrating solution and on the size of the liposome. The huge range of molecules used in the experiments is due to this last parameter, since the choice of vesicles with even slightly different dimensions has a big difference on the number of molecules encapsulated, as this scales with the cube of the diameter.

2.2.7 DISCUSSION

In the field of chemotaxis, the generation of gradients of stimuli has always been a big issue. Many different approaches to tackle this technical limitation have been proposed, but they all require micro- and nano-fabrication facilities, a strong know-how in chemistry or do not allow an easy control of the positioning of the stimulus.

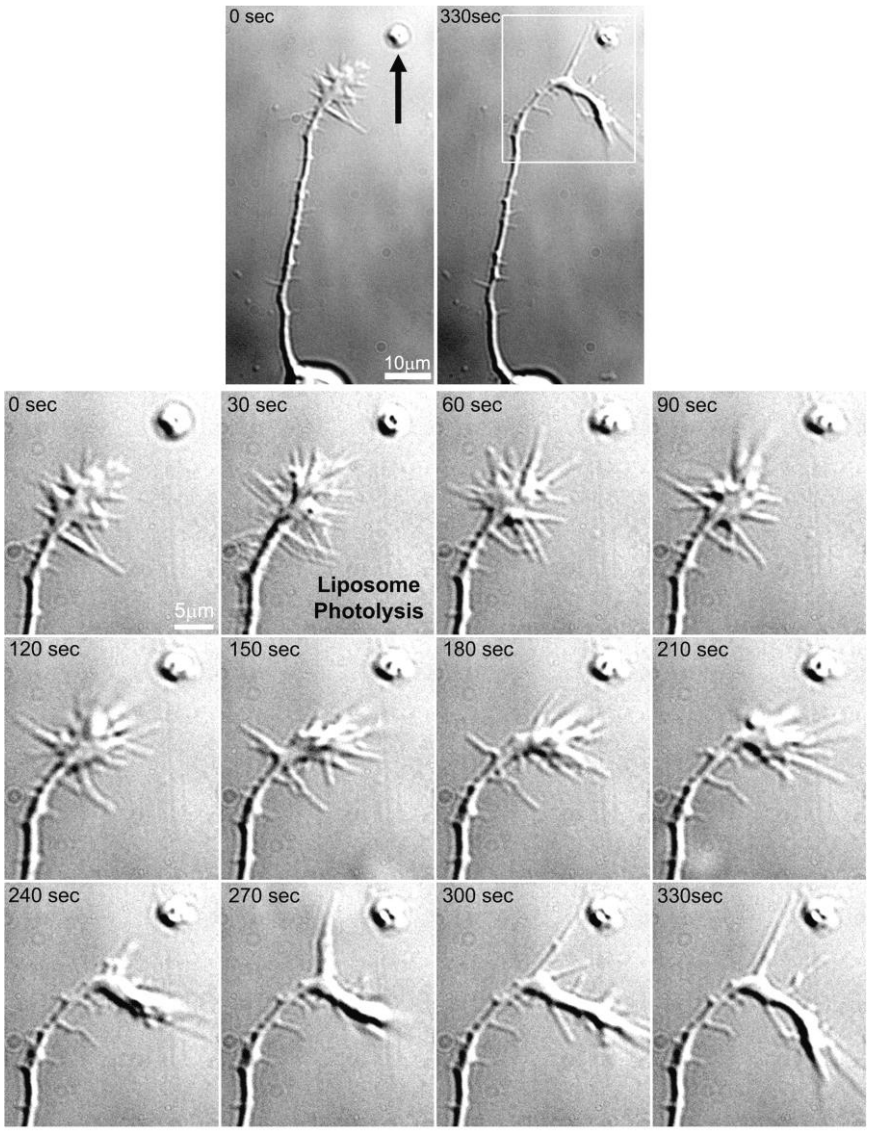

Figure 2.15: Neurite guidance by Sema3A released from a micrometric size liposome. (**Upper panel**) A liposome (indicated by the black arrow) is positioned near the neurite of a neuron. At 30 sec (2nd frame) the photolysis takes place. (**Lower panel**) Time laps and enlargement of the area are indicated in the upper panel

A new, robust and simple technique for the local stimulation of neurons with gradients of molecules was developed. No constraints are placed to the choice of stimulation site: the position of the vector can be decided according to the cell's morphology and to the biological issue that has to be observed. The liposome technology allows the delivery of almost any molecule with a high spatial and temporal resolution. Indeed, both ions and molecules encapsulated within liposomes induced an effect on neurons (**Figure 2.11** and **Figure 2.14**).

With respect to other vectors used for the generation of gradients (i.e. microsources, Kress et al., 2009), liposomes do not require a particularly trained operator for their preparation. Indeed, their preparation is really simple and does not require long time. Moreover, the experimental conditions in which liposomes are prepared allow the encapsulation of proteins without affecting their biological activity. In addition, molecules should not be chemically modified with caging groups that may have unwanted effects on cells (Canepari et al., 2001). It is not possible to rule out the possibility that lipid molecules reach the cell and alter its activity, influencing the experimental responses. However, this risk

is low since the photolysis of the liposomes does not destroy them but it rather creates temporary holes that close shortly after the end of the UV pulse. We can thus assume that there is no leakage of lipids.

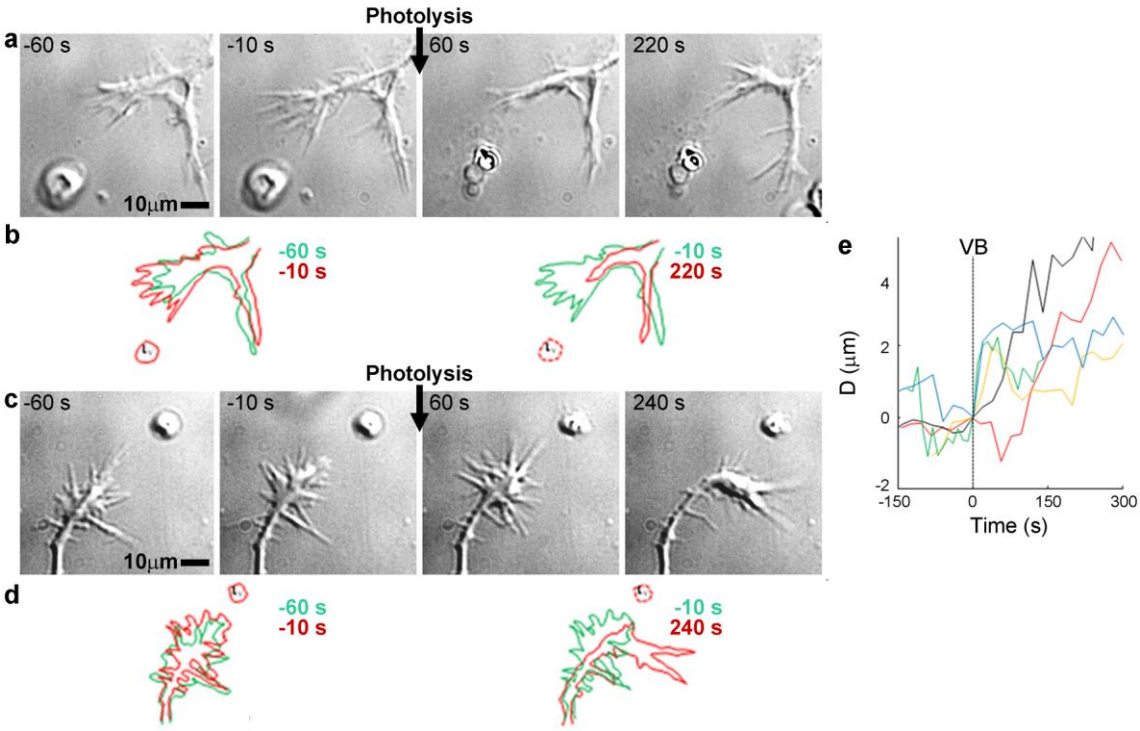

Figure 2.16: The release of Sema3A from vesicles induces either retraction or turning. (**a**) DIC images of a GC before VB (-60 s and -10 s) and after VB (60 s and 220 s). (**b**) Profiles of the GC at -60 s (green) and at -10 s (red) before VB (right). The GC before VB explored the environment, but after VB retracted significantly as shown by its profile at -10 (green) and 220 s (red) (left). The estimated average number of Sema3A molecules inside the vesicle (N_{mol}) was 2500. (**c**) The same as a, but in this case the GC 2 minutes after VB turned away from vesicle. (**d**) As in b but profiles obtained from the GC shown in c. In this experiment N_{mol} was 540. (**e**) Time evolution of the distance (Dist) between liposome and the nearest tip of the GC for 5 different experiments. The vertical broken line indicated the time of VB. Following VB the GC started to retract with a delay varying from 20 to 120 s. From Pinato et al., paper in preparation.

The spatial resolution that can be achieved with the proposed approach is really high with respect to that of ejection systems or microfluidics platforms. The former may allow a higher temporal control but the diffusion of the molecules occurs over large areas. The diffusion of the molecules, moreover, is present both in front and on the back of the target. Hence, the readout of the experiments can be unclear. The main drawback of microfluidic platforms is flexibility: the geometry of the system cannot be changed in real time according to the shape of the cell. The position of the cells can be guided treating the surface but direction and exact location of the stimulus cannot be chosen.

Lastly, the instrumentation required (i.e pulsed UV laser and continuous wave IR laser for the trapping) is cheaper that the systems with similar characteristics (2 photon uncaging).

The proposed technique was initially validated with KCl, that causes a strong depolarization in neurons and an increase in Calcium levels (**Figure 2.11**). In this first step the goal was not a high resolution delivery, but the evaluation of the releasing efficiency. Molecules were able to travel in the medium and stimulate cells about 10 μm distant. This can also explain the delayed (5-10 seconds) cellular response observed in the Calcium dynamics. Moreover, we could not evaluate the encapsulation

efficiency of KCl. We assumed that the concentration of the molecule within liposomes is the same of the hydration solution but it likely is slightly lower.

The steric volume occupied by proteins is, obviously, larger than the one occupied by KCl. Thus, the fact that also proteins can be encapsulated within liposomes is not straightforward. The experiments with Netrin-1 and Semaphorin 3A demonstrated that also large molecules can be used and their biological activity is not affected by both the protocol for the preparation of vesicles and the optical manipulation (**Figure 2.13** and **Figure 2.15**). The high resolution of the technique was proven in these experiments, by placing the liposomes exactly in the desired position with respect to hippocampal growth cones and namely about 45° away from the direction of development of the structure. As expected from literature, Sema3A showed a repellant behavior while Netrin-1 was attractant. In the case of Netrin-1, we can assume that the receptors which were activated, were dimers of DCC. However, further experiments are necessary to confirm this hypothesis.

It should be noticed that Netrin-1 had attractive effects in all the experiments that were performed. We cannot exclude that this positive response is influenced by the dynamics of Netrin-1 release. Indeed, when stimulated with high amounts of proteins, growth cones can desensitize endocyting the receptors (Piper et al., 2005). The number of molecules released with liposomes is probably lower that the other approaches and this fact may be an explanation for the different observed outcomes.

In conclusion, we demonstrated that, beside beads, also liposomes can be used as vectors for the local delivery of molecules, being them small molecules or entire proteins. This technique shows a high flexibility both in terms of molecules that can be used and in terms of positioning of the stimulus. Liposomes permit also the use of different concentrations of stimulus by simply changing the concentration of the hydration solution or choosing larger vesicles.

2.3 NANOSIZED VECTORS

Vectors developed in the previous chapters are micron-sized vectors, which can be used for the delivery of molecules. However, the fate of these molecules cannot be investigated, since we cannot image them. Indeed, ligands may remain at a surface level or be endocyted and ultimately transported to different cellular compartments. Visualization of these processes requires single molecule sensitivity, which cannot be provided by organic dyes. On the contrary, quantum dots are bright, photostables nanoparticles, which can be bound to a molecule of interest, allowing its visualization in live imaging experiments. For this reasons we decided to use quantum dots nanovectors to track the retrograde transport of BDNF, that undergoes endocytosis through its receptor TrkB but whose transport dynamics are unknown.

2.3.1 QUANTUM DOTS: BIOLOGICAL APPLICATIONS & TOXICITY

Quantum dots (Qdots) are nanocrystals with peculiar properties, which are given by their small dimensions in all the three dimensions and that change with their size. Qdots have a core of semiconductor material (cadmium mixed with selenium, tellurium or sulfur) and semiconductor shell, that protect the core against surface oxidation and leaching of toxic ions. Moreover, the shell serves as platform for ligand exchange and bioconjugate reactions. Finally, a coating of the surface with amphiphilic or hydrophilic molecules is possible. This coating makes Qdots biocompatible and allows their functionalization, which can be achieved by conjugating reactive biomolecules (**Figure 2.17a**).

One of the most valuable properties of Qdots is their fluorescence spectrum, which renders them as optimal fluorophores. The energy of the emitted photon is determined by the size of the quantum dot due to quantum confinement effects. This means that they have a size-dependent tunable absorption and emission in visible and near IR regions.

Other peculiarities that make Qdots such an useful tool in biology are the brightness, the photostability, the narrow emission and broad absorption bands, the large one- and multi-photon absorption cross-section and their dimensions, that allow the precise localization of single crystals (for reviews see Biju et al., 2010; Pinaud et al., 2010).

Qdots can be covalently or non-covalently linked to the molecule of interest (antibodies, proteins, nucleic acids), allowing the labeling of proteins, cellular structures and organelles and providing a high signal-to-noise ratio.

The simplest application of Qdots in biology is their use in immunohistochemistry experiments on fixed samples. This application was proposed by Burchez (Bruchez et al., 1998), who used Qdots to detect actin filaments in cultured fibroblast. Later on, not only single- but also multiple staining have been performed. Indeed, different sizes of nanocrystals may be excited with monochromatic light, resulting in many emission colors that may be detected simultaneously (Zahavy et al., 2005)(for reviews see Byers and Hitchman, 2010; Chan et al., 2002). Immunohistochemistry experiments rely on the combination of biotinylated primary/secondary antibodies and streptavidin coated Qdots. The same approach can be used in flow cytometry (Wu et al., 2007). Qdots–labeled oligonucleotide probes were used in fluorescence *in situ* hybridization (Pathak et al., 2001) not only for qualitative experiments but also for quantification (Xiao and Barker, 2004), and were used to detect both DNA or RNA.

Beside their applications on fixed samples, Qdots provide a powerful tool for live imaging experiments (Michalet et al., 2005). Qdots have been used in animals for long-term experiments. Large amounts of Qdots can be transferred into live mammalian cells, either by non-specific pinocytosis, microinjection or peptide-induced transport. Labelled cells have been used to study embryogenesis,

cancer metastasis, stem-cells therapy, and lymphocyte homing, without apparently altering function and viability of the cells (for a review on the application Byers and Hitchman, 2010).

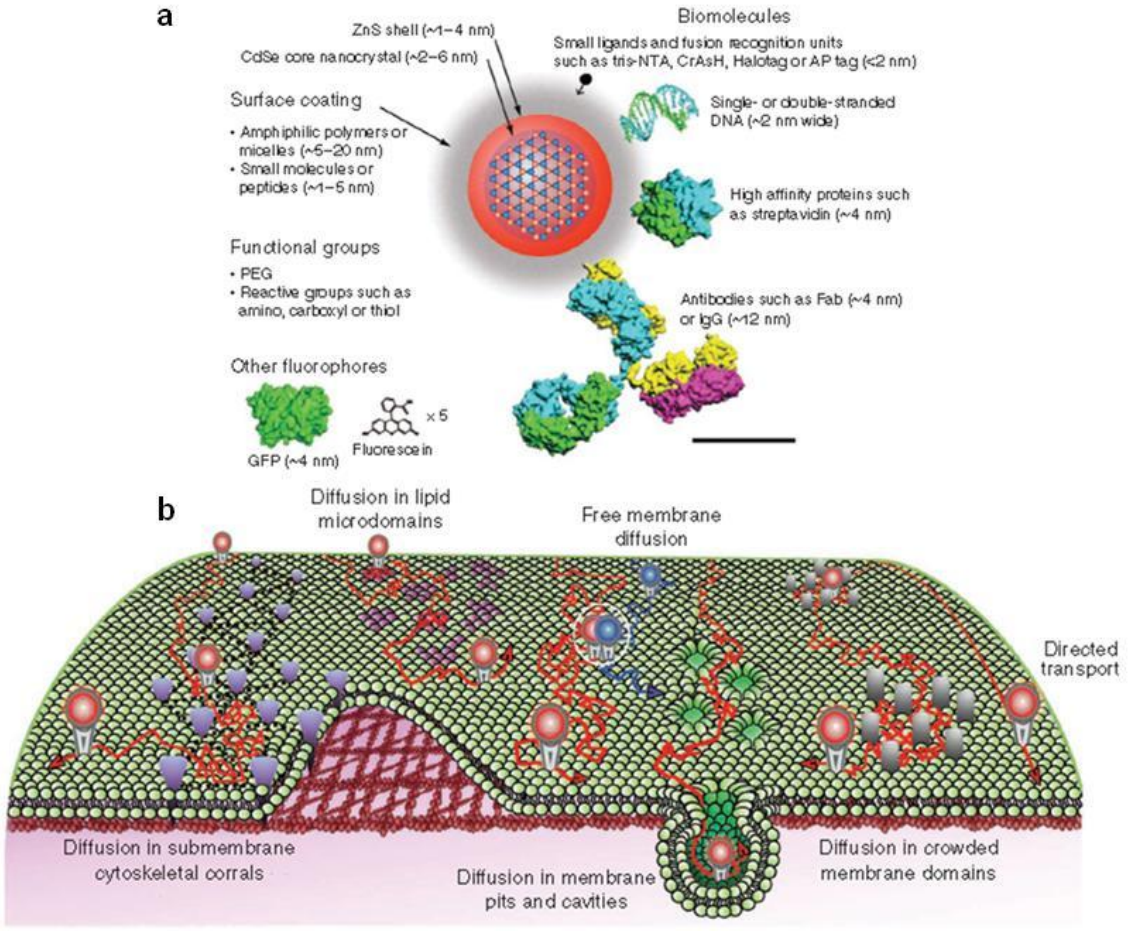

Figure 2.17: Structure and properties of Qdots probes and their use to study membrane dynamics and organization. (**a**) Schematic representation of a Qdots probe. The inorganic CdSe core nanocrystal and ZnS shell (red) dictate the optical properties in a size-dependent manner. Organic surface coatings (gray) such as small molecules, peptides and amphiphilic micelles or polymers provide colloidal stability in biological buffers. Key features of the surface coating include PEG to reduce nonspecific interactions and reactive groups to enable conjugation of biomolecules. Biomolecules such as DNA, streptavidin and antibodies are conjugated to the surface to enable specific binding to biological targets. GFP and fluorescein dye are shown for size comparison. Scale bar, 5 nm. (**b**) Schematic representation of diverse lateral diffusion for plasma membrane lipids or proteins detected by single Qdot tracking (SQT). Constrained membrane diffusion can be induced by a variety of structures and microdomains, including submembranous skeleton corrals, lipid microdomains, membrane pits and cavities, crowded membrane domains or sites of protein/protein interactions (white circle). From Pinaud et al., 2010.

On living cultured cells, Qdots are used for localisation and tracking of molecules, with a particular interest on membrane dynamics and organization. Tracking and quantification of the movement of Qdots-labelled proteins is possible, and it may indicate the cytoskeletal elements that actively participate in the distribution and constrained diffusion of many membrane proteins (Pinaud et al., 2010). The first application was proposed by Lidke, who used EGF-Qdots and revealed a previously unreported mechanism of retrograde transport of endosomes to the cell body (Lidke et al., 2004). Analysis of the lateral diffusion of Qdot-tagged proteins can provide information on protein-protein interaction in

membrane or on structures such as microdomains and membrane cavities (Pinaud et al., 2009) and the entry-exit kinetics of receptors (for a review Triller and Choquet, 2008) (**Figure 2.17b**). In particular, lateral diffusion of surface neurotransmitter receptors is a key pathway to regulate receptor trafficking to and from synapses. Indeed, receptors enter and exit synapses mainly by lateral diffusion within the plane of the membrane while their retrieval and addition from and to the plasma membrane by endo- and exocytotic processes occur largely at extrasynaptic sites. Quantum dots are a useful tool for the labeling and tracking of surface receptors, with an appropriate spatial and temporal resolution (Groc and Choquet, 2008; Groc et al., 2007).

Beside the dynamics at the membrane level, Qdots probes allow real-time visualization of cellular internalization pathways and long-term tracking of molecules directly inside cells. In particular, Qdots functionalized with receptor ligands provide means to both activate membrane receptors and follow their intracellular fate. Endosomal retrograde transport of EGF (Lidke et al., 2005; Lidke et al., 2004) and NGF (Cui et al., 2007; Echarte et al., 2007; Rajan et al., 2008; Zhang et al., 2010) were investigated through this approach.

Given their applications for live experiments and their heavy metal core, the issue of toxicity of Qdots should be taken into account. Many studies indicated that they can be delivered into cells without any detectable effect on cellular viability, morphology or functions, even with long exposure times. As an example, Qdots were injected in mice tail veins and 4 month later there was no evident necrosis in the tissues where they had deposited (liver, skin, bone marrow and other organs) (Ballou et al., 2004). However, their stability may be compromised via photolysis or oxidation. Indeed, extended UV illumination may cause photolysis and release of cadmium ions (Derfus et al., 2004). Another important issue that should be considered when using Qdots is the surface modification: it changes not only the physicochemical properties but also the cytotoxicity (Hoshino et al., 2004). These and other results suggested that there is a dependency on the surface coating in determining the toxicity experienced by the cells, which affects both the level of toxic material released from the nanoparticles and their localisation. Indeed, non-functionalised Qdots often end up in the cytoplasm because of non-specific entry, while functionalised ones reach different organelles, according to the moiety attached (for a review on Qdots toxicity Bottrill and Green, 2011). Overall, it is better to keep the concentration of Qdots as low as possible and to carefully choose their capping.

2.3.2 TRK RECEPTOR RETROGRADE TRANSPORT

Ligand binding stimulates receptors in nerve terminals. Receptors are packed into discrete membrane-bound vesicles that are internalized to form signaling endosomes, with the active domain exposed to the cell cytosol (Beattie et al., 1996). Thus, receptors within endosomes remain catalytically active. These vesicles are then loaded onto microtubule motor transport highways within the cell and continue signaling as they travel through axons to cell bodies. This mechanism works to propagate biochemical signaling cascades within cells and in neurons. Thus, intracellular responses to target-derived neurotrophins can be divided into two categories based on location. The first group constitutes the local signaling that takes place within axons, which might or might not require the formation of signaling endosomes. The second group of responses occurs at the cell bodies, and represents signaling events that emanate from transported, activated receptors within signaling endosomes (Heerssen and Segal, 2002; Segal, 2003). The importance of signaling endosomes is given by the evidence that an aberrant retrograde transport of BDNF is observed in some models of amyotrophic lateral sclerosis (Devon et al., 2006).

The dynamics and kinetics of the trafficking of Nerve growth factor (NGF) and its receptor TrkA have been extensively dissected, using also Qdots. The first paper reporting NGF coupled to Qdots appeared in 2005 and demonstrated that biotinylated NGF bound to streptatividin-Qdots retain

bioactivity, activate TrkA receptors, and initiate neuronal differentiation in PC12 cells (Vu et al., 2005). The same group observed that 15min after treatment Qdots-NGF bind to PC12 cell membranes in a punctuate pattern. At longer times, a majority of membrane-bound Qdots-NGF are rapidly internalized into the cell cytosol (Rajan et al., 2008). Internalized Qdots are contained in microtubule-associated vesicles and possess transport properties that reflect TrkA receptor dynamics (Sundara Rajan and Vu, 2006).

The dynamics of the retrograde transport of NGF in the processes of differentiated PC12 cells were analyzed by Echarte and colleagues using streptavidin-Qdots coupled to monobiotin-NGF (Echarte et al., 2007). Authors demonstrated that 10-35% of the Qdot-NGF-receptor complexes were mobile and had a bidirectional step-like motion. This trafficking requires intact microtubules and has a mean velocity of 0,15 μm/s on individual runs and a net retrograde speed of 0,054 μm/s.

At the same time Cui et al. investigated the retrograde transport of NGF in compartmentalized cultures of rat dorsal root ganglion (DRG) (Cui et al., 2007). Streptavidin-Qdots coupled to NGF with 3 biotin monomers were used. They saw a "stop-and-go", unidirectional retrograde motion, even if short-distance anterograde movements were occasionally observed. The average speed was 1,31 μm/s. The authors also saw that the majority of NGF-endosomes contain only a single NGF dimer and have 50-150nm diameter.

Later on, the same tool was used on microfluidic devices to analyze the effect of the temperature on the retrograde transport (Zhang et al., 2010). In these devices, cell bodies and axon termini of DRG cells can be controlled separately and Qdot-NGF showed again a movement exclusively toward the cell body with a characteristic stop-and-go motion. The rate of retrograde transport decreased exponentially with temperature.

Although the dynamics of TrkA trafficking have been so exhaustively studied, little information is available on the TrkB dynamics. Recently superparamagnetic nanoparticles (MNPs) functionalized with TrkB agonist antibodies were used. MNPs were endocytosed into signaling endosomes by primary retinal ganglion cells that activate TrkB-dependent signaling, gene expression and promote neurite growth. These MNP signaling endosomes are trafficked into nascent and existing neurites bidirectionally (Steketee et al., 2011).

Thus, we want to study the transport of the TrkB-BDNF complex in hippocampal neurons exploiting the Qdots technology, since it might be different from the one observed in DRG and it would unveil new aspects of the cellular response to BDNF.

In order to be as similar as possible with the experiments performed using beads as vectors for local delivery, in which the protein BDNF was covalently attached to carboxylic groups present on the surface of beads, we decided to use carboxylated Qdots.

These Qdots have been used to study the kiss-and-run process, a nonclassical mode of fusion wherein vesicles fuse transiently with plasma membrane to release neurotransmitter and are quickly recaptured on site without loss of shape and possibly other aspects of their identity (Zhang et al., 2007; Zhang et al., 2009). Qdots with carboxyl-exposed coating were seen to bind to neuronal processes in strong preference to neighbouring glia. Moreover no significant effect was observed in EPSC (evoked post-synaptic current) amplitude at synapses loaded with Qdots or sham-treated (Zhang et al., 2007).

2.3.3 MATERIALS AND METHODS

2.3.3.1 QUANTUM DOTS FUNCTIONALIZATION

Qdot® 655 ITK™ carboxyl quantum dots were purchased from Invitrogen (cat. Q21321MP). EDAC, BDNF, and BSA were the same as the one used for beads functionalization (see **paragraph 2.1.3.2**). Coupling was performed in borate buffer 10mM pH 7.4 in glass vials, at room temperature (RT) and under shaking. After the reaction of the protein with Qdots (details will be described in **paragraph 2.3.4.1**) the conjugates were filtered through ultrafiltration units with 100 kDa cutoff (Millipore, Amicon Ultra-2 Centrifugal Filter Unit with Ultracel-100 membrane, cat. UFC210024PL). Qdots were washed 5 times with 500 µL borate buffer 50 mM pH 8.3 (boric acid and borax, 50 mM each) and centrifuged 5 min at 25°C and 4000 rpm. Elution was performed by inverting the ultrafiltration units and spinning 2 min at 1000 rpm.

Borate buffers were prepared starting from 200 mM sodium borate and 200 mM boric acid stock solutions. The two solutions were mixed together until the desired pH was reached. Stock solutions, which were 200 mM, were then diluted to 10mM or 50 mM with de-ionized water.

The reaction was controlled in 0,5% agarose gel electrophoresis, run at 80 V. For dot blot experiments, a drop of solution was placed on a nitrocellulose membrane. Membrane was hydrated 30 min in PBS. Then 45 min at RT with 2% blocking solution (Amersham ECL™ Advance Western Blotting Detection Kit) were performed, followed by 1h incubation with primary antibodies in the same buffer (anti-BSA Sigma 1:2000; anti-BDNF N20 SantaCruz 1:1000). After 3 washes 10 min each in 2% blocking solution, incubation with secondary antibodies conjugated to HRP (1:10000) was performed. Subsequently, membrane was washed 3 times in blocking solution and once in PBS. For the detection ECL or ECL Advanced (both Amersham) were used.

2.3.3.2 CELL CULTURE AND TRANSFECTION

Primary hippocampal neurons were prepared as previously described (**paragraph 2.1.3.1**).

SHSY-5Y cells were grown in DMEM medium supplemented with 10% FBS and 5% Penicillin/Streptomycin (all reagents from Euroclone). Cultures were grown in a 5% CO_2-humidified incubator at 37°C.

For transfection experiments, cells were plated in 24-well plates. Growing medium was replaced just before the transfection with a medium without antibiotics. Transfection was performed using Lipofectamine 2000 (Invitrogen, cat 11668-019) (2 µL in 50 µL MEM) and 1 µg DNA (diluted in 50 µL MEM). After 5 min incubation at RT, the two solutions with Lipofectamin and DNA were mixed and added to the cell culture 20 min later. Medium was replaced with complete DMEM 2-5h after transfection.

2.3.3.3 LIPOSOME PREPARATION, MANIPULATION AND IMAGING

Liposomes with Qdots encapsulated inside were prepared according to the protocol described in **paragraph 2.2.5.2**. Manipulation and imaging were performed on the same setup described in **paragraph 2.2.5.2.**

2.3.4 RESULTS

Several issues should be considered when using Qdots as nanovectors for tracking of BDNF retrograde transport. First of all, BDNF coupling to Qdots should be optimized, using a reaction that does

not alter the biological activity of the protein. Later on, our imaging capacity of single Qdot should be tested, as well as the possibility of delivering small amounts of nanocrystals, in order to reduce their toxic effects.

2.3.4.1 Optimization of Qdots functionalization

In order to use Qdots for the tracking of single molecules, it is necessary to generate a bioconjugate, in which the molecule of interest is linked to the reporter (the Qdot). Usually, streptavidin-Qdots are bound to biotinylated proteins. The use of this approach has two main drawbacks: firstly, even if the binding of streptavidin to biotin is strong, the protein is not covalently bound to the Qdot so it may detach from it under certain conditions. Secondly, the dimension of the bioconjugate becomes larger and this feature may interfere with the endocytotic process.

Thus, the first goal was the direct coupling of the desired proteins (BSA and BDNF) to the carboxyl-Qdots. The chemistry used for the binding is the same used for silica beads, since we demonstrated that it does not alter the biological activity of BDNF (**Figure 2.3**). Hence, the carboxylic groups present on the surface of Qdots should form amide bonds with the amines of proteins. This reaction was performed in presence of the coupling reagent EDAC. A strong scale-down of the reagents' quantities with respect to the manufacturers' protocol was required given the small amounts of BDNF available (1 µg) and thus new experimental conditions were tested. To be sure that every Qdot had at least one molecule crosslinked to its surface, we used a ratio 1:3 between Qdots and protein.

First of all different EDAC concentration were tested and the best one was 200 µg/mL (data not shown). Then, different incubation times were tested, namely 30 min, 60 min, 90 min, and 120 min. This test was performed using 1 µg of BSA (which corresponds to 9 x 10^{12} molecules) and 0,6 µL of Qdots stock solution (3 x 10^{12} nanocrystals) in a total volume of about 120 µL. The reaction was performed as follows:

- 0,6µL Qdots stock solution 8µM;
- 10µL BSA 100ng/µL diluted in borate buffer 10mM pH 7,4;
- 90µL borate buffer 10mM pH 7,4;
- 18µL EDAC 10mg/mL (in water).

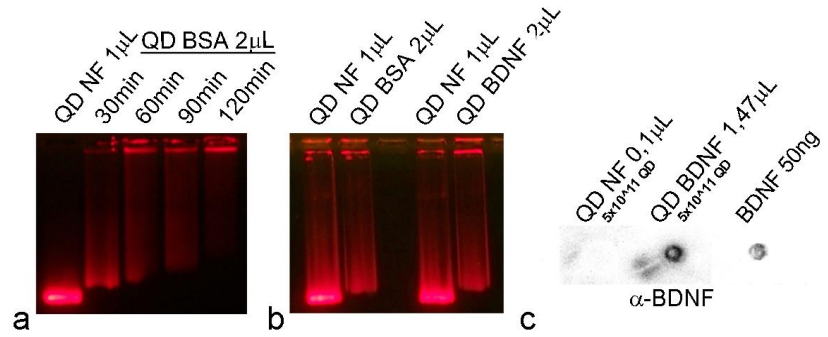

Figure 2.18: Qdots functionalization. (**a**) Test of different functionalization times. QD NF: Qdots non-functionalized. QD BSA: Qdots functionalized with BSA. (**b**) Successful functionalization of Qdots with both BSA and BDNF (QD BDNF) proven in agarose gel electrophoresis. (**c**) Dot blot of Qdots functionalized with BDNF.

Following the reaction, bioconjugates were washed on ultracentrifugation units, recovered in borate buffer 50 mM pH 8,3 and analyzed using agarose gel electrophoresis. As depicted in **Figure 2.18a**, at all the times tested the electrophoretic mobility of treated Qdots was different from non-functionalized

ones, indicating that the coupling occurred. However, while at 30min a smeared band can be seen, at longer times, the mobility of the bioconjugates decreases, indicating that larger aggregates are forming. After 2 hr of incubation, most of Qdots cannot even enter the agarose gel matrix and remain in the well, indicating that their dimension is too large. Thus, 30 min of incubation with EDAC was chosen as the best condition.

2.3.4.2 BIOLOGICAL ACTIVITY

We then tested the ability of functionalized Qdots to bind the BDNF receptor TrkB and to be endocyted together with it. To this aim we transfected SHSY-5Y cells (a human derived neuroblastoma cell line) with a TrkB-GFP fusion protein. Cells were incubated 30 min with Qdots before being fixed. Indeed, after half an hour Qdots should be already endocyted (Rajan et al., 2008). Non-functionalized Qdots and BSA-Qdots did not colocalize with TrkB-GFP (**Figure 2.19**), while BDNF-Qdots colocalize with the receptor. This indicates that BDNF-Qdots were endocyted together with the receptor, along the specific receptor-mediated endocytotic pathway. Indeed, Qdots may be brought inside a cell also through other non specific mechanisms, such as phagocytosis. Thus, this images demonstrate the possibility of using Qdots for the tracking of BDNF-endocyted molecules, and hence to study the trafficking of BDNF signaling endosomes.

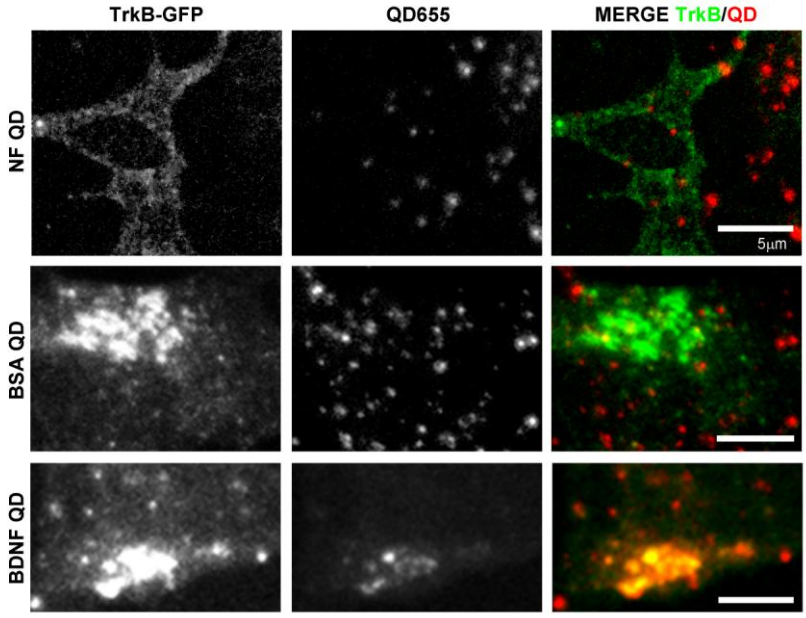

Figure 2.19: BDNF Qdots colocalize with TrkB. SHSY-5Y cells were transfected with TrkB-GFP and incubated 30min with Qdots. Confocal images show colocalization between TrkB and Qdots functionalized with BDNF. On the contrary, no colocalization was observed for non functionalized Qdots or for BSA-Qdots. Scalebar 5µm.

When applied to rat primary hippocampal neurons, functionalized Qdots immediately sticked to the membrane of cells. Most of them exhibited a Brownian motion probably caused by the rearrangements of the membrane (**Figure 2.20**). BDNF-Qdots may attach to TrkB receptors on the surface of cells and thus indicate the dynamics of the receptor, but at the moment we cannot exclude an unspecific binding to the membrane. However, among all these Qdots that do not show a clear trafficking, there are some that travel along the neuronal processes with a well established direction (**Figure 2.20**). Considering their velocity (about 4 µm/s), this particle can only be actively transported inside the cell by cargos that shuttle vesicles. Hence, it is reliable that these Qdots have been endocyted and are within

signaling endosomes. Further experiments are necessary to prove this hypothesis and to study the dynamics of Qdots endocytosis.

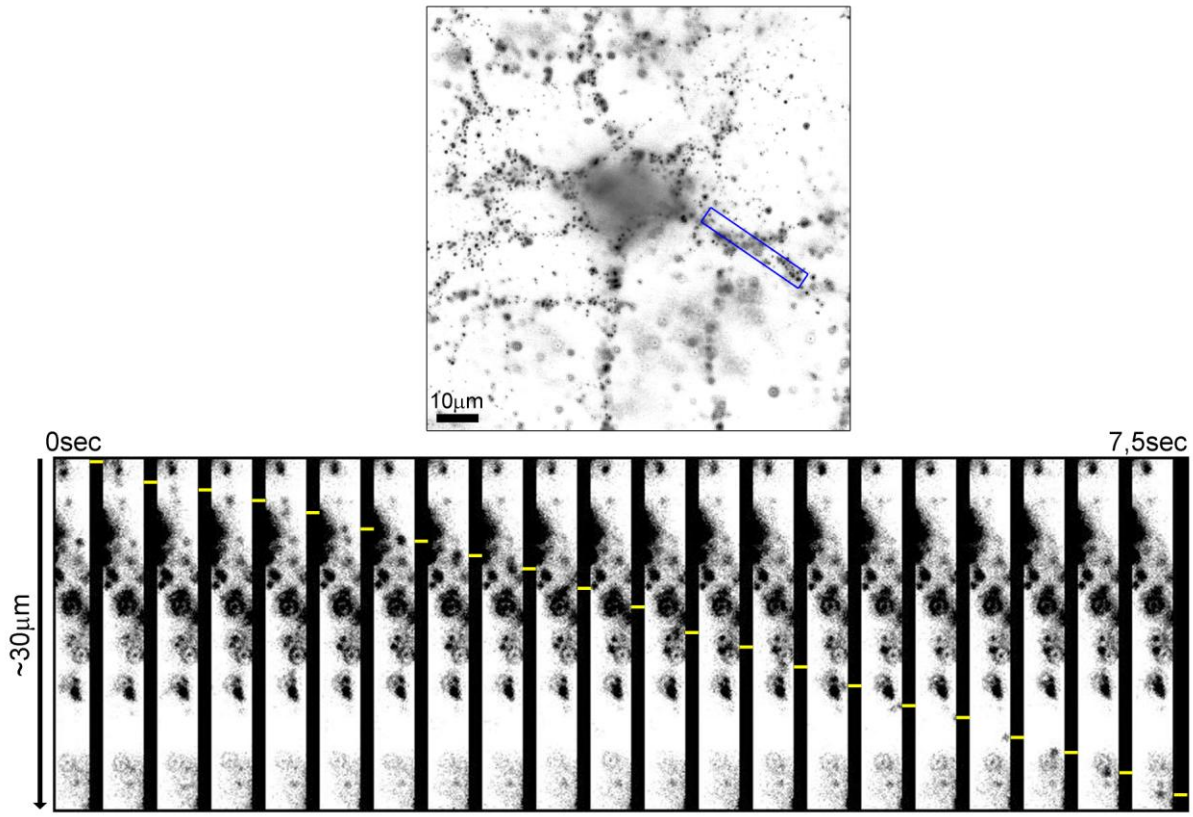

Figure 2.20: Qdots trafficking. BDNF-Qdots bath applied to hippocampal neurons deposit on their membrane and show a confined motion. 10 seconds-long time lapse sequence of the indicated area, in which a BDNF-Qdot is moving along a neuronal process. The position of the Qdot is indicated by the yellow lines.

2.3.4.3 QDOTS DELIVERY WITH LIPOSOMES

Considering the toxic effects that Qdots may have and the fact that they can interfere with the cellular responses, we decided to encapsulate them within liposomes. Indeed, with the technique described in the previous section (**2.2**), we should be able to locally deliver small number (tens) of Qdots. This would allow us to study the retrograde transport from specific cellular compartments of neurons and to reduce the side effects of Qdots. Moreover, delivery of small numbers of nanocrystals would significantly reduce the background of the images acquired and allow an easier analysis of the experiments.

Qdots have already been encapsulated inside liposomes (Sigot et al., 2010). These liposomes were biotinylated-lipid particles (BLP) produced by a detergent dialysis technique, where the inclusion of a small amount of PEG-lipids allowed the self-assembly of stable BLPs. The lipid vesicles produced were 100 nm large and contain 2-5 Qdots. Since BLPs are smaller than the diffraction limit, they cannot be visualized when manipulated in conventional transmission microscopy. Thus, they are not suitable for our purpose, in which micrometric vesicles are needed.

The possibility of encapsulation of nanocrystals in large unilamellar vesicles was successfully tested, as shown in **Figure 2.21**. Liposomes were prepared in the same conditions that were used for Sema3A and Netrin-1 (see **section 2.2** for details). Lipidic films were hydrated with the desired solution (in this case Qdots at the desired concentration, sucrose 100mM and PBS) and shaken. According to the

Qdots concentration and size of liposome, different numbers of Qdots can be placed inside the vesicle. For instance, on average a single Qdot could be encapsulated in a liposome of 1 µm diameter using a Qdot solution of 1 nM concentration. Encapsulation was successful for both non-functionalized nanocrystals (**Figure 2.21A, D**) and functionalized ones (data not shown). Qdots can freely move inside the lumen of the vesicle, as demonstrated in **Figure 2.21D** by the trajectory obtained from Qdot tracking. This free movement supports the hypothesis of an effective delivery by liposome photolysis.

Qdots delivery by photolysis was effectively tested for manipulated liposomes. A liposome was positioned in the proximity of a neuron with optical tweezers (**Figure 2.21E**). It contained several Qdots moving inside its lumen (**Figure 2.21F, G**). The vector was broken by a UV-pulse. Membrane rearrangements occurred (**Figure 2.21H**), suggesting a successful photolysis. Indeed, fluorescence images demonstrated that there were no Qdots left in the vector (**Figure 2.21I**). Bleaching or damaging of Qdots due to the UV-pulse can be ruled out, since some aggregates of crystals attached to the outer membrane of the liposome were still visible.

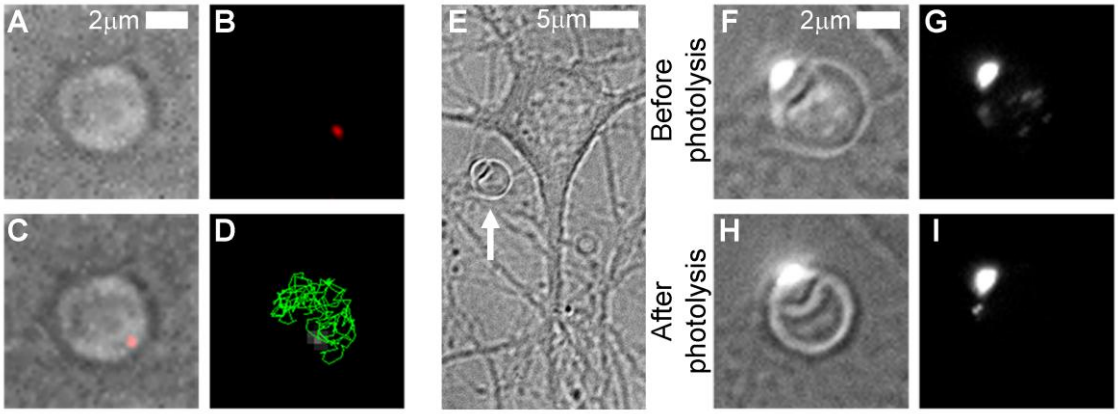

Figure 2.21: Encapsulation of Qdots within liposomes and their release. (**A-D**) A single non-functionalized Qdot is encapsulated in a liposome and it freely moves inside its lumen. Rehydrating solution had a Qdots concentration of 80 nM. (**A**) transmission image of the liposome. (**B**) Fluorescence image of the Qdot. (**C**) Merging of the transmission and fluorescence images. (**D**) Trajectory of the Qdot moving inside the liposome imaged 1 frame every 50 msec for about 15 sec. (**E-I**) Manipulation and release of Qdots from a liposome (250nM). (**E**) Liposome was manipulated with optical tweezers and position at the site of interest. The liposome is indicated with the arrow. (**F, G**) Transmission and fluorescence image of the liposome before the photolysis. Several Qdots can be seen inside the vesicle (G). (**H, I**) Liposome after the photolysis. Some rearrangements in the shape of the liposome occurred, indicating that it was hit by the UV pulse. Moreover no Qdots are detected inside the lumen of the liposome (I).

2.3.5 DISCUSSION

Quantum dots are nanocrystals with exceptional optical properties which are becoming a powerful tool for the study of cellular events at a single molecule level. Qdots brightness, in particular, allows their visualization also with conventional epi-fluorescence microscopy (Pinaud et al., 2010). Moreover, thanks to surface modifications, the coupling of almost any desired chemical group or molecule to their surface is Nowadays possible. These properties make Qdots an extraordinary alternative to organic fluorescence dyes. and permit experiments that were impossible before, such as the tracking of single receptors dynamics.

In the case of neurotrophins, tracking of receptors trafficking may unveil new signaling mechanisms related to the so-called “signaling endosomes”, a cellular mechanism for long distance

communication. These signals are intended to transmit information from the pre-synaptic terminal receiving the secreted factors to its corresponding cell body. These signaling factors are packed into a discrete, coherent, membrane-bounded organelle that moves along the length of the axon via a cytoskeleton-based transport machine (Howe and Mobley, 2004). Among the factors that use the signaling endosomes mechanism, the family of neurotrophins is one of the most interesting, since the signals should travel along the neurites for long distances. While trafficking of TrkA (the NGF receptor) has been characterized in different cell types (Cui et al., 2007; Echarte et al., 2007; Howe and Mobley, 2004; Vu et al., 2005), to our knowledge the retrograde transport of TrkB/BDNF has never been dissected. Therefore, we decided to use the approaches employed for the experiments on NGF (i.e. Qdots) to tackle this questions.

With respect to the papers on NGF, in which the biotinylated protein was coupled to steptavidin-coated Qdots, we decided to directly bind BDNF to Qdots through the formation of amide bonds. In this way, the complex BDNF-Qdots is smaller, and hence its internalization in signaling endosomes should be easier. The ability of our bioconjugates to be internalized together with TrkB receptor was successfully tested in transfected SHSY-5Y cells. However, further experiments should be done in order to study the dynamics of this process and to define the best time point at which specific endocytosis occurs not only in cell lines but also in primary cultures.

Considering the toxic effects that Qdots may have on cells (Bottrill and Green, 2011), the delivery of small amounts of nanocrystals was also investigated. Optical trapping of single Qdots was already demonstrated (Jauffred and Oddershede, 2010) but for our purpose it is not feasible for two reasons: first trapping of a single Qdot is not easy (usually more Qdots are attracted in the trap), second if one wants to visualize the Qdot, only fluorescence light should be turned on. However, without transmission imaging the precise delivery at the desired cellular compartment is not possible. Finally, considering the fact that not every BDNF-Qdot undergoes internalization, the delivery of more bioconjugates is preferable, in order to increase the chances of success. For all these reasons, we decided to encapsulate Qdots inside the liposome, a well-established technology. In this way, tens of Qdots can be released at the site of interest. The possibility to manipulate Qdots-filled liposomes was experimented, as well as their delivery after the photolysis of the vector with a UV-pulse. Interesting, UV pulses do not affect Qdots fluorescence and therefore this method of delivery can be used.

Concluding, we developed a tool to study the trafficking of BDNF signaling endosomes in primary neurons and minimized the side effects related to the use of Qdots. Additional experiments should be performed for the optimization of the technique. In particular the kinetic of internalization should be studied and the efficiency of neuronal stimulation should be improved. Indeed, sometimes Qdots are released from liposomes following photolysis but they cannot be seen on the neighbor cells. This problem can be related both to the control of the direction of release and to imaging limitations. Indeed, the objectives that were used during the experiments had a small depth of focus and the signal that was coming from parts of the specimen which is out of focus could not be detected. If the Qdot reaches the cell on its top, it might not be detected. However, after the addressing of these problems the technique will be efficiently used for the study of all the different aspects of the biological question proposed. Moreover, the proposed approach can be applied also to microfluidic devices in which cell bodies are physically separated by the axon and hence a better imaging will be possible.

2.4 SUPER-RESOLUTION IMAGING OF GROWTH CONES

Super-resolution fluorescence microscopy was designated as the method of the year 2008 by Nature Methods for its extraordinary impact in biological research. Indeed, it allows the visualization of structures that before could be seen only with electron microscopy. This method is unique in providing enough resolution to highlight features that would otherwise be impossible to distinguish with conventional microscopy. An interesting field of application of super-resolution microscopy is imaging of the cytoskeleton of cells, considering the density and complexity of its network. Within neuronal growth cones, in particular, actin networks or bundles are fundamental, since they establish the shape and morphology of these structures. Hence, super-resolution imaging of growth cones will help researchers to unveil new aspects of their dynamics.

2.4.1 SUPER-RESOLUTION OPTICAL MICROSCOPY: NOVEL TECHNIQUES AND PERSPECTIVES FOR BIO-SAMPLES IMAGING

Fluorescence microscopy is currently one of the more powerful and versatile techniques available for biological studies (Lichtman and Conchello, 2005). Taking advantage of the optical transparency of cells, light microscopy uniquely provides non invasive imaging of the interior of cells in three dimensions (3D). Moreover, it allows the detection of specific cellular constituents through fluorescence tagging (Hell, 2007).

Although the most specifically labelled cellular constituents can readily be detected in a conventional light microscope, the resolution of light microscopy (hundreds of nanometers, see **paragraph 1.3**) is approximately the size of an intracellular organelle. Thus, it is inadequate for dissecting the inner architecture of many subcellular structures. Super-resolution fluorescence microscopy techniques that break the diffraction barrier, improving lateral resolution, have been developed starting from the middle of ‘90.

The most popular super-resolution techniques are SPEM/SSIM (Saturated Pattern Excitation Microscopy or Saturated Structured Illumination Microscopy), STED (STimulated Emission Depletion microscopy), PALM/STORM (PhotoActivation Localization Microscopy, STochastic Optical Reconstruction Microscopy), GSD (Ground State Depletion microscopy) and RESOLFT (REversible Saturable/Switchable Optical Linear Fluorescence Transition) (for reviews on the super-resolution microscopy techniques see Hell, 2007; Hell, 2009; Huang et al., 2010; Leung and Chou, 2011).

The common characteristic of all these super-resolution techniques is the use of reversible switching on and off mechanisms in order to discern objects that are closer than 200 nm. The switching of a fluorescent molecule on or off requires two states: a fluorescent (on) state and a dark (off) state, connected by a transition representing the actual switch (Hell, 2009).

The aforementioned super-resolution techniques can be divided into groups according to the approach used for the illumination and readout. In the ensemble, targeted readout mode, one of the two states (on or off) is established by patterned illumination, which generates a subdiffraction-sized spot at the position of a zero to read out an unknown number of fluorophore molecules. The image is assembled by deliberate translation of the zero. In the stochastic readout mode, a single switchable fluorophore from a random position within the diffraction zone is switched to a stable activated state, while the other molecules remain in dark state. The coordinate is calculated from the centroid of the diffraction fluorescence spot measured by a pixelated detector. The coordinate pops up stochastically depending on where the interrogated marker molecule is located (Hell, 2007). Among super-resolution techniques, only PALM/STORM uses a stochastic read-out. All the other ones have a targeted read-out.

The nature of the switching mechanism is another feature that can be used to classify super-resolution techniques. STED, GSD and SPEM utilize photophysical transitions, while in RESOLFT and PALM/STORM the transition is photochemical. Photophysical transitions are transitions between the different states of the fluorophore, which can be the ground state S_0, the singlet state S_1 or the metastable triplet state T_1. On the contrary, photochemistry transitions, rely on isomerisation processes, in which atoms are relocated or bonds formed and broken.

The maximum achievable resolution can be improved by a factor of ~2 for SPEM/SSIM, while it can be reduced down to few tens of nanometers with the other types of nanoscopy.

The advantages and application fields of super-resolution techniques are evident in particular in the cell biology, microbiology and neurobiology areas, where they helped to solve several biological questions related to colocalization issues or regarding subcellular structures.

2.4.2 STIMULATED EMISSION DEPLETION (STED) MICROSCOPY: PRINCIPLE AND APPLICATION TO CELL IMAGING

The STED principle was proposed in 1994 (Hell and Wichmann, 1994). The basic idea behind scanning STED microscopy is to confine the emission of fluorescent markers to a region that is much smaller than that covered by the diffraction-limited excitation spot. Beside the canonical excitation laser, a second, red-shifted beam (called the STED beam) is applied. This laser has the ability to annihilate the molecular excitation and thereby prevents the molecules from fluorescing. Indeed, it brings an excited fluorophore down to the lowest energy state before it can emit fluorescence signal. The depletion light is applied as doughnut surrounding the excitation laser, in order to de-excite molecules only in the outer region of the excitation spot (**Figure 2.22**). The STED photons act primarily on the excited state S_1, inducing stimulated emission down to a vibrational sublevel of the ground state S_0^{vib} (**Figure 2.22**). Subpicosecond vibrational decay empties S_0^{vib}, so repumping into S_1 is largely ineffective (Willig et al., 2009). STED microscopy has been implemented mostly with pulsed beams, whereby the STED pulses of typical 0.1–1.0 ns duration have followed (shorter) excitation pulses. By the time the STED pulse has vanished, the population of the S_1 is $N(h_{STED}) = N0 \exp(-\sigma h_{STED})$, where $N0$ is the initial population, $\sigma \cong 10^{-16} cm^2$ the cross-section for stimulated emission, and h_{STED} is the point-spread function (PSF) of the STED pulse in photons per area per pulse. This formula assumes that the STED pulse is shorter than the fluorescence lifetime, which is a few nanoseconds for organic dyes. Hence, the fluorescence is reduced by a factor $\eta(h_{STED}) = \exp(-\sigma h_{STED})$.

Using a doughnut-shaped STED pulse with a local zero ($h_{STED}(0) = 0$) implies that the fluorescence emission is unaffected at $r = 0$ but is increasingly suppressed with increasing r (**Figure 2.22, right**). Thus, the STED PSF confines the fluorescence emission to a region that is much narrower than the excitation spot. The effective PSF h_{eff} can be shown to scale with the STED intensity according to the following formula:

$$\Delta r \cong \frac{\lambda}{2n\sin\alpha\sqrt{1+\zeta}}$$

where the intensity I is given as the "saturation factor" $\zeta = I/I_s$. That is, it is given in multiples of the saturation intensity I_s at which the fluorescence drops to 1/e of its initial value. I_s is characteristic of the dye used. Scanning this reduced focal spot through the sample yields images of subdiffraction resolution (Willig et al., 2009).

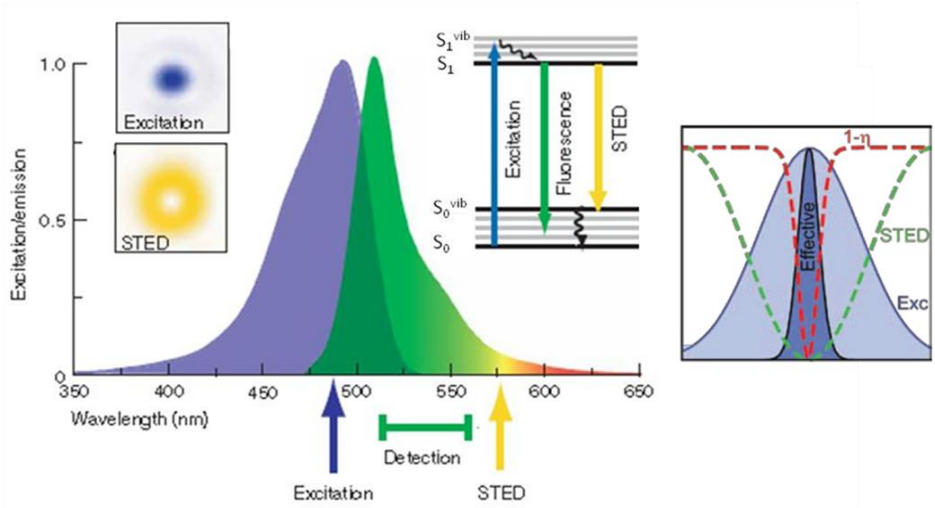

Figure 2.22: STED principle. The STED beam is red-shifted with respect to the excitation beam specific for a certain fluorophore. The detection windows is chosen so that both the excitation and the STED wavelengths are avoided. The shape of the two beams is shown (upper left) as well as the transition between the different energy states they induce. **Right**: breaking the diffraction limit using STED. Normalized intensity profiles of the excitation PSF (exc), STED PSF (STED), De-excitation probability (1-η) and effective PSF. Adapted from Willig et al., 2009; Willig et al., 2006.

STED microscopes can be built using both pulsed or continuous wave (CW) lasers. STED microscopy with pulsed lasers relies on tightly synchronized trains of pulses: excitation pulses of <80 ps duration are typically followed by 250-ps pulses for STED. The 200-fs pulses originating from the laser system have to be stretched by 1,000 folds using optical fibers or gratings and should be synchronized with their excitation counterparts (Willig et al., 2007). CW STED microscopes are easier to implement since no synchronization is required. Indeed, temporal separation between excitation and STED is not crucial as long as the rate of population of the excited state is much lower than the depletion rate (Willig et al., 2007). CW STED, however, needs greater average power than pulsed-STED, since the dye is continuously illuminated.

A reduction in the required power of lasers (Hofmann et al., 2005) can be obtained with REversible Saturable Optically Linear Fluorescence Transition microscopy, which exploits the property of some proteins to be switched on and off at the appropriate wavelength. During illumination with light these proteins change their conformation. In this process they gain or lose their ability to emit fluorescence. Relatively low power intensities are required to induce this conformational changes in proteins (Hofmann et al., 2005).

STED microscopy has been applied in many biological fields. For instance it was used to demonstrate that the native lipid environment is not sufficient for correct Syntaxin 1 (a proteins that defines sites at which secretory granules fuse with the membrane) clustering and that additional cytoplasmic protein-protein interactions are required (Sieber et al., 2006). With STED the diffusion of single lipid molecules in nanosized areas in the plasma membrane of living cells can be detected, allowing the study of lipid rafts (Eggeling et al., 2009). Several are applications of STED in the neurobiology field. For example, STED allowed the mapping and description of the vesicle mobility within the highly confined space of synaptic buttons (Westphal et al., 2008). Actin remodeling in the spines of living brain slices was observed (Urban et al., 2011) as well as living synapses re-shaping (Nagerl and Bonhoeffer, 2010). Finally, very recently STED on living mice was also demonstrated (Berning et al., 2012).

To our knowledge, no super-resolution fluorescence images of cytoskeleton in growth cones are available. Considering the limitation of conventional optical microscopy, two approaches were used to study this structure: electron microscopy (Gordon-Weeks, 1989; Letourneau, 1983; Lewis and Bridgman, 1992) or model organisms which have large growth cones. In particular *Aplysia californica*, a sea slug, has growth cones that are five to ten times larger than growth cones from other species, making them suitable for quantitative high-resolution imaging of cytoskeletal protein dynamics and biophysical properties (Suter, 2011).

Considering our interest in growth cones and the lack of real fluorescence super-resolution images of these structures, we collected STED image of both actin and tubulin. The final goal would be to understand the cytoskeletal rearrangements induces by chemotactic stimuli. However, at the beginning images of fixed samples are required.

2.4.3 MATERIALS AND METHODS

2.4.3.1 GROWTH CONES PREPARATION AND STAINING

Rat hippocampal neurons were kindly provided by the lab of Prof. Dr. Professor Emeritus Erwin Neher (Max-Planck-Institut für biophysikalische Chemie, Göttingen). 10-15 x 10^3 cells were plated on each coverslip.

Neurons were then washed in PBS, fixed in PFA 3% and 0.1% Glutaraldehyde for 15 min, quenched with NH_4Cl 100 mM for 15 min and permeabilized with Triton X-100 0,1% for other 5 min. Then, neurons were incubated with primary antibody (anti-β-Tubulin 1:100, Sigma cat. T5201) in PBS 1 hr at RT. After washing them in PBS, they were incubated for 1 hr at RT with secondary antibody (sheep anti-mouse Atto- 647N 1:100) and phalloidin Atto-590 (1:50, Attotec cat. AD590-81). Samples were then washed three times in PBS, once in H_20 and mounted using Mowiol.

2.4.3.2 STED SETUP

The setup used (described by Bückers et al., 2011) was a STED microscope optimized for colocalization experiments with up to three colors, located at the Max-Planck-Institut für biophysikalische Chemie, Department of Nanobiophotonics, Göttingen (Germany).

The images were recorded with a custom-built STED microscope combining two pairs of excitation and STED laser beams, all stemming from a single supercontinuum laser source. Whereas the excitation wavelengths (570±2 nm and 650±2 nm) were selected from the supercontinuum source using an acousto-optical tunable filter (AOTF, AA Opto-Electronic, Orsay Cedex, France) the STED wavelengths (720±10 nm, 755±15 nm) were extracted using prism monochromators ensuring strict wavelength selections. After filtering the appropriate wavelength ranges, the four beams were coupled into separate polarization-maintaining single mode fibers. At the fiber outputs the beams were collimated and sent to the objective lens. The corresponding excitation and STED beams were combined using dichroic mirrors to give two pairs of beams with orthogonal polarization. The beam pairs were then combined with a polarizing beam splitter cube and coupled into the objective lens (PL APO 100×/1.40–0.7 oil, Leica Microsystems, Wetzlar, Germany). Two vortex phase plates (RPC Photonics, Rochester, NY, USA.) placed into the STED beams followed by a superachromatic quarterwave plate (600–2700 nm, B. Halle GmbH, Berlin, Germany) placed at the back of the objective lens afforded ring-shaped STED foci with a zero-intensity minimum in their centre.

To ensure spatial overlap of the excitation and the STED foci, the diffraction patterns (“point spread functions”) of the four beams were measured sequentially by recording scattered light from gold

nanoparticles (80 nm) as they were scanned through the focal region. The alignment precision was on the order of 5 nm, i.e. below the resolution achievable with the setup.

Since all four laser beams originated from a single source, no pulse synchronization was necessary. Still, the simultaneous arrival of the excitation and the respective STED beam in the sample had to be adjusted by matching the optical path lengths for each pair of beams. On the contrary, the pairs of excitation and STED beams for the two color channels were time-shifted by about 40 ns using optical fibers of different lengths. This pulse-interleaved acquisition scheme enabled the (quasi-)simultaneous recording of both color channels: in addition to the spectral separation photons were assigned to a dye according to their arrival time at the detector. Due to the simultaneous recording of both color channels hardly any shift of the sample was possible during the recording time.

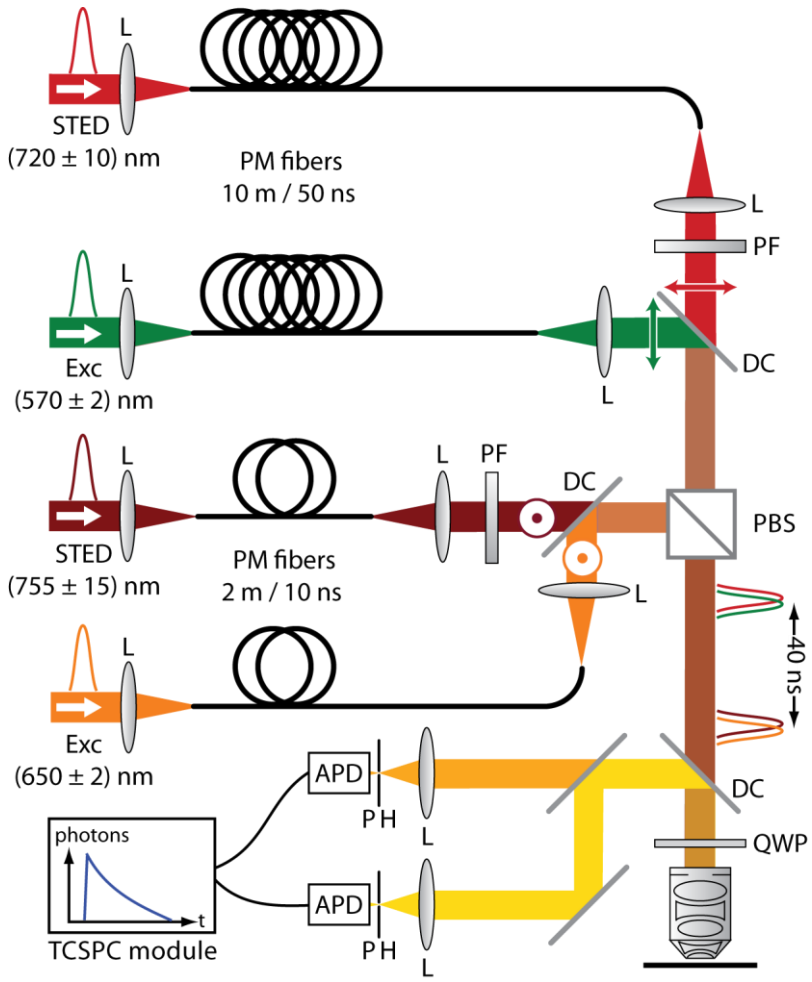

Figure 2.23: Setup of the multi-color STED microscope. From Bückers et al., 2011.

The fluorescence from the two fluorophores was separated from the laser beams with a custom made multiband dichroic mirror (Chroma Technology, Rockingham, VT, USA). It was subsequently split up with a second dichroic mirror (Z635RDC, Chroma Technology) according to the emission maxima of the different dyes, and was finally cleaned up with bandpass and longpass filters (M620/40, M670/40 nm and Z660LP, all from Chroma Technology). The fluorescence was then focused into separate multimode optical fibers (Ø = 62.5 µm, Thorlabs, Dachau, Germany) which served as confocal pinholes. The fibers were attached to single-photon counting modules (SPC-AQRH-13-FC, Perkin Elmer, Salem, MA) which were connected to custom time gating electronics extracting the fluorescence signals following each of the excitation/STED pulse pairs. Optionally, for the acquisition of fluorescence lifetime data, the time

trace of the fluorescent signals was measured by a time-correlated single-photon counting (TCSPC) module (SPC-730, Becker & Hickl GmbH, Berlin, Germany). Typically, images were acquired with pixel sizes of 20 nm × 20 nm and a pixel dwell-time of 1 ms (Bückers et al., 2011).

2.4.4 RESULTS

STED images of cultured hippocampal neurons were acquired in order to unveil features of the cytoskeleton, that are not visible with diffraction-limited microscopy. In particular, we focused our attention on actin a tubulin, the two proteins that determine the morphology of growth cones (see **section 2.2.1** for details on the cytoskeleton of growth cones).

2.4.4.1 ACTIN IMAGING

Actin has two different kind of organization in growth cones: bundles or network (see **paragraph 2.2.1**). Bundles are present within filopodia and actin network in lamellipodia. Actin was stained using phalloidin in primary rat hippocampal neurons the day after plating. At this time point cells haven't yet established a well connected network and hence growth cones are present.

Phalloidin was conjugated to Atto590 dye, which can be used for STED at 690 nm wavelength (Wildanger et al., 2009) and at 720 nm (Bückers et al., 2011). Examples of STED and confocal images can be seen in **Figure 2.24**. Confocal and STED images were acquired subsequently on the same region of interest by simply turning on and off the STED beams. The improvement of resolution given by the STED beam can be immediately appreciated. The resolution achieved with STED imaging was about 70 nm. While in most of the cases with confocal microscopy it is not possible to discern actin bundles within filopodia, STED allows the discrimination of the single bundles. Striking examples are provided in the close-up images (**Figure 2.24C, E, I, K**). In confocal images only a blurred line is present, which turns out to be the signal coming from three (**Figure 2.24C**) or four (**Figure 2.24I**) different bundles when using STED. These bundles can be clearly seen in line scan profile: separate picks can be distinguished in the STED images (**Figure 2.24D, J**), while basically a single pick is observed in confocal images (**Figure 2.24F, L**).

It is however not possible to determine whether actin bundles are composed by a single filament or more than one. However, in some cases, at the base of filopodia, more bundles can be distinguished, even if on the tip of the structure they cannot be seen as separated (**Figure 2.24A, G**, indicated by the solid wedges). In the corresponding confocal images a single, blurry filament is visualized (**Figure 2.24B, H**).

In the growth cone depicted in **Figure 2.24G** the different regions characterizing the structure of the cytoskeleton can be recognized (**Figure 2.24**). In particular, the central domain, can be seen where no signal from phalloidin is present (**Figure 2.24G**, indicated with the asterisk). Close to the C domain, actin arcs of the transition zone (T zone) can be observed (**Figure 2.24G**, indicated with empty wedge). Differently to what was expected from literature, not all the actin bundles seem to originate from the transition zone (**Figure 2.24A, G**). This fact may be due to a lack of sensitivity of the technique, to a larger and less defined T zone or simply to the morphology of the two growth ones, since they have many and closely packed filopodia and almost no actin network. A nice actin network is evident in **Figure 2.26E**, in which a growth cone with a large lamellipodia and almost no filopodia is shown. It should be noticed how, with confocal imaging, the actin network can be appreciated as well. However, the image is not so clear and sharp as the STED one.

2.4.4.2 ACTIN AND TUBULIN IMAGING

STED allows also multicolor imaging. In particular, the setup previously described (**paragraph 2.4.3.2**) has two excitation beams at 570 nm and 650 nm respectively. Hence, we exploited the possibility of using two staining. Besides actin, we marked tubulin, the other key element of the growth cone cytoskeleton. Tubulin was stained according to immunofluorescence protocols with Atto647N, a dye which is highly suitable for STED imaging (Willig et al., 2007). In both **Figure 2.25C** and **Figure 2.26C** tubulin is present in thick fiber (stable microtubules) in the axon shaft and in the C domain. They form dense, parallel arrays, characteristic of axon. Stable microtubules end where the T zone begins. However, in the presented images, the distinction between C domain, T zone and periphery domain (P domain) is not so evident as in the previous case (**Figure 2.24G**). Indeed, even if increasing levels of actin can be observed towards the tip of the growth cones, no actin arcs are visible.

Nevertheless an interesting feature can be noticed in the P domain: thin, dynamic pioneer microtubules are departing from the C domain and pointing towards the tip of growth cones (**Figure 2.25C** and **Figure 2.26C**, indicated with the solid wedges). As expected, colocalization between dynamic microtubules and actin can be observed in some instances (**Figure 2.26E**).

In **Figure 2.25C** another interesting feature is present, and namely branched microtubules. Branched microtubule array is indicative of an actively growing terminal (Conde and Caceres, 2009). Curiously, in this growth cone the C domain is large compared to the P domain and no evident actin organization is present. These signs may indicate the "engorgement", that is the phase in with actin arcs re-orient and T zone is invaded by microtubules of the C domain. In the confocal image of the same structure (**Figure 2.25D**) it is not even possible to see these branching and actin structure appears noisy. On the contrary, STED resolves that actin simply doesn't have an organized structure.

2.4.5 DISCUSSION

Actin and microtubules are highly organized in growth cones and have always attracted the interest of scientists for their complex regulation and dynamics. Fluorescence microscopy provided fundamental hints for their understanding but electron microscopy was necessary for a deeper structural analyses. However, with respect to electron microscopy, far-field nanoscopy requires an easier sample preparation and permits also live imaging experiments. The use of fluorescence imaging is hence preferable.

Structure of the both actin and microtubules in rat hippocampal growth cones was analyzed using STED microscopy. The STED beam allowed an improvement of the resolution, which dropped down to 70 nm. In this way details which were not discernible with confocal microscopy were visualized. The, in particular regarding actin bundles in filopodia and branching of microtubules. Is should be noticed that the actual dimension of actin filaments is of 7 nm, while microtubules are 25 nm large. Hence, an improvement in the resolution in still possible.

To our knowledge these STED images are the first super-resolution images of actin and tubulin structures within growth cones. These data confirmed the possibility of using STED microscopy for the study of cytoskeleton of growth cones. Future experiments will be done on living, stimulated growth cones to analyze the response of actin and microtubules to a defined and localized chemical cue. However, to achieve this goal a different and faster setup for imaging is required.

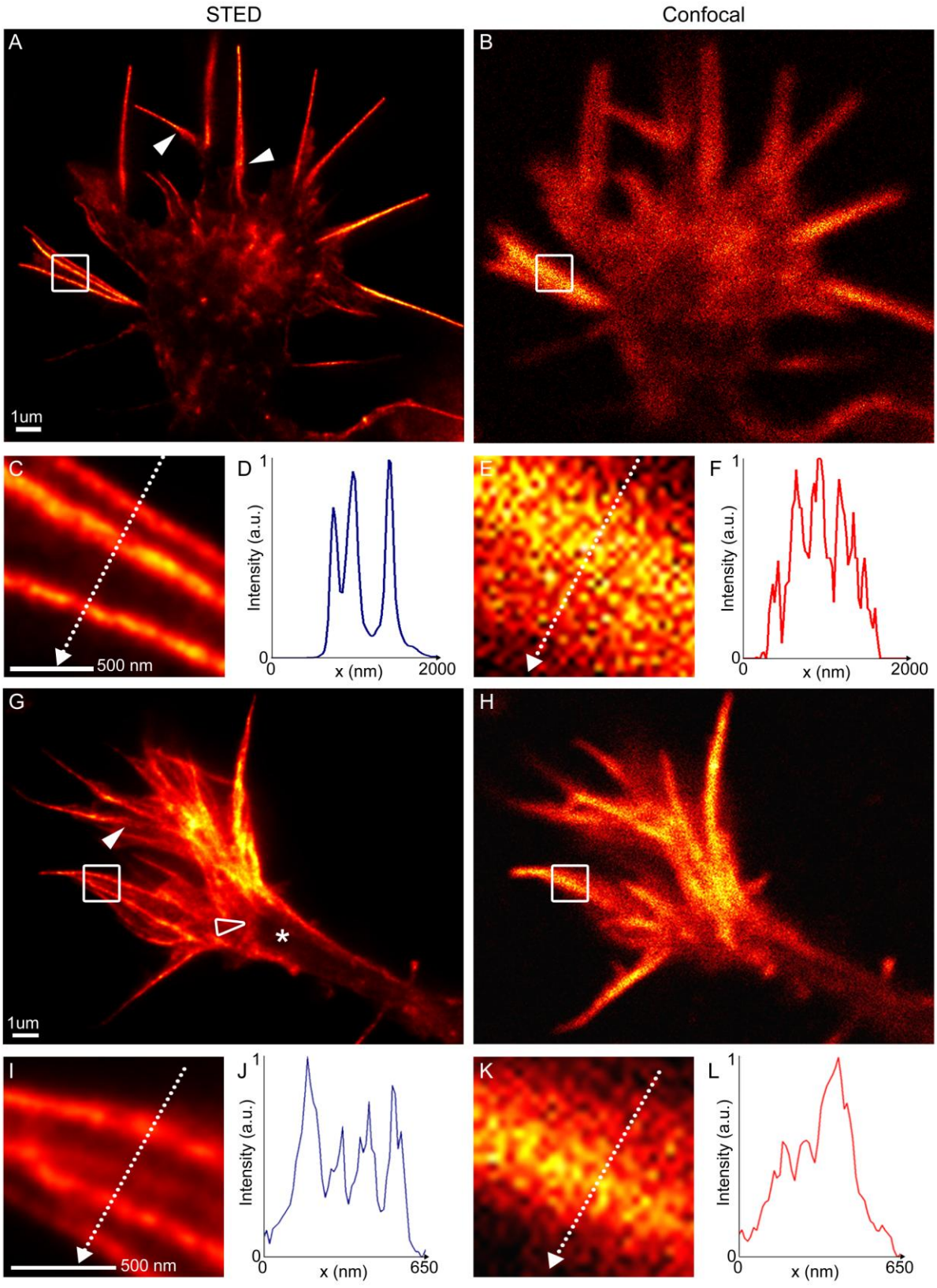

Figure 2.24: STED imaging of actin in growth cones. STED (**A, C** and **G, I**) and confocal (**B, E** and **H, K**) images of two different hippocampal growth cones are compared. Squares in A, B, G and H indicate the region that is enlarged respectively in C, E, I and K. (**D, F, J** and **L**) Plot profile of the linescans indicated by the dashed lines in close-up images. Solid wedges in A and G indicate filopodia at whose base more actin bundles can be seen. In G, * indicates the C domain. Empty wedge indicates

the T zone. Images are shown in pseudocolors, according to the number of photon counts for each pixel.

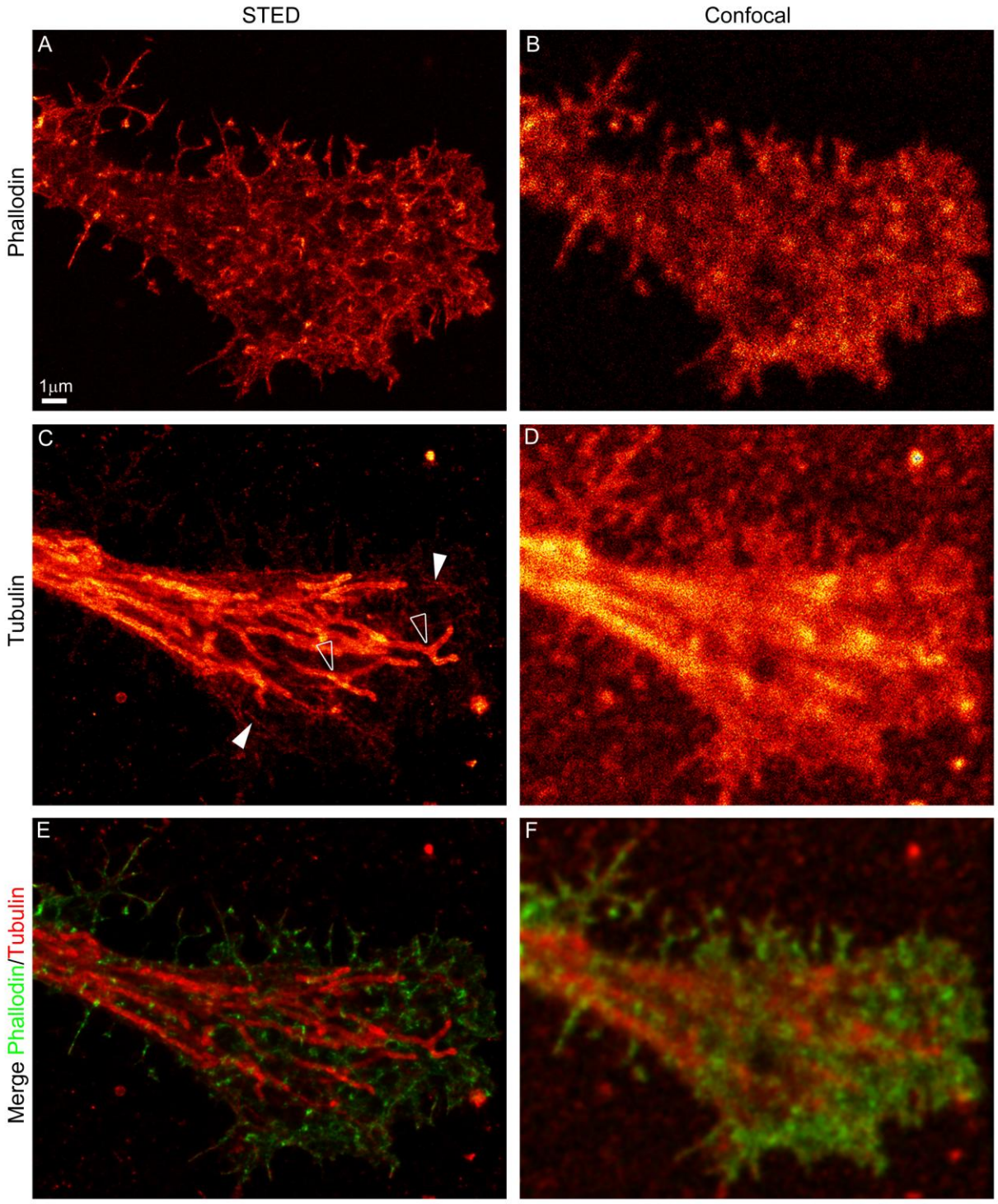

Figure 2.25: Double staining of tubulin and actin imaged with STED microscopy. (**A, C, E**) STED images. (**B, D, F**) Corresponding confocal images. (**A, B, C, D**) Single staining, and (**E, F**) merging of the two channels. Solid wedges indicate pioneer microtubules. Empty wedges indicate branching microtubules.

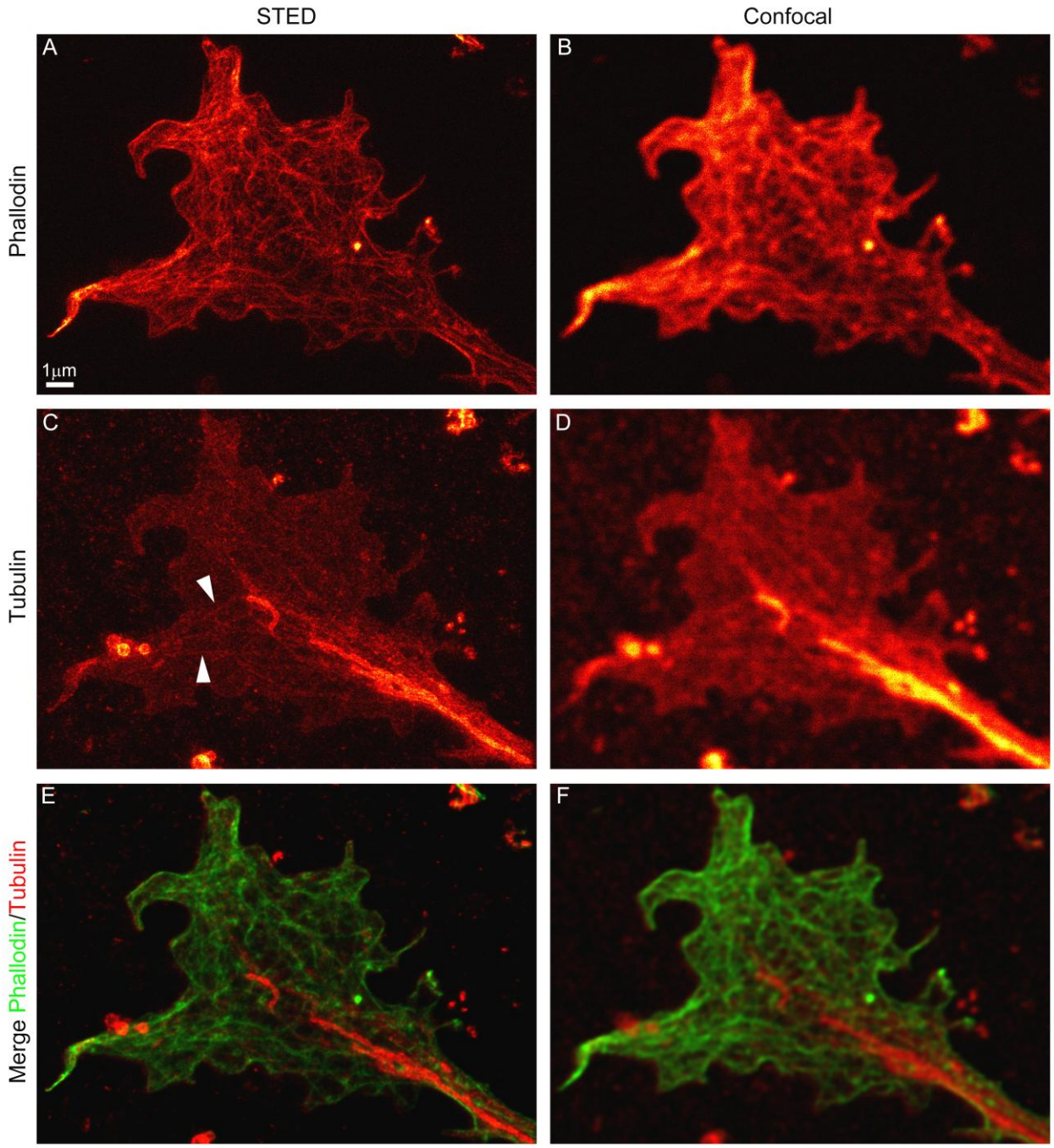

Figure 2.26: Double staining of tubulin and actin imaged with STED microscopy. (**A, C, E**) STED images. (**B, D, F**) Corresponding confocal images. (**A, B, C, D**) Single staining and (**E, F**) merging of the two channels. Solid wedges indicate pioneer microtubules.

3.FINAL REMARKS AND CONCLUSIONS

Polarized cells are those in which a spatial asymmetry in their organization causes the plasma membrane to be divided into discrete domains. Each domain has specific functions, characteristics, and receptors. This means that the same stimulus applied to different domains may have different readouts. Neurons are extremely polarized cells and in the last decades several techniques for the stimulation of specific neuronal compartments were proposed. However, they have limitations (e.g. low handiness, low spatial and temporal resolution) or are optimized only for few, well-established molecules. As a result, most of the experiments are still being performed by bath application of the molecule of interest. Therefore, the effects observed are not specific and correspond to the response of the whole cell to the stimulus. However, in physiological conditions molecules are released mainly in a spatially and temporally confined fashion.

In this Thesis we developed novel techniques for the local delivery of molecules based on optical manipulation, as well as imaging tools. Indeed, it is important to see what you are manipulating and vice versa. We focused our attention on two different kind of vectors (i.e. silica beads and liposomes), which can carry the molecules to the site of interest. Their common characteristic is that they can be easily trapped and manipulated with optical tweezers.

The first tested vectors were silica beads, which can be functionalized on their surface with the molecule of interest. Through optical tweezers, single functionalized beads can be placed in contact with the domain of interest of a cell. In this way, the proteins that coat the bead may bind their corresponding receptor present on the cell membrane. Interestingly, internalization of the ligand is avoided with beads. Indeed, since molecules are covalently linked to the vector, endocytosis is prevented. Beads system was validated with the neurotrophin BDNF, a protein which exerts its functions by binding a receptor on cell surface. We demonstrated that a single BDNF-coated bead is sufficient to activate different intracellular signaling pathways and induce a cellular response.

Beads allow focal stimulation of cells and mimic systems in which a protein is either bound to the extra cellular matrix or exposed on the membrane to stimulate the neighbour cell, or systems in which molecules should travel along short distances. At synaptic level, for instance, neurotransmitters and trophic factors are released from pre-synaptic sites and act on post-synaptic sites, which are few tens of nanometers away.

However, in physiological conditions molecules can be released also by sources that are distant from the target cell, which therefore senses a gradient. For instance, chemotactic stimuli influence the movements of cells according to their concentration in the environment. Chemotaxis is a key mechanism exploited by nature during development but it plays an important role also in other functions, such as immune response or metastatic process. With beads, gradients of molecules cannot be generated. Therefore, we decided to develop a second kind of vectors, which allowed the formation of a gradient of molecules. These vectors are micron-sized liposomes, i.e. vesicles with a lipid bilayer and a lumen within which almost any soluble molecule can be encapsulated. The release from liposomes is achieved by temporary breaking the liposome membrane with a UV-pulse. In this way, molecules that are restrained in the lumen can diffuse outside and generate a gradient. Liposomes have some advantages with respect to beads: first, ligand can be endocyted and signaling endosomes can form. Second, the number of molecules inside the liposome can be finely tuned, by simply changing the concentration of the

rehydrating solution or the dimension of liposomes. Third, liposomes can be bath applied in the medium and then a single vesicle can be chosen. Fourth, molecules are not chemically modified since they should not be crosslinked to the vector. Indeed, stimuli are encapsulated inside the lumen and there confined. Hence, there is no undesired leakage of molecules. On the other hand, only small amount of molecules can be delivered with liposomes and the spatial resolution of the stimulation is poorer with respect to beads.

The liposome technique was initially validated with KCl-filled vesicles. In the experimental setup adopted, a depolarization in cultured hippocampal neurons was observed. Subsequently, the technique was used to study the effect of two chemotactic proteins (Netrin-1 and Semaphorin-3A) on growth cone motility. Netrin-1 showed an attractive behaviour, while Sema-3A was repellent. The fast morphological changes in responses to these cues are due to rapid rearrangements of the cytoskeleton, and in particular to actin and tubulin dynamics, which would be interesting to investigate. A first step in this direction was done with the acquisition of super-resolution fluorescence (STED) images of actin and tubulin structures in growth cones. Comparing to Abbe-limited microscopy, with STED we were able to outline much more details, see single actin bundles, branching of microtubules and pioneer microtubules. These results demonstrate that, thanks to its resolution, live imaging of actin and tubulin dynamics with STED microscopy may allow the solution of many biological problems related to this topic.

Finally, nanovectors have been developed as well. In particular, functionalized quantum dots may be used for the intracellular tracking of the endosomes. Indeed, given their small size and their brightness Qdots are suitable for single molecule dynamic studies. In this Thesis we prepared BDNF-functionalized Qdots, which were able to bind BDNF receptor and to be endocyted. Considering the toxic effects they may have, we delivered Qdots with liposomes. This tool might now be used in two distinct ways: first of all the dynamics of endocytosis and retrograde transport of signaling endosomes will be analyzed. Second, it would be interesting to evaluate the differences in the biological response due to different location of the signaling endosomes along the axon. Lastly, a comparison between the different delivery techniques (i.e. beads, liposomes, Qdots) may unveil mechanisms or parts of signaling pathways which are still unclear.

Concluding, different tools that respond to different experimental needs have been developed. The best vector should be chosen according to each specific biological problem. Both beads and liposomes are highly flexible as vectors, meaning that they can be exploited for different biological problems and are not restricted only to the biological questions presented in this Thesis. In particular, the presented technique may have several applications not only in neurobiology, but also in all the fields in which gradients of molecules or a spatially restricted stimulation are required.

ACKNOWLEDGMENTS

The very first person I would like to thank is Dan Cojoc, who has been more than a supervisor and more than a mentor for me. A warm thank you for the fundamental teamwork goes also to all the other members of the OM lab: Giulietta Pinato, Sara Finaurini, Enrico Ferrari, Federica Tavano, Tiziano Raffaelli, and Paolo Beuzer.

I would like to acknowledge also the other labs that took part to my PhD project. In particular, prof. Enrico Tongiorgi's lab at the University of Trieste for hosting me during the experiments on beads and on Qdots; prof. Vincent Torre's lab at SISSA for the collaboration during the experiments on growth cones with Semaphorin and Netrin; Prof. Dr. rer. nat. Dr. med. h. c. Stefan Hell's lab at the Max Planck Institute in Göttingen for the part on STED images.

Thanks to Stefania, Anna, and Andriy for the critical reading of this work.

Viva l'A e po' bon!

Vorrei ringraziare tutte le persone che mi sono state vicino psicologicamente, fisicamente e a suon di spritz e/o birrini in questi 3 anni. Premetto che l'ordine è puramente CASUALE!!! Un infinito a Svampi per aver portato una ventata di ottimismo, positività e festa festa nella mia vita. Fagiana! Sei il mio orgoglio! Un grazie infinito va anche alla Comelliiiiii per tutte le sue perle di saggezza di ogni mattina e per tutte le cose che solo lei riesce a dire in faccia schiettamente (la mia autostima ringrazia). Grazie alla Migliorins, mia gemella di vita degli ultimi 5 anni per aver potuto sempre e comunque contare su di te. Grazie a Fra: dopo 7 anni di convivenza è difficile stare senza di te! Ma tranquilla che imparerò la strada per arrivare a Flaibano.

Grazie a coloro che mi hanno fatto divertire nei vari lab, rendendo gli esperimenti un po' meno pesanti, e che ora sono da altre parti del mondo: ValeVaghi, Beuzeeeeeeer, Tiz. Quando vi penso, sorrido!

Grazie a tutti i compagni di dottorato, molto più di semplici colleghi. Un enorme in bocca al lupo a tutti voi! Viva il XXIV ciclo! Firmato: la maestra. Un pensiero anche a tutti i compagni dell'MCA: l'esperienza con voi segnerà di sicuro la mia vita! Grazie ai soci Allergenius per la pazienza in questi due mesi con il loro project manager…

Thanks to the "german" guys. Dirk for your never-ending patience when "I think I have a problem with the setup" and for your "mandiiii", which makes me so proud of you; Andriy and Ila for introducing me to the life in Göttingen and to Feuerzangebowle...and for the "unforgettable" concerts. See you very soon guys!!

Last but not least, grazie alla mia famiglia. Ai miei genitori per avermi sempre sostenuto, pur non facendo domande. Grazie a Francesca ed Enrico, per la comprensione umano/scientifica e per quello spettacolo che è Davide.

BIBLIOGRAPHY

Abbe, E. (1873). Beiträge zur Theorie des Mikroskops und der mikroskopischen Wahrnehmung. Archiv für Mikroskopische Anatomie *9*, 413-468.

Akselrod, G. M., Timp, W., Mirsaidov, U., Zhao, Q., Li, C., Timp, R., Timp, K., Matsudaira, P., and Timp, G. (2006). Laser-guided assembly of heterotypic three-dimensional living cell microarrays. Biophys J *91*, 3465-3473.

Allen, J. W., and Bhatia, S. N. (2003). Formation of steady-state oxygen gradients in vitro: application to liver zonation. Biotechnol Bioeng *82*, 253-262.

Amaral, M. D., Chapleau, C. A., and Pozzo-Miller, L. (2007). Transient receptor potential channels as novel effectors of brain-derived neurotrophic factor signaling: potential implications for Rett syndrome. Pharmacol Ther *113*, 394-409.

Amaral, M. D., and Pozzo-Miller, L. (2007). BDNF induces calcium elevations associated with IBDNF, a nonselective cationic current mediated by TRPC channels. J Neurophysiol *98*, 2476-2482.

Arevalo, J. C., Conde, B., Hempstead, B. L., Chao, M. V., Martin-Zanca, D., and Perez, P. (2000). TrkA immunoglobulin-like ligand binding domains inhibit spontaneous activation of the receptor. Mol Cell Biol *20*, 5908-5916.

Ashkin, A. (1970). Acceleration and Trapping of Particles by Radiation Pressure. Physical Review Letters *24*, 156-159.

Ashkin, A. (1992). Forces of a single-beam gradient laser trap on a dielectric sphere in the ray optics regime. Biophys J *61*, 569-582.

Ashkin, A. (2006). Optical trapping and manipulation of neutral particles using lasers: a reprint volume with commentaries (Singapore: World Scientific Publishing Co. Pte. Ltd.).

Ashkin, A., and Dziedzic, J. M. (1987). Optical trapping and manipulation of viruses and bacteria. Science *235*, 1517-1520.

Ashkin, A., Dziedzic, J. M., Bjorkholm, J. E., and Chu, S. (1986). Observation of a single-beam gradient force optical trap for dielectric particles. Opt Lett *11*, 288.

Ashkin, A., Dziedzic, J. M., and Yamane, T. (1987). Optical trapping and manipulation of single cells using infrared laser beams. Nature *330*, 769-771.

Ashkin, A., Schutze, K., Dziedzic, J. M., Euteneuer, U., and Schliwa, M. (1990). Force generation of organelle transport measured in vivo by an infrared laser trap. Nature *348*, 346-348.

Ashok, P. C., and Dholakia, K. (2011). Optical trapping for analytical biotechnology. Curr Opin Biotechnol *23*, 1-6.

Ballou, B., Lagerholm, B. C., Ernst, L. A., Bruchez, M. P., and Waggoner, A. S. (2004). Noninvasive imaging of quantum dots in mice. Bioconjug Chem *15*, 79-86.

Bankapur, A., Zachariah, E., Chidangil, S., Valiathan, M., and Mathur, D. (2010). Raman tweezers spectroscopy of live, single red and white blood cells. PLoS One *5*, e10427.

Barde, Y. A., Edgar, D., and Thoenen, H. (1982). Purification of a new neurotrophic factor from mammalian brain. Embo J *1*, 549-553.

Barrett, L. E., Sul, J. Y., Takano, H., Van Bockstaele, E. J., Haydon, P. G., and Eberwine, J. H. (2006). Region-directed phototransfection reveals the functional significance of a dendritically synthesized transcription factor. Nat Methods *3*, 455-460.

Bashaw, G. J., and Klein, R. (2010). Signaling from axon guidance receptors. Cold Spring Harb Perspect Biol *2*, a001941.

Beattie, E. C., Zhou, J., Grimes, M. L., Bunnett, N. W., Howe, C. L., and Mobley, W. C. (1996). A signaling endosome hypothesis to explain NGF actions: potential implications for neurodegeneration. Cold Spring Harb Symp Quant Biol *61*, 389-406.

Berning, S., Willig, K. I., Steffens, H., Dibaj, P., and Hell, S. W. (2012). Nanoscopy in a living mouse brain. Science *335*, 551.

Berridge, M. J., Bootman, M. D., and Lipp, P. (1998). Calcium--a life and death signal. Nature *395*, 645-648.

Biju, V., Itoh, T., and Ishikawa, M. (2010). Delivering quantum dots to cells: bioconjugated quantum dots for targeted and nonspecific extracellular and intracellular imaging. Chem Soc Rev *39*, 3031-3056.

Blake, A. J., Pearce, T. M., Rao, N. S., Johnson, S. M., and Williams, J. C. (2007). Multilayer PDMS microfluidic chamber for controlling brain slice microenvironment. Lab Chip *7*, 842-849.

Block, S. M., Goldstein, L. S., and Schnapp, B. J. (1990). Bead movement by single kinesin molecules studied with optical tweezers. Nature *348*, 348-352.

Bosques, C. J., and Imperiali, B. (2003). Photolytic control of peptide self-assembly. J Am Chem Soc *125*, 7530-7531.

Bottrill, M., and Green, M. (2011). Some aspects of quantum dot toxicity. Chem Commun (Camb) *47*, 7039-7050.

Bruchez, M., Jr., Moronne, M., Gin, P., Weiss, S., and Alivisatos, A. P. (1998). Semiconductor nanocrystals as fluorescent biological labels. Science *281*, 2013-2016.

Bückers, J., Wildanger, D., Vicidomini, G., Kastrup, L., and Hell, S. W. (2011). Simultaneous multi-lifetime multi-color STED imaging for colocalization analyses. Opt Express *19*, 3130-3143.

Bustamante, C., Bryant, Z., and Smith, S. B. (2003). Ten years of tension: single-molecule DNA mechanics. Nature *421*, 423-427.

Byers, R. J., and Hitchman, E. R. (2010). Quantum dots brighten biological imaging. Prog Histochem Cytochem *45*, 201-237.

Cahagan, K. T., and Swartzlander, G. A. (1998). Trapping of low-index microparticles in an optical vortex. Journal of the Optical Society of America B *15*, 524-534.

Campenot, R. B. (1977). Local control of neurite development by nerve growth factor. Proc Natl Acad Sci U S A *74*, 4516-4519.

Canepari, M., Nelson, L., Papageorgiou, G., Corrie, J. E., and Ogden, D. (2001). Photochemical and pharmacological evaluation of 7-nitroindolinyl-and 4-methoxy-7-nitroindolinyl-amino acids as novel, fast caged neurotransmitters. J Neurosci Methods *112*, 29-42.

Canossa, M., Griesbeck, O., Berninger, B., Campana, G., Kolbeck, R., and Thoenen, H. (1997). Neurotrophin release by neurotrophins: implications for activity-dependent neuronal plasticity. Proc Natl Acad Sci U S A *94*, 13279-13286.

Carnegie, D. J., Cizmar, T., Baumgartl, J., Gunn-Moore, F. J., and Dholakia, K. (2009). Automated laser guidance of neuronal growth cones using a spatial light modulator. J Biophotonics *2*, 682-692.

Castellani, V., Falk, J., and Rougon, G. (2004). Semaphorin3A-induced receptor endocytosis during axon guidance responses is mediated by L1 CAM. Mol Cell Neurosci *26*, 89-100.

Chan, W. C., Maxwell, D. J., Gao, X., Bailey, R. E., Han, M., and Nie, S. (2002). Luminescent quantum dots for multiplexed biological detection and imaging. Curr Opin Biotechnol *13*, 40-46.

Chao, M. V. (2003). Neurotrophins and their receptors: a convergence point for many signalling pathways. Nat Rev Neurosci *4*, 299-309.

Chao, M. V., Rajagopal, R., and Lee, F. S. (2006). Neurotrophin signalling in health and disease. Clin Sci (Lond) *110*, 167-173.

Chedotal, A., Del Rio, J. A., Ruiz, M., He, Z., Borrell, V., de Castro, F., Ezan, F., Goodman, C. S., Tessier-Lavigne, M., Sotelo, C., and Soriano, E. (1998). Semaphorins III and IV repel hippocampal axons via two distinct receptors. Development *125*, 4313-4323.

Chen, X., Kis, A., Zettl, A., and Bertozzi, C. R. (2007). A cell nanoinjector based on carbon nanotubes. Proc Natl Acad Sci U S A *104*, 8218-8222.

Chisholm, A., and Tessier-Lavigne, M. (1999). Conservation and divergence of axon guidance mechanisms. Curr Opin Neurobiol *9*, 603-615.

Choudhury, D., van Noort, D., Iliescu, C., Zheng, B., Poon, K. L., Korzh, S., Korzh, V., and Yu, H. (2012). Fish and Chips: a microfluidic perfusion platform for monitoring zebrafish development. Lab Chip.

Cojoc, D., Difato, F., Ferrari, E., Shahapure, R. B., Laishram, J., Righi, M., Di Fabrizio, E. M., and Torre, V. (2007). Properties of the force exerted by filopodia and lamellipodia and the involvement of cytoskeletal components. PLoS One *2*, e1072.

Conde, C., and Caceres, A. (2009). Microtubule assembly, organization and dynamics in axons and dendrites. Nat Rev Neurosci *10*, 319-332.

Cuerrier, C. M., Lebel, R., and Grandbois, M. (2007). Single cell transfection using plasmid decorated AFM probes. Biochem Biophys Res Commun *355*, 632-636.

Cui, B., Wu, C., Chen, L., Ramirez, A., Bearer, E. L., Li, W. P., Mobley, W. C., and Chu, S. (2007). One at a time, live tracking of NGF axonal transport using quantum dots. Proc Natl Acad Sci U S A *104*, 13666-13671.

D'Este, E., Baj, G., Beuzer, P., Ferrari, E., Pinato, G., Tongiorgi, E., and Cojoc, D. (2011). Use of optical tweezers technology for long-term, focal stimulation of specific subcellular neuronal compartments. Integr Biol (Camb) *3*, 568-577.

Dai, J., and Sheetz, M. P. (1995). Mechanical properties of neuronal growth cone membranes studied by tether formation with laser optical tweezers. Biophys J *68*, 988-996.

Dasgupta, R., Verma, R. S., Ahlawat, S., Uppal, A., and Gupta, P. K. (2011). Studies on erythrocytes in malaria infected blood sample with Raman optical tweezers. J Biomed Opt *16*, 077009.

Denk, W., Strickler, J. H., and Webb, W. W. (1990). Two-photon laser scanning fluorescence microscopy. Science *248*, 73-76.

Derfus, A. M., Chan, W., and Bhatia, S. N. (2004). Probing the Cytotoxicity of Semiconductor Quantum Dots. Nano Lett *4*, 11-18.

Dertinger, S. K., Jiang, X., Li, Z., Murthy, V. N., and Whitesides, G. M. (2002). Gradients of substrate-bound laminin orient axonal specification of neurons. Proc Natl Acad Sci U S A *99*, 12542-12547.

Desmond, N. L., and Levy, W. B. (1985). Granule cell dendritic spine density in the rat hippocampus varies with spine shape and location. Neurosci Lett *54*, 219-224.

Devon, R. S., Orban, P. C., Gerrow, K., Barbieri, M. A., Schwab, C., Cao, L. P., Helm, J. R., Bissada, N., Cruz-Aguado, R., Davidson, T. L., *et al.* (2006). Als2-deficient mice exhibit disturbances in endosome trafficking associated with motor behavioral abnormalities. Proc Natl Acad Sci U S A *103*, 9595-9600.

Dholakia, K., MacDonald, M. P., Zemanek, P., and Cizmar, T. (2007). Cellular and colloidal separation using optical forces. Methods Cell Biol *82*, 467-495.

Du, J., Feng, L., Zaitsev, E., Je, H. S., Liu, X. W., and Lu, B. (2003). Regulation of TrkB receptor tyrosine kinase and its internalization by neuronal activity and Ca2+ influx. J Cell Biol *163*, 385-395.

Echarte, M. M., Bruno, L., Arndt-Jovin, D. J., Jovin, T. M., and Pietrasanta, L. I. (2007). Quantitative single particle tracking of NGF-receptor complexes: transport is bidirectional but biased by longer retrograde run lengths. FEBS Lett *581*, 2905-2913.

Eggeling, C., Ringemann, C., Medda, R., Schwarzmann, G., Sandhoff, K., Polyakova, S., Belov, V. N., Hein, B., von Middendorff, C., Schonle, A., and Hell, S. W. (2009). Direct observation of the nanoscale dynamics of membrane lipids in a living cell. Nature *457*, 1159-1162.

Ehrlicher, A., Betz, T., Stuhrmann, B., Gogler, M., Koch, D., Franze, K., Lu, Y., and Kas, J. (2007). Optical neuronal guidance. Methods Cell Biol *83*, 495-520.

Ehrlicher, A., Betz, T., Stuhrmann, B., Koch, D., Milner, V., Raizen, M. G., and Kas, J. (2002). Guiding neuronal growth with light. Proc Natl Acad Sci U S A *99*, 16024-16028.

Ellis-Davies, G. C. (2007). Caged compounds: photorelease technology for control of cellular chemistry and physiology. Nat Methods *4*, 619-628.

Ellis-Davies, G. C. (2011). Two-photon microscopy for chemical neuroscience. ACS Chem Neurosci *2*, 185-197.

Ernfors, P., Kucera, J., Lee, K. F., Loring, J., and Jaenisch, R. (1995). Studies on the physiological role of brain-derived neurotrophic factor and neurotrophin-3 in knockout mice. Int J Dev Biol *39*, 799-807.

Esposito, D., Patel, P., Stephens, R. M., Perez, P., Chao, M. V., Kaplan, D. R., and Hempstead, B. L. (2001). The cytoplasmic and transmembrane domains of the p75 and Trk A receptors regulate high affinity binding to nerve growth factor. J Biol Chem *276*, 32687-32695.

Fan, J., Mansfield, S. G., Redmond, T., Gordon-Weeks, P. R., and Raper, J. A. (1993). The organization of F-actin and microtubules in growth cones exposed to a brain-derived collapsing factor. J Cell Biol *121*, 867-878.

Fan, J., and Raper, J. A. (1995). Localized collapsing cues can steer growth cones without inducing their full collapse. Neuron *14*, 263-274.

Fazal, F. M., and Block, S. M. (2011). Optical tweezers study life under tension. Nat Photonics *5*, 318-321.

Finkbeiner, S., Tavazoie, S. F., Maloratsky, A., Jacobs, K. M., Harris, K. M., and Greenberg, M. E. (1997). CREB: a major mediator of neuronal neurotrophin responses. Neuron *19*, 1031-1047.

Fournier, A. E., Nakamura, F., Kawamoto, S., Goshima, Y., Kalb, R. G., and Strittmatter, S. M. (2000). Semaphorin3A enhances endocytosis at sites of receptor-F-actin colocalization during growth cone collapse. J Cell Biol *149*, 411-422.

Frade, J. M., and Barde, Y. A. (1998). Nerve growth factor: two receptors, multiple functions. Bioessays *20*, 137-145.

Galbraith, C. G., and Sheetz, M. P. (1999). Keratocytes pull with similar forces on their dorsal and ventral surfaces. J Cell Biol *147*, 1313-1324.

Gallo, G., Lefcort, F. B., and Letourneau, P. C. (1997). The trkA receptor mediates growth cone turning toward a localized source of nerve growth factor. J Neurosci *17*, 5445-5454.

Goeppert-Mayer, M. (1931). Uber Elementarakte mit zwei Quantensprungen. Ann Phys *9*, 273-295.

Gomez, T. M., and Zheng, J. Q. (2006). The molecular basis for calcium-dependent axon pathfinding. Nat Rev Neurosci *7*, 115-125.

Gordon-Weeks, P. R. (1989). Growth at the growth cone. Trends Neurosci *12*, 238-240.

Grier, D. G. (2003). A revolution in optical manipulation. Nature *424*, 810-816.

Grimes, M. L., Zhou, J., Beattie, E. C., Yuen, E. C., Hall, D. E., Valletta, J. S., Topp, K. S., LaVail, J. H., Bunnett, N. W., and Mobley, W. C. (1996). Endocytosis of activated TrkA: evidence that nerve growth factor induces formation of signaling endosomes. J Neurosci *16*, 7950-7964.

Groc, L., and Choquet, D. (2008). Measurement and characteristics of neurotransmitter receptor surface trafficking (Review). Mol Membr Biol *25*, 344-352.

Groc, L., Lafourcade, M., Heine, M., Renner, M., Racine, V., Sibarita, J. B., Lounis, B., Choquet, D., and Cognet, L. (2007). Surface trafficking of neurotransmitter receptor: comparison between single-molecule/quantum dot strategies. J Neurosci *27*, 12433-12437.

Han, L., Wen, Z., Lynn, R. C., Baudet, M. L., Holt, C. E., Sasaki, Y., Bassell, G. J., and Zheng, J. Q. (2011). Regulation of chemotropic guidance of nerve growth cones by microRNA. Mol Brain *4*, 40.

Han, S. W., Nakamura, C., Kotobuki, N., Obataya, I., Ohgushi, H., Nagamune, T., and Miyake, J. (2008). High-efficiency DNA injection into a single human mesenchymal stem cell using a nanoneedle and atomic force microscopy. Nanomedicine *4*, 215-225.

Harada, A., and Asakura, T. (1996). Radiation forces on a dielectric sphere in the Rayleigh scattering regime. Optics Communications *124*, 529-541.

Hart, S. J., Terray, A., Leski, T. A., Arnold, J., and Stroud, R. (2006). Discovery of a significant optical chromatographic difference between spores of Bacillus anthracis and its close relative, Bacillus thuringiensis. Anal Chem *78*, 3221-3225.

Heerssen, H. M., and Segal, R. A. (2002). Location, location, location: a spatial view of neurotrophin signal transduction. Trends Neurosci *25*, 160-165.

Hell, S. W. (2007). Far-field optical nanoscopy. Science *316*, 1153-1158.

Hell, S. W. (2009). Microscopy and its focal switch. Nat Methods *6*, 24-32.

Hell, S. W., and Wichmann, J. (1994). Breaking the diffraction resolution limit by stimulated emission: stimulated-emission-depletion fluorescence microscopy. Opt Lett *19*, 780-782.

Henle, S. J., Wang, G., Liang, E., Wu, M., Poo, M. M., and Henley, J. R. (2011). Asymmetric PI(3,4,5)P3 and Akt signaling mediates chemotaxis of axonal growth cones. J Neurosci *31*, 7016-7027.

Hofmann, M., Eggeling, C., Jakobs, S., and Hell, S. W. (2005). Breaking the diffraction barrier in fluorescence microscopy at low light intensities by using reversibly photoswitchable proteins. Proc Natl Acad Sci U S A *102*, 17565-17569.

Hong, K., Nishiyama, M., Henley, J., Tessier-Lavigne, M., and Poo, M. (2000). Calcium signalling in the guidance of nerve growth by netrin-1. Nature *403*, 93-98.

Horch, H. W., and Katz, L. C. (2002). BDNF release from single cells elicits local dendritic growth in nearby neurons. Nat Neurosci *5*, 1177-1184.

Hoshino, A., Fujioka, K., Oku, T., Suga, M., Sasaki, Y. F., Ohta, T., Yasuhara, M., Suzuki, K., and Yamamoto, K. (2004). Physicochemical Properties and Cellular Toxicity of Nanocrystal Quantum Dots Depend on Their Surface Modification. Nano Lett *4*, 2163-2169.

Howe, C. L., and Mobley, W. C. (2004). Signaling endosome hypothesis: A cellular mechanism for long distance communication. J Neurobiol *58*, 207-216.

Huang, B., Babcock, H., and Zhuang, X. (2010). Breaking the diffraction barrier: super-resolution imaging of cells. Cell *143*, 1047-1058.

Huang, E. J., and Reichardt, L. F. (2003). Trk receptors: roles in neuronal signal transduction. Annu Rev Biochem *72*, 609-642.

Huang, Y., Agrawal, B., Clark, P. A., Williams, J. C., and Kuo, J. S. (2011). Evaluation of cancer stem cell migration using compartmentalizing microfluidic devices and live cell imaging. J Vis Exp.

Hub, H. H., Zimmermann, U., and Ringsdorf, H. (1982). Preparation of large unilamellar vesicles FEBS Letters *140*, 254-256.

Huber, A. B., Kolodkin, A. L., Ginty, D. D., and Cloutier, J. F. (2003). Signaling at the growth cone: ligand-receptor complexes and the control of axon growth and guidance. Annu Rev Neurosci *26*, 509-563.

Ichikawa, M., and Yoshikawa, K. (2001). Optical transport of a single cell-sized liposome. Applied Physics Letters *79*, 4598.

Irimia, D., Liu, S. Y., Tharp, W. G., Samadani, A., Toner, M., and Poznansky, M. C. (2006). Microfluidic system for measuring neutrophil migratory responses to fast switches of chemical gradients. Lab Chip *6*, 191-198.

Jauffred, L., and Oddershede, L. B. (2010). Two-photon quantum dot excitation during optical trapping. Nano Lett *10*, 1927-1930.

Ji, Y., Lu, Y., Yang, F., Shen, W., Tang, T. T., Feng, L., Duan, S., and Lu, B. (2010). Acute and gradual increases in BDNF concentration elicit distinct signaling and functions in neurons. Nat Neurosci *13*, 302-309.

Jurney, W. M., Gallo, G., Letourneau, P. C., and McLoon, S. C. (2002). Rac1-mediated endocytosis during ephrin-A2- and semaphorin 3A-induced growth cone collapse. J Neurosci *22*, 6019-6028.

Kaplan, D. R., and Miller, F. D. (2000). Neurotrophin signal transduction in the nervous system. Curr Opin Neurobiol *10*, 381-391.

Kepler, J. (1619). De cometis libelli tres, typis Andreae Apergeri, sumptibus Sebastiani Mylii bibliopolae augustani. Avgvstae Vindelicorum.

Kohli, V., and Elezzabi, A. Y. (2009). Prospects and developments in cell and embryo laser nanosurgery. Wiley Interdiscip Rev Nanomed Nanobiotechnol *1*, 11-25.

Korte, M., Carroll, P., Wolf, E., Brem, G., Thoenen, H., and Bonhoeffer, T. (1995). Hippocampal long-term potentiation is impaired in mice lacking brain-derived neurotrophic factor. Proc Natl Acad Sci U S A *92*, 8856-8860.

Kossel, A. H., Cambridge, S. B., Wagner, U., and Bonhoeffer, T. (2001). A caged Ab reveals an immediate/instructive effect of BDNF during hippocampal synaptic potentiation. Proc Natl Acad Sci U S A *98*, 14702-14707.

Kothapalli, C. R., van Veen, E., de Valence, S., Chung, S., Zervantonakis, I. K., Gertler, F. B., and Kamm, R. D. (2010). A high-throughput microfluidic assay to study neurite response to growth factor gradients. Lab Chip *11*, 497-507.

Kress, H., Park, J. G., Mejean, C. O., Forster, J. D., Park, J., Walse, S. S., Zhang, Y., Wu, D., Weiner, O. D., Fahmy, T. M., and Dufresne, E. R. (2009). Cell stimulation with optically manipulated microsources. Nat Methods *6*, 905-909.

Kumanogoh, A., and Kikutani, H. (2010). Semaphorins and their receptors: novel features of neural guidance molecules. Proc Jpn Acad Ser B Phys Biol Sci *86*, 611-620.

Lang, S. B., Stein, V., Bonhoeffer, T., and Lohmann, C. (2007). Endogenous brain-derived neurotrophic factor triggers fast calcium transients at synapses in developing dendrites. J Neurosci *27*, 1097-1105.

Leclerc, E., David, B., Griscom, L., Lepioufle, B., Fujii, T., Layrolle, P., and Legallaisa, C. (2006). Study of osteoblastic cells in a microfluidic environment. Biomaterials *27*, 586-595.

Lee, S. S., Horvath, P., Pelet, S., Hegemann, B., Lee, L. P., and Peter, M. (2012). Quantitative and dynamic assay of single cell chemotaxis. Integr Biol (Camb).

Leitz, G., Fallman, E., Tuck, S., and Axner, O. (2002). Stress response in Caenorhabditis elegans caused by optical tweezers: wavelength, power, and time dependence. Biophys J *82*, 2224-2231.

Lessmann, V., Gottmann, K., and Malcangio, M. (2003). Neurotrophin secretion: current facts and future prospects. Prog Neurobiol *69*, 341-374.

Letokhov, V. S. (1968). Narrowing of the Doppler width in a standing light wave. JETP Letters *7*, 272-274.

Letourneau, P. C. (1983). Differences in the organization of actin in the growth cones compared with the neurites of cultured neurons from chick embryos. J Cell Biol *97*, 963-973.

Leung, B. O., and Chou, K. C. (2011). Review of super-resolution fluorescence microscopy for biology. Appl Spectrosc *65*, 967-980.

Lewis, A. K., and Bridgman, P. C. (1992). Nerve growth cone lamellipodia contain two populations of actin filaments that differ in organization and polarity. J Cell Biol *119*, 1219-1243.

Li Jeon, N., Baskaran, H., Dertinger, S. K., Whitesides, G. M., Van de Water, L., and Toner, M. (2002). Neutrophil chemotaxis in linear and complex gradients of interleukin-8 formed in a microfabricated device. Nat Biotechnol *20*, 826-830.

Li, X., Saint-Cyr-Proulx, E., Aktories, K., and Lamarche-Vane, N. (2002). Rac1 and Cdc42 but not RhoA or Rho kinase activities are required for neurite outgrowth induced by the Netrin-1 receptor DCC (deleted in colorectal cancer) in N1E-115 neuroblastoma cells. J Biol Chem *277*, 15207-15214.

Li, Y., Jia, Y. C., Cui, K., Li, N., Zheng, Z. Y., Wang, Y. Z., and Yuan, X. B. (2005). Essential role of TRPC channels in the guidance of nerve growth cones by brain-derived neurotrophic factor. Nature *434*, 894-898.

Liang, H., Vu, K. T., Krishnan, P., Trang, T. C., Shin, D., Kimel, S., and Berns, M. W. (1996). Wavelength dependence of cell cloning efficiency after optical trapping. Biophys J *70*, 1529-1533.

Lichtman, J. W., and Conchello, J. A. (2005). Fluorescence microscopy. Nat Methods *2*, 910-919.

Lidke, D. S., Lidke, K. A., Rieger, B., Jovin, T. M., and Arndt-Jovin, D. J. (2005). Reaching out for signals: filopodia sense EGF and respond by directed retrograde transport of activated receptors. J Cell Biol *170*, 619-626.

Lidke, D. S., Nagy, P., Heintzmann, R., Arndt-Jovin, D. J., Post, J. N., Grecco, H. E., Jares-Erijman, E. A., and Jovin, T. M. (2004). Quantum dot ligands provide new insights into erbB/HER receptor-mediated signal transduction. Nat Biotechnol *22*, 198-203.

Lin, A. C., and Holt, C. E. (2007). Local translation and directional steering in axons. Embo J *26*, 3729-3736.

Linnarsson, S., Willson, C. A., and Ernfors, P. (2000). Cell death in regenerating populations of neurons in BDNF mutant mice. Brain Res Mol Brain Res *75*, 61-69.

Liu Tsang, V., Chen, A. A., Cho, L. M., Jadin, K. D., Sah, R. L., DeLong, S., West, J. L., and Bhatia, S. N. (2007). Fabrication of 3D hepatic tissues by additive photopatterning of cellular hydrogels. Faseb J *21*, 790-801.

Lohof, A. M., Quillan, M., Dan, Y., and Poo, M. M. (1992). Asymmetric modulation of cytosolic cAMP activity induces growth cone turning. J Neurosci *12*, 1253-1261.

Lowery, L. A., and Van Vactor, D. (2009). The trip of the tip: understanding the growth cone machinery. Nat Rev Mol Cell Biol *10*, 332-343.

Luo, C., Li, H., Xiong, C., Peng, X., Kou, Q., Chen, Y., Ji, H., and Ouyang, Q. (2007). The combination of optical tweezers and microwell array for cells physical manipulation and localization in microfluidic device. Biomed Microdevices *9*, 573-578.

MacInnis, B. L., and Campenot, R. B. (2002). Retrograde support of neuronal survival without retrograde transport of nerve growth factor. Science *295*, 1536-1539.

Mao, H., Cremer, P. S., and Manson, M. D. (2003). A sensitive, versatile microfluidic assay for bacterial chemotaxis. Proc Natl Acad Sci U S A *100*, 5449-5454.

Maxell, J. C. (1873). Treatise On Electricity And Magnetism).

McAllister, A. K., Lo, D. C., and Katz, L. C. (1995). Neurotrophins regulate dendritic growth in developing visual cortex. Neuron *15*, 791-803.

McDougall, C., Stevenson, D. J., Brown, C. T., Gunn-Moore, F., and Dholakia, K. (2009). Targeted optical injection of gold nanoparticles into single mammalian cells. J Biophotonics *2*, 736-743.

Meister, A., Gabi, M., Behr, P., Studer, P., Voros, J., Niedermann, P., Bitterli, J., Polesel-Maris, J., Liley, M., Heinzelmann, H., and Zambelli, T. (2009). FluidFM: combining atomic force microscopy and nanofluidics in a universal liquid delivery system for single cell applications and beyond. Nano Lett *9*, 2501-2507.

Mendel, E. (1991). Friendly communication is key to effective client interactions. J Am Vet Med Assoc *198*, 1707-1708.

Meyvantsson, I., and Beebe, D. J. (2008). Cell culture models in microfluidic systems. Annu Rev Anal Chem (Palo Alto Calif) *1*, 423-449.

Michalet, X., Pinaud, F. F., Bentolila, L. A., Tsay, J. M., Doose, S., Li, J. J., Sundaresan, G., Wu, A. M., Gambhir, S. S., and Weiss, S. (2005). Quantum dots for live cells, in vivo imaging, and diagnostics. Science *307*, 538-544.

Moffitt, J. R., Chemla, Y. R., Smith, S. B., and Bustamante, C. (2008). Recent advances in optical tweezers. Annu Rev Biochem *77*, 205-228.

Mogilner, A. (2006). On the edge: modeling protrusion. Curr Opin Cell Biol *18*, 32-39.

Monneret, S., Belloni, F., and Soppera, O. (2007). Combining fluidic reservoirs and optical tweezers to control beads/living cells contacts. Microfluid Nanofluid *3*, 645-652.

Mowla, S. J., Farhadi, H. F., Pareek, S., Atwal, J. K., Morris, S. J., Seidah, N. G., and Murphy, R. A. (2001). Biosynthesis and post-translational processing of the precursor to brain-derived neurotrophic factor. J Biol Chem *276*, 12660-12666.

Muralidharan, V., and Muir, T. W. (2006). Protein ligation: an enabling technology for the biophysical analysis of proteins. Nat Methods *3*, 429-438.

Nagerl, U. V., and Bonhoeffer, T. (2010). Imaging living synapses at the nanoscale by STED microscopy. J Neurosci *30*, 9341-9346.

Naka, Y., Kitazawa, A., Akaishi, Y., and Shimizu, N. (2004). Neurite outgrowths of neurons using neurotrophin-coated nanoscale magnetic beads. J Biosci Bioeng *98*, 348-352.

Neuman, K. C., and Block, S. M. (2004). Optical trapping. Rev Sci Instrum *75*, 2787-2809.

Neuman, K. C., Chadd, E. H., Liou, G. F., Bergman, K., and Block, S. M. (1999). Characterization of photodamage to Escherichia coli in optical traps. Biophys J *77*, 2856-2863.

Nishiyama, M., Hoshino, A., Tsai, L., Henley, J. R., Goshima, Y., Tessier-Lavigne, M., Poo, M. M., and Hong, K. (2003). Cyclic AMP/GMP-dependent modulation of Ca2+ channels sets the polarity of nerve growth-cone turning. Nature *423*, 990-995.

Ostroff, L. E., Fiala, J. C., Allwardt, B., and Harris, K. M. (2002). Polyribosomes redistribute from dendritic shafts into spines with enlarged synapses during LTP in developing rat hippocampal slices. Neuron *35*, 535-545.

Pakhomov, A. G., Semenov, I., Brenner, R., and Toney, G. M. (2006). Hydraulically coupled microejection technique for precise local solution delivery in tissues. J Neurosci Methods *155*, 231-240.

Park, T. H., and Shuler, M. L. (2003). Integration of cell culture and microfabrication technology. Biotechnol Prog *19*, 243-253.

Patapoutian, A., and Reichardt, L. F. (2001). Trk receptors: mediators of neurotrophin action. Curr Opin Neurobiol *11*, 272-280.

Pathak, S., Choi, S. K., Arnheim, N., and Thompson, M. E. (2001). Hydroxylated quantum dots as luminescent probes for in situ hybridization. J Am Chem Soc *123*, 4103-4104.

Perkins, T. T. (2009). Optical traps for single molecule biophysics: a primer. Laser & Photonics Reviews *3*, 203-220.

Pidoplichko, V. I., and Dani, J. A. (2005). Applying small quantities of multiple compounds to defined locations of in vitro brain slices. J Neurosci Methods *142*, 55-66.

Pinato, G., Lien, L. T., D'Este, E., Torre, V., and Cojoc, D. (2011a). Neuronal chemotaxis by optically manipulated liposomes. Journal of the European Optical Society Rapid Publications *6*, 11042.

Pinato, G., Pegoraro, S., Iacono, G., Ruaro, M. E., and Torre, V. (2009). Calcium control of gene regulation in rat hippocampal neuronal cultures. J Cell Physiol *220*, 727-747.

Pinato, G., Raffaelli, T., D'Este, E., Tavano, F., and Cojoc, D. (2011b). Optical delivery of liposome encapsulated chemical stimuli to neuronal cells. J Biomed Opt *16*, 095001.

Pinaud, F., Clarke, S., Sittner, A., and Dahan, M. (2010). Probing cellular events, one quantum dot at a time. Nat Methods *7*, 275-285.

Pinaud, F., Michalet, X., Iyer, G., Margeat, E., Moore, H. P., and Weiss, S. (2009). Dynamic partitioning of a glycosyl-phosphatidylinositol-anchored protein in glycosphingolipid-rich microdomains imaged by single-quantum dot tracking. Traffic *10*, 691-712.

Pine, J., and Chow, G. (2009). Moving live dissociated neurons with an optical tweezer. IEEE Trans Biomed Eng *56*, 1184-1188.

Piner, R. D., Zhu, J., Xu, F., Hong, S., and Mirkin, C. A. (1999). "Dip-Pen" nanolithography. Science *283*, 661-663.

Piper, M., Salih, S., Weinl, C., Holt, C. E., and Harris, W. A. (2005). Endocytosis-dependent desensitization and protein synthesis-dependent resensitization in retinal growth cone adaptation. Nat Neurosci *8*, 179-186.

Rajan, S. S., Liu, H. Y., and Vu, T. Q. (2008). Ligand-bound quantum dot probes for studying the molecular scale dynamics of receptor endocytic trafficking in live cells. ACS Nano *2*, 1153-1166.

Ramser, K., Logg, K., Goksor, M., Enger, J., Kall, M., and Hanstorp, D. (2004). Resonance Raman spectroscopy of optically trapped functional erythrocytes. J Biomed Opt *9*, 593-600.

Rao, S., Balint, S., Cossins, B., Guallar, V., and Petrov, D. (2009). Raman study of mechanically induced oxygenation state transition of red blood cells using optical tweezers. Biophys J *96*, 209-216.

Raucher, D. (2008). Chapter 17: Application of laser tweezers to studies of membrane-cytoskeleton adhesion. Methods Cell Biol *89*, 451-466.

Ravula, S. K., Wang, M. S., McClain, M. A., Asress, S. A., Frazier, B., and Glass, J. D. (2007). Spatiotemporal localization of injury potentials in DRG neurons during vincristine-induced axonal degeneration. Neurosci Lett *415*, 34-39.

Reichardt, L. F. (2006). Neurotrophin-regulated signalling pathways. Philos Trans R Soc Lond B Biol Sci *361*, 1545-1564.

Reichardt, L. F., and Mobley, W. C. (2004). Going the distance, or not, with neurotrophin signals. Cell *118*, 141-143.

Rittweger, E., Young Han, K., Irvine, S. E., Eggeling, C., and Hell, S. W. (2009). STED microscopy reveals crystal colour centres with nanometric resolution. Nature Photonics *3*, 144-147.

Rodriguez-Tebar, A., Dechant, G., and Barde, Y. A. (1990). Binding of brain-derived neurotrophic factor to the nerve growth factor receptor. Neuron *4*, 487-492.

Rosenberg, M. B., Hawrot, E., and Breakefield, X. O. (1986). Receptor binding activities of biotinylated derivatives of beta-nerve growth factor. J Neurochem *46*, 641-648.

Round, J., and Stein, E. (2007). Netrin signaling leading to directed growth cone steering. Curr Opin Neurobiol *17*, 15-21.

Sawano, A., Takayama, S., Matsuda, M., and Miyawaki, A. (2002). Lateral propagation of EGF signaling after local stimulation is dependent on receptor density. Dev Cell *3*, 245-257.

Schaff, U. Y., Xing, M. M., Lin, K. K., Pan, N., Jeon, N. L., and Simon, S. I. (2007). Vascular mimetics based on microfluidics for imaging the leukocyte--endothelial inflammatory response. Lab Chip *7*, 448-456.

Schecterson, L. C., and Bothwell, M. (2010). Neurotrophin receptors: Old friends with new partners. Dev Neurobiol *70*, 332-338.

Segal, R. A. (2003). Selectivity in neurotrophin signaling: theme and variations. Annu Rev Neurosci *26*, 299-330.

Shaevitz, J. W. (2006). A Practical Guide to Optical Trapping.

Shan, J., Munro, T. P., Barbarese, E., Carson, J. H., and Smith, R. (2003). A molecular mechanism for mRNA trafficking in neuronal dendrites. J Neurosci *23*, 8859-8866.

Shekarabi, M., and Kennedy, T. E. (2002). The netrin-1 receptor DCC promotes filopodia formation and cell spreading by activating Cdc42 and Rac1. Mol Cell Neurosci *19*, 1-17.

Shen, K., and Cowan, C. W. (2010). Guidance molecules in synapse formation and plasticity. Cold Spring Harb Perspect Biol *2*, a001842.

Sheng, M., McFadden, G., and Greenberg, M. E. (1990). Membrane depolarization and calcium induce c-fos transcription via phosphorylation of transcription factor CREB. Neuron *4*, 571-582.

Sieber, J. J., Willig, K. I., Heintzmann, R., Hell, S. W., and Lang, T. (2006). The SNARE motif is essential for the formation of syntaxin clusters in the plasma membrane. Biophys J *90*, 2843-2851.

Sigot, V., Arndt-Jovin, D. J., and Jovin, T. M. (2010). Targeted cellular delivery of quantum dots loaded on and in biotinylated liposomes. Bioconjug Chem *21*, 1465-1472.

Snook, R. D., Harvey, T. J., Correia Faria, E., and Gardner, P. (2009). Raman tweezers and their application to the study of singly trapped eukaryotic cells. Integr Biol (Camb) *1*, 43-52.

Steketee, M. B., Moysidis, S. N., Jin, X. L., Weinstein, J. E., Pita-Thomas, W., Raju, H. B., Iqbal, S., and Goldberg, J. L. (2011). Nanoparticle-mediated signaling endosome localization regulates growth cone motility and neurite growth. Proc Natl Acad Sci U S A *108*, 19042-19047.

Steubing, R. W., Cheng, S., Wright, W. H., Numajiri, Y., and Berns, M. W. (1991). Laser induced cell fusion in combination with optical tweezers: the laser cell fusion trap. Cytometry *12*, 505-510.

Stevenson, D. J., Gunn-Moore, F., and Dholakia, K. (2010a). Light forces the pace: optical manipulation for biophotonics. J Biomed Opt *15*, 041503.

Stevenson, D. J., Gunn-Moore, F. J., Campbell, P., and Dholakia, K. (2010b). Single cell optical transfection. J R Soc Interface *7*, 863-871.

Sun, B., and Chiu, D. T. (2003). Spatially and temporally resolved delivery of stimuli to single cells. J Am Chem Soc *125*, 3702-3703.

Sundara Rajan, S., and Vu, T. Q. (2006). Quantum dots monitor TrkA receptor dynamics in the interior of neural PC12 cells. Nano Lett *6*, 2049-2059.

Suter, D. M. (2011). Live cell imaging of neuronal growth cone motility and guidance in vitro. Methods Mol Biol *769*, 65-86.

Taylor, A. M., Blurton-Jones, M., Rhee, S. W., Cribbs, D. H., Cotman, C. W., and Jeon, N. L. (2005). A microfluidic culture platform for CNS axonal injury, regeneration and transport. Nat Methods *2*, 599-605.

Theveneau, E., and Mayor, R. (2011). Beads on the run: beads as alternative tools for chemotaxis assays. Methods Mol Biol *769*, 449-460.

Thompson, A. W., Pujic, Z., Richards, L. J., and Goodhill, G. J. (2011). Cyclic nucleotide-dependent switching of mammalian axon guidance depends on gradient steepness. Mol Cell Neurosci *47*, 45-52.

Tirlapur, U. K., and Konig, K. (2002). Targeted transfection by femtosecond laser. Nature *418*, 290-291.

Tlusty, T., Meller, A., and Bar-Ziv, R. (1998). Optical gradient forces of the strongly localized fields. Phys Rev Lett *81*, 1738-1741.

Tojima, T., Hines, J. H., Henley, J. R., and Kamiguchi, H. (2011). Second messengers and membrane trafficking direct and organize growth cone steering. Nat Rev Neurosci *12*, 191-203.

Tongiorgi, E. (2008). Activity-dependent expression of brain-derived neurotrophic factor in dendrites: facts and open questions. Neurosci Res *61*, 335-346.

Tongiorgi, E., Righi, M., and Cattaneo, A. (1997). Activity-dependent dendritic targeting of BDNF and TrkB mRNAs in hippocampal neurons. J Neurosci *17*, 9492-9505.

Toresson, H., and Grant, S. G. (2005). Dynamic distribution of endoplasmic reticulum in hippocampal neuron dendritic spines. Eur J Neurosci *22*, 1793-1798.

Townes-Anderson, E., St Jules, R. S., Sherry, D. M., Lichtenberger, J., and Hassanain, M. (1998). Micromanipulation of retinal neurons by optical tweezers. Mol Vis *4*, 12.

Triller, A., and Choquet, D. (2008). New concepts in synaptic biology derived from single-molecule imaging. Neuron *59*, 359-374.

Underwood, C. K., and Coulson, E. J. (2008). The p75 neurotrophin receptor. Int J Biochem Cell Biol *40*, 1664-1668.

Urban, N. T., Willig, K. I., Hell, S. W., and Nagerl, U. V. (2011). STED nanoscopy of actin dynamics in synapses deep inside living brain slices. Biophys J *101*, 1277-1284.

Valero, V., Nevian, T., Ho, D., and Lindau, M. (2008). Tethering forces of secretory granules measured with optical tweezers. Biophys J *95*, 4972-4978.

Vu, T. Q., Maddipati, R., Blute, T. A., Nehilla, B. J., Nusblat, L., and Desai, T. A. (2005). Peptide-conjugated quantum dots activate neuronal receptors and initiate downstream signaling of neurite growth. Nano Lett *5*, 603-607.

Walde, P., and Ichikawa, S. (2001). Enzymes inside lipid vesicles: preparation, reactivity and applications. Biomol Eng *18*, 143-177.

Walker, J. W., Gilbert, S. H., Drummond, R. M., Yamada, M., Sreekumar, R., Carraway, R. E., Ikebe, M., and Fay, F. S. (1998). Signaling pathways underlying eosinophil cell motility revealed by using caged peptides. Proc Natl Acad Sci U S A *95*, 1568-1573.

Wang, X., Boreiko, A., Schlossmacher, U., Brandt, D., Schroder, H. C., Li, J., Kaandorp, J. A., Gotz, H., Duschner, H., and Muller, W. E. (2008). Axial growth of hexactinellid spicules: formation of cone-like structural units in the giant basal spicules of the hexactinellid Monorhaphis. J Struct Biol *164*, 270-280.

Westphal, V., Rizzoli, S. O., Lauterbach, M. A., Kamin, D., Jahn, R., and Hell, S. W. (2008). Video-rate far-field optical nanoscopy dissects synaptic vesicle movement. Science *320*, 246-249.

Wildanger, D., Medda, R., Kastrup, L., and Hell, S. W. (2009). A compact STED microscope providing 3D nanoscale resolution. J Microsc *236*, 35-43.

Willig, K. I., Harke, B., Medda, R., and Hell, S. W. (2007). STED microscopy with continuous wave beams. Nat Methods *4*, 915-918.

Willig, K. I., Kastrup, L., Nägerl, V., and Hell, S. W. (2009). STED Microscopy: Different Approaches and Applications: Washington, DC: Society for Neuroscience).

Willig, K. I., Kellner, R. R., Medda, R., Hein, B., Jakobs, S., and Hell, S. W. (2006). Nanoscale resolution in GFP-based microscopy. Nat Methods *3*, 721-723.

Wu, Y., Campos, S. K., Lopez, G. P., Ozbun, M. A., Sklar, L. A., and Buranda, T. (2007). The development of quantum dot calibration beads and quantitative multicolor bioassays in flow cytometry and microscopy. Anal Biochem *364*, 180-192.

Wu, Y. I., Frey, D., Lungu, O. I., Jaehrig, A., Schlichting, I., Kuhlman, B., and Hahn, K. M. (2009). A genetically encoded photoactivatable Rac controls the motility of living cells. Nature *461*, 104-108.

Xiao, Y., and Barker, P. E. (2004). Semiconductor nanocrystal probes for human metaphase chromosomes. Nucleic Acids Res *32*, e28.

Yoshii, A., and Constantine-Paton, M. (2007). BDNF induces transport of PSD-95 to dendrites through PI3K-AKT signaling after NMDA receptor activation. Nat Neurosci *10*, 702-711.

Zahavy, E., Freeman, E., Lustig, S., Keysary, A., and Yitzhaki, S. (2005). Double labeling and simultaneous detection of B- and T cells using fluorescent nano-crystal (q-dots) in paraffin-embedded tissues. J Fluoresc *15*, 661-665.

Zhang, K., Osakada, Y., Vrljic, M., Chen, L., Mudrakola, H. V., and Cui, B. (2010). Single-molecule imaging of NGF axonal transport in microfluidic devices. Lab Chip *10*, 2566-2573.

Zhang, Q., Cao, Y. Q., and Tsien, R. W. (2007). Quantum dots provide an optical signal specific to full collapse fusion of synaptic vesicles. Proc Natl Acad Sci U S A *104*, 17843-17848.

Zhang, Q., Li, Y., and Tsien, R. W. (2009). The dynamic control of kiss-and-run and vesicular reuse probed with single nanoparticles. Science *323*, 1448-1453.

Zhang, X., and Poo, M. M. (2002). Localized synaptic potentiation by BDNF requires local protein synthesis in the developing axon. Neuron *36*, 675-688.

Zhang, Y., Moheban, D. B., Conway, B. R., Bhattacharyya, A., and Segal, R. A. (2000). Cell surface Trk receptors mediate NGF-induced survival while internalized receptors regulate NGF-induced differentiation. J Neurosci *20*, 5671-5678.

Zheng, J. Q. (2000). Turning of nerve growth cones induced by localized increases in intracellular calcium ions. Nature *403*, 89-93.

Zhou, F. Q., and Cohan, C. S. (2004). How actin filaments and microtubules steer growth cones to their targets. J Neurobiol *58*, 84-91.

APPENDIX

Papers published:

- D'Este, E., Baj, G., Beuzer, P., Ferrari, E., Pinato, G., Tongiorgi, E., and Cojoc, D. (2011). Use of optical tweezers technology for long-term, focal stimulation of specific subcellular neuronal compartments. Integr Biol (Camb) *3*, 568-577;
- Pinato, G., Lien, L. T., D'Este, E., Torre, V., and Cojoc, D. (2011). Neuronal chemotaxis by optically manipulated liposomes. Journal of the European Optical Society Rapid Publications *6*, 11042;
- Pinato, G., Raffaelli, T., D'Este, E., Tavano, F., and Cojoc, D. (2011). Optical delivery of liposome encapsulated chemical stimuli to neuronal cells. J Biomed Opt *16*, 095001.